

---

Electronic Thesis and Dissertation Repository

---

4-27-2012 12:00 AM

## Applicability of the Eshelby Formalism to Viscous Power-Law Materials: A Numerical Validation

Zhenyu Zhong  
*The University of Western Ontario*

Supervisor  
Dr. Dazhi Jiang  
*The University of Western Ontario*

Graduate Program in Geology  
A thesis submitted in partial fulfillment of the requirements for the degree in Master of Science  
© Zhenyu Zhong 2012

Follow this and additional works at: <https://ir.lib.uwo.ca/etd>



Part of the [Tectonics and Structure Commons](#)

---

### Recommended Citation

Zhong, Zhenyu, "Applicability of the Eshelby Formalism to Viscous Power-Law Materials: A Numerical Validation" (2012). *Electronic Thesis and Dissertation Repository*. 541.

<https://ir.lib.uwo.ca/etd/541>

This Dissertation/Thesis is brought to you for free and open access by Scholarship@Western. It has been accepted for inclusion in Electronic Thesis and Dissertation Repository by an authorized administrator of Scholarship@Western. For more information, please contact [wlsadmin@uwo.ca](mailto:wlsadmin@uwo.ca).

**Applicability of the Eshelby Formalism to Viscous Power-Law Materials: A  
Numerical Validation**

(Thesis format: Monograph)

by

Zhenyu Zhong

Graduate Program in Geology

A thesis submitted in partial fulfillment  
of the requirements for the degree of  
Master of Science

The School of Graduate and Postdoctoral Studies  
The University of Western Ontario  
London, Ontario, Canada

© Zhenyu Zhong 2012

**CERTIFICATE OF EXAMINATION**

Supervisor

\_\_\_\_\_  
Dr. Dazhi Jiang

Supervisory Committee

\_\_\_\_\_  
Dr. Robert Shcherbakov

Examiners

\_\_\_\_\_  
Dr. Gerhard Pratt

\_\_\_\_\_  
Dr. Robert Shcherbakov

\_\_\_\_\_  
Dr. Liying Jiang

The thesis by

**Zhenyu Zhong**

entitled:

**Applicability of the Eshelby Formalism to Viscous Power-Law Materials: A  
Numerical Validation**

is accepted in partial fulfillment of the  
requirements for the degree of  
**Master of Science**

April 26, 2012

\_\_\_\_\_  
Date

Dr. Stephen R. Hicock

\_\_\_\_\_  
Chair of the Thesis Examination Board

## Abstract

Fabric is important for the interpretation of tectonic evolutions. In the process of extrapolating small-scale fabric to tectonics, modeling frameworks are needed. Neither the early kinematic models nor the contemporary computational geodynamics are able to capture the complexities of the fabric development in natural deformation systems. Eshelby proposed a formalism in micro-mechanics, and it is now well understood that this formalism works well for the linear viscous deformations. However, given that most of the natural rocks are power-law materials, the Eshelby Formalism cannot be directly applied to geological problems. This problem was largely solved when Lebensohn and Tomé (1993, *Acta Metallurgica et Materialia*, vol 41, 2611-2624) incorporated a linearization scheme with Eshelby Formalism, known as the Tangent Linearization. The purpose of this project is to validate the applicability of the Eshelby Formalism with Tangent Linearization (*EFTL*) or with Secant Linearization (*EFSL*) to power-law material deformations. Two types of simulations are proceeded, one is based on *EFTL / EFSL*, while the other one based on 2D finite difference geodynamic method. Comparisons of the two simulations show that even in the most general situation of power-law material deformations, *EFSL* has major differences with the simulated power-law behavior while *EFTL* has only an approximately 10% deviation. Through this project, *EFTL* is validated to be a new, sufficient framework for fabric modeling, which marks a new era of fabric interpretation both in theoretical simulations and in field work practice.

## Keywords

Fabric Modeling; Eshelby Formalism; Tangent Linearization; Secant Linearization;  
Finite difference model; Validation

## Acknowledgments

First of all, I want to express my gratitude to my supervisor Professor Dazhi Jiang. Without his vivid lectures, his fruitful discussions, expertise and enthusiasm in supervision, this thesis will not be possible. It is him that guides me through the mist so that I can gain so much insight into my program and discover the beauty of science. I will also remember all the kind words he said, all the supports he gave me, and all the encouragements that keeps me marching on throughout these years. I'm truly grateful for everything that he teaches me, which is going to be beneficial for a whole lifetime. In all these years, I always enjoy working with Professor Jiang and feel honored to be one of his students.

I also want to dedicate this work to my parents. Every parent loves their child, but not all of them have to suffer the pain of being apart from each other. I have not been home for nearly two years, and I can sense how hard it is for my parents to go through this time, although they hid it so well on every single call. They never stop loving me and never lose faith in me, even when I was in the most frustrating period. My mother had two surgeries during these two years, but she always tried so hard to hide her pain and sugarcoat her illness in order for me to concentrate on my own research. I hate myself so much that I cannot be with her in her hardest time. Without their love, I will not have the courage to face all the difficulties and finish this work. Please let me dedicate this work as well as my deepest love to them. In the future, I hope that I can be a better son to them.

Xinting Hu, my fiancée, is the next person to whom I owe so much. She has been supporting me and never stops loving me through all these years. Long-distance

relationship is so hard for most of people, but we make it possible. This is all because of her. She is already a family to me.

Changcheng Li is another person to whom I always desire to express my gratitude. His friendship, his company, his unconditional help in both research and finance, his encouragement, his help with my research etc., provide me the best research environment that one can ever dream of. From day one when I arrive in Canada, he has been taking care of me. He manages to make it much easier for me to part with my family and find some comfort in here. I am extremely lucky to have met him and worked with him.

In addition, I want to thank all my fellow graduate students working with me, fulfilling my daily life. Xinyang Liu has brought so many joys and supports to me that I learn to embrace the beauty of life. Pengfei Chen, Qin Ma, Peng Jiang, we share wonderful memories behind us and may we all have glorious future before us.

Last but not least, I am grateful for all the professors, administrative staff and fellow students in my department. It is all of you who make this department a warm and invincible family. I am proud of myself for being one of the family members.

# Table of Contents

<b>CERTIFICATE OF EXAMINATION</b> .....	ii
Abstract .....	iii
Acknowledgments .....	v
Table of Contents .....	vii
List of Tables .....	xi
List of Figures .....	xii
List of Appendices .....	xiv
Chapter 1 .....	1
1 Introduction .....	1
1.1 Scale Gap in Fabric Modeling .....	1
1.2 Early Framework: Kinematic Models .....	3
1.3 Contemporary Framework: Computational Geodynamics .....	5
1.4 New Approach in Fabric Modeling – Eshelby Inclusion Formalism .....	7
1.4.1 The ‘Inhomogeneity-Matrix’ System in Eshelby theory .....	8
1.4.2 Advantages of the Eshelby Formalism .....	11
1.5 Extension of Eshelby Formalism to Power-Law Materials .....	12
1.6 Objectives and Methodology of this Project .....	13
1.7 Thesis Outline .....	18
Chapter 2 .....	19
2 Theoretical Background .....	19
2.1 Terminology of Continuum Mechanics .....	19
2.1.1 Flow Kinematics .....	19
2.1.2 Strain Ellipsoid and Strain Ellipse .....	23



2.1.3	Flow Types.....	24
2.1.4	Rheology.....	27
2.2	Eshelby Formalism and Tangent Linearization Scheme .....	29
2.2.1	Eshelby Formalism for linear elastic and viscous materials.....	30
2.2.2	Extension of Eshelby Formalism to Power-Law Materials – Tangent Linearization Scheme.....	31
2.3	Mathcad Program.....	35
2.4	Finite Difference Simulations in FLAC.....	36
2.4.1	Finite Difference .....	37
2.4.2	Grid and Zone Generation.....	37
2.4.3	FISH Programming Language .....	40
Chapter 3	.....	41
3	Simulation Designs .....	41
3.1	Simulation Design for <i>EFTL</i> and <i>EFSL</i> .....	41
3.1.1	Step Length Settings .....	41
3.1.2	2D Plane Strain Deformation Settings .....	42
3.2	Design for Finite Difference Simulation.....	44
3.2.1	Grid Generation.....	46
3.2.2	Material Property Assignment .....	47
3.2.3	Boundary Conditions .....	48
3.2.4	Timestep Selection for FLAC modeling.....	52
3.2.5	Obtaining Results in FLAC .....	54
3.3	Optimization in Finite Difference Simulation .....	61
3.3.1	Elastic Relaxation Time .....	61
3.3.2	Grid Density Selection.....	63
3.3.3	The Finite Model Size Effect.....	70

3.3.4	Boundary Velocity Updating .....	71
3.4	Result Post-Processing and Comparisons .....	73
Chapter 4	.....	75
4	Simulations and Results .....	75
4.1	Verification Simulations .....	75
4.1.1	A Newtonian Inhomogeneity in a Newtonian Matrix.....	75
4.1.2	A Power-Law Inhomogeneity in a Newtonian Matrix .....	79
4.1.3	A Newtonian Inhomogeneity in a Power-Law Matrix .....	84
4.2	Simulations on General Power-law Deformation .....	87
4.2.1	Shear Flow Type Variations .....	87
4.2.2	Initial Orientation/Shape Variations .....	92
4.2.3	Mechanical Property Variations.....	96
Chapter 5	.....	102
5	Result Discussions and Conclusions .....	102
5.1	Result Summary and Discussions .....	102
5.1.1	Newtonian Inhomogeneity in Newtonian Matrix .....	102
5.1.2	Power-Law Inhomogeneity in Newtonian Matrix .....	103
5.1.3	Newtonian Inhomogeneity in Power-Law Matrix .....	103
5.1.4	Power-Law Inhomogeneity in Power-Law Matrix .....	105
5.2	Applicability of the Eshelby Formalism with Tangent Linearization Scheme ...	108
5.2.1	Applicability Quantification .....	108
5.2.2	Mechanical Condition Requirement .....	113
5.3	Appropriate Modifications .....	114
5.3.1	Practical Implementations.....	115
5.4	Conclusions and Future Work .....	118

References.....	120
Appendices.....	125
Curriculum Vitae.....	134

## List of Tables

Table 3-1 Material properties Assignment in FLAC2D in one experiment. ....	62
Table 3-2 Material property of wet quartzite (Gleason and Tullis, 1995) .....	63
Table 4-1 Initial Conditions for the verification simulation where a Newtonian inhomogeneity is embedded in a Newtonian matrix .....	76
Table 4-2 Initial conditions for the simulation where a power-law inhomogeneity is embedded in a Newtonian matrix. ....	81
Table 4-3 Initial conditions for the simulation where a Newtonian inhomogeneity is embedded in a power-law matrix.....	84
Table 4-4 Initial conditions for simulations with shear flow type variations. ....	88
Table 4-5 Initial conditions for simulations on different initial inhomogeneity orientations. ....	93
Table 4-6 Initial mechanical conditions for simulations on different mechanical properties. ....	97
Table 5-1 Initial conditions for a general power-law simulation.....	108
Table 5-2 Resulted axial ratios and orientations of the inhomogeneity.....	109
Table 5-3 Initial conditions for simulation on <i>neff</i> value. ....	115

## List of Figures

Figure 1-1 Fabric in Dynamic Recrystallized Quartz. ....	2
Figure 1-2 ‘Inhomogeneity-Matrix’ System in Eshelby Formalism.....	10
Figure 1-3 Procedure of the methodology in this project. ....	16
Figure 1-4 <i>EFTL</i> Computation design in Mathcad. ....	17
Figure 2-1 A homogenous domain of 2D general shear used as the flow field in this project.....	22
Figure 2-2 Strain ellipsoid and its three principal axes. ....	23
Figure 2-3 Strain resulting from simple shear, general shear and pure shear. Modified from (Fossen, 2010). ....	26
Figure 2-4 Grid generation in FLAC. ....	39
Figure 3-1 Length change in the z-axis of the elongated ellipsoid during a complete computation.....	43
Figure 3-2 Simulation Design in FLAC.....	45
Figure 3-3 Velocity boundary conditions of the FLAC model. ....	51
Figure 3-4 Orientation of the elliptical inhomogeneity. ....	56
Figure 3-5 Axial ratio history of an elliptical inhomogeneity modeled in FLAC. ....	58
Figure 3-6 Initial state and final state of the matrix and the elliptical inhomogeneity. ....	60
Figure 3-7 History of the Inhomogeneity orientation for two different grid densities. ....	65
Figure 3-8 Inhomogeneity axial ratio plot with different grid densities. ....	66

Figure 3-9 Error in the calculated long axis.....	68
Figure 3-10 Actual Evolution Curve in FLAC simulation. ....	69
Figure 3-11 Result curve figure for comparisons. ....	74
Figure 4-1 Results from FLAC and Eshelby Formalism for a Newtonian inhomogeneity embedded in a Newtonian matrix. ....	78
Figure 4-2 Response of effective viscosity ratio in respect to the variations of axial ratio and power-law stress exponent of the inhomogeneity. Figure modified from Mancktelow (2011). ....	80
Figure 4-3 Results from FLAC and Esheby formalism for a power-law inhomogeneity embedded in a Newtonian matrix. ....	83
Figure 4-4 Results from FLAC and Eshelby Formalism for a Newtonian inhomogeneity embedded in a power-law matrix.....	86
Figure 4-5 Results from FLAC and Eshelby Formalism for $Wk$ variation simulations....	91
Figure 4-6 Axial ratio simulation results from FLAC and Eshelby Formalism with initial orientation variations. ....	95
Figure 4-7 Results from FLAC and Eshelby Formalism on varying power-law stress exponent. ....	101
Figure 5-1 Schematic strain history of an inhomogeneity modeled by the Secant Behavior, Tangent Behavior and the Real Power-law Behavior as <b><i>nm</i></b> varies. ....	107
Figure 5-2 The ‘inhomogeneity-matrix’ system after 1 million years deformation in the example simulation. ....	109
Figure 5-3 Late-period general shear deformation. ....	112
Figure 5-4 Results from Eshelby Formalism and FLAC on <b><i>neff</i></b> .....	117

## List of Appendices

Appendix A: Added adjustment command to Jiang's (2012) worksheet in Mathcad to assign initial material settings. Through this algorithm the initial effective viscosity is calculated. ....	125
Appendix B: FISH commands to generate ellipse geometry in FLAC2D.....	126
Appendix C: Mechanical Property Assignment in Power-Law Model in FLAC2D .....	127
Appendix D: Velocity Boundary Condition Updating FISH in FLAC2D .....	128
Appendix E: Von Mises Stress Invariant Calculation in FISH command by ITASCA .	130
Appendix F: Fish Command to Obtain and History-Tracked Ellipse Orientation and Axial Ratio .....	132

# Chapter 1

## 1 Introduction

Strain localization along shear zones is common on Earth (Brun et al., 1980; Hobbs et al., 1990; Riggs and Green, 2001). The deformation fabrics, resulting from strain localization, include lineations and foliations in rocks that are observed on many different scales particularly on outcrops and smaller scale. Such fabrics are of crucial importance for structural geologists to unravel the history, mechanism and rheological property of lithospheric processes that are many orders of magnitude larger in scale dimension than the fabrics themselves (Passchier, 1988, 1990) (Figure 1). Important information of the tectonic evolution held by deformation fabrics makes it desirable to theoretically model the development of such fabrics during deformation. With these theoretical models, one is able to shed light on the tectonic evolution history from the fabric observations. However, there are a number of problems facing current approaches in fabric modeling as discussed below.

### 1.1 Scale Gap in Fabric Modeling

As important as it is, fabric modeling has long been a research focus and captured a large number of geologists' interests (e.g., Ramsay and Graham, 1970; Passchier, 1991; Simpson, 1993; Jiang and Williams, 1998). In the process of such modeling, one is faced with a problem here referred to as the 'scale gap' in this project.



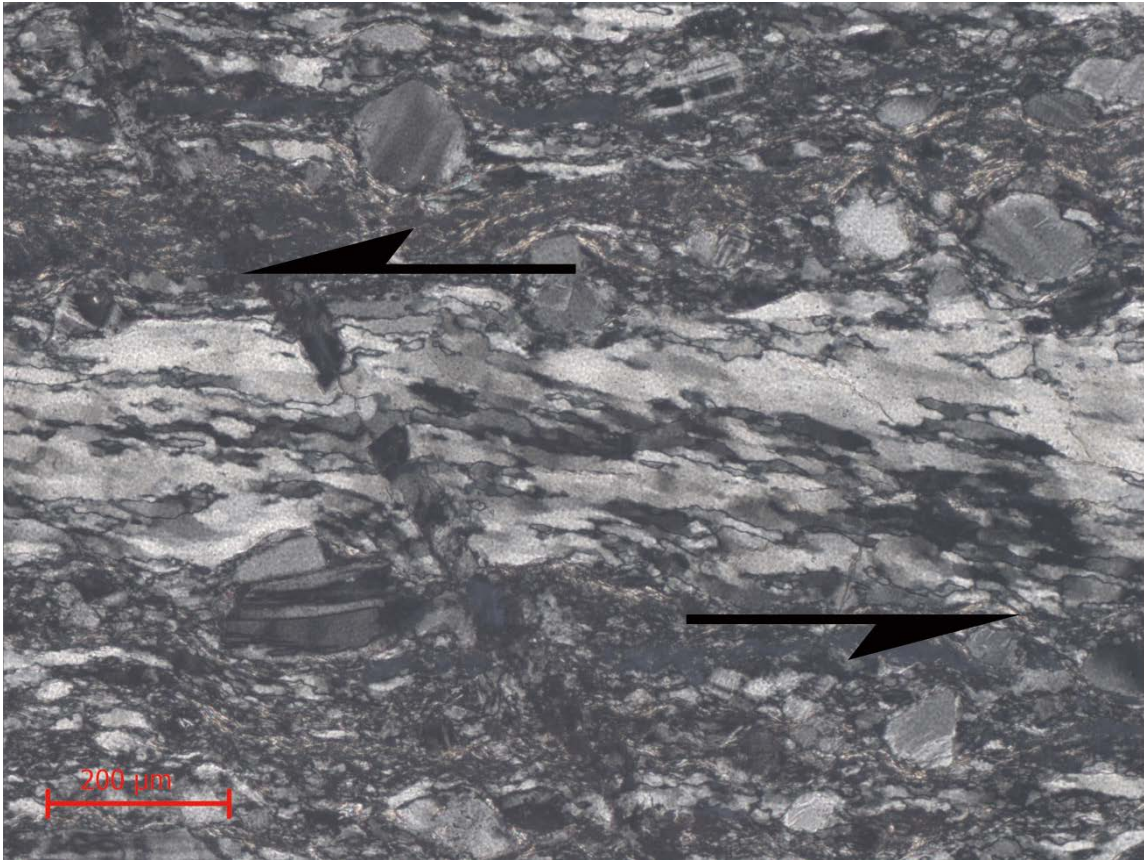


**Figure 1-1 Fabric in Dynamic Recrystallized Quartz.**

*A microscopic sample of the dynamic recrystallized quartz is shown (modified from Li, 2012). By observing the foliations on the quartz, one is able to interpret the shear sense of the shear zone. Shear sense in this mylonite shear zone is top to the west, as indicated by the black arrows.*

The fact that most frequently observed fabrics are in the scale range of meters or even in microscopic scale while the tectonic deformation is often tens of thousands of meters (Passchier, 1990), forms a scale gap when one intends to interpret the whole tectonic process from the fabric observations. Besides the scale gap, the fact that heterogeneity and strain partitioning (Jiang and Williams, 2005) existing in deformation fabrics introduce great complexity to the relationship between the microscopic fabrics and the large-scale rock deformations, making the extrapolation not uniform. Therefore, heterogeneity in natural fabrics ultimately makes the scale gap a serious problem in fabric models where the relationship between the micro scale and the large scale is complicated.

To tackle the gap problem in fabric modeling, an extrapolation framework that is able to simultaneously address multi-scale situations is needed. Such a framework would serve as an information link between the micro-scale fabrics and the large-scale deformations.

## 1.2 Early Framework: Kinematic Models

In designing framework for the extrapolation, simple kinematic models are often used to gain insight into fabrics in natural shear zones. The early framework first proposed by Ramsay and Graham (1970) uses a model that is homogeneous, steady and purely kinematic. The primary justification for using this simple model is that a certain scale can often be chosen where deformation approximates the homogenous state (Twiss and Moores, 1992, p238). In this scale, the rock material is homogenous and the fabric-defining elements are all of the same order therefore the relationship between the flow field and the resulting fabrics is much simpler. Ramsay and Graham's homogeneous,

steady, purely kinematic model was adopted by many for the development of more general types of progressive homogeneous deformation (e.g. Ramberg, 1975; Sanderson and Marchini, 1984; Simpson and De Paor, 1993; Fossen and Tikoff, 1993; Jiang and Williams, 1998; Passchier, 1998).

However, the kinematic models neglect two important complexities in natural rock deformations: heterogeneity and non-steadiness (e.g. Jiang, 1998; Goodwin and Tikoff, 2002). Such neglects lead to an applicability problem when one uses these kinematic models to investigate an important and common type of foliation in nature: transposition foliation. Transposition foliations exist in all crustal scale shear zones and are now understood as the product from the whole-zone scale progressive deformation of an initially heterogeneous rock mass (Williams and Jiang, 2005). The rock units (hereafter 'element') in such crustal scale shear zones are inevitably of different shapes and sizes, randomly dispersed and even show hierarchical embedding relationships where some elements lie within the other. Such compositionally and texturally heterogeneities in the fabrics can no longer be captured by the previous featureless kinematic models.

Thus, using the existing kinematic models limit the understanding of the specific field data. This limitation prompts geologists to find an alternative framework, which can address the heterogeneity and non-steadiness in nature deformation, while also being based on physical principles. Moreover, it can be applied to multi-scale deformation in a deforming system.

## 1.3 Contemporary Framework: Computational Geodynamics

With the rapid development of computers, computational geodynamics has been frequently developed in engineering science. The potential to capture the heterogeneous/non-steady complexities in fabric development deformation makes the computational geodynamics a newly accepted framework in structural geology field (e.g., Currie et al., 2004, 2008; Segurado et al., 2012). However, the big question that most of the structural geologists want to ask is: to what extent can the geodynamics be a framework qualified for fabric development modeling? In order to answer this question, some essential aspects of the geodynamics must first be introduced.

Two current computational geodynamics methods are known as the finite element method (FEM) and the finite difference method (FDM). The most manifest characteristic of these two methods is that they are both mesh-based. The idea of the mesh basis is to divide the whole modeling object into finite meshes. In the modeling process, calculations of conservative equations and constitutive equations in each mesh are undertaken. This meshing basis helps the improvement of the solution precision; however, it also leads to an inevitable computational problem in the following two situations.

### ***1. Multi-Scale Situation***

As mentioned above, to apply a model to the deformation of rocks and the resulting fabric development, one must solve the scale gap problem and address multi-scale deformation simultaneously. Such multi-scale deformation is the main reason that usually

makes the mesh-based geodynamics methods arduous to be applied. Imagine that a geodynamics model is built to simulate the deformations of microscopic elements (in micrometer scale) within a kilometer-scale matrix simultaneously. The minimum mesh size requires being at least in micrometer scale to capture the deformation information of the elements. Moreover, most fabrics in geology like lineations and foliations result from 3D deformation. To model such fabrics, elements in the model must all be 3D to capture all the deformation information. Then the whole matrix will need at least  $10^{27}$  meshes ( $10^9$  for one dimension,  $10^{27}$  for three dimensions) to address the kilometer-scale deformation. Even if the tedious mesh-generation can be done, the variable-calculation on this number of meshes will be a devastating computational challenge.

Thus, simulating both the large scale and the small scale deformation simultaneously is a huge obstacle for the current mesh-based modeling methods.

## ***2. History Tracking Situation***

History tracking is another compulsory work in fabric development modeling. To investigate the development of fabrics, certain deformation information of the each fabric should be recorded in each deformation time duration (e.g., shape, vorticity or strain rate). This recording process is the so-called history tracking process and it is crucial for the interpretation of the fabric deformation evolution. However, as important as the history tracking process is, it brings technical difficulties to the current mechanics modeling methods and such difficulties still remain unsolved. Consider the following example: even in a simplest geodynamics model in geology, histories of one or more of the

following properties: velocities, pressures, stress, strain rate etc. may be tracked (Jiang, 2012). This history tracking process will consequently exert an extra pressure on the memory allocation of the computer. The situation comes even worse in serialization calculation, where in each step in the process of simulation, the system needs to store the histories and use them as the initial conditions for the next-step calculation. In such a case, not only the availability of memory is the problem, the computational time is also a problem that needs to be addressed. For instance, in a specific fabric development model where 100 fabric elements dispersed in the deforming body, both the orientation and the shape properties of all the fabric elements need to be tracked and these properties are also the factors to influence the next step calculations. In such a case, consider each fabric contains about 50 mesh points, then in each step at least 10000 extra variables will be calculated and must be stored in memory before the next step can be proceeded. This is a devastating impact on both memory availability and on CPU power, thus it is computationally impossible under contemporary computer conditions.

In summary, although being able to account for the heterogeneity, non-steadiness complexities, the fact that geodynamic mechanics model can only tackle a single-scale problem makes it limited to be applied to fabric deformations.

## 1.4 New Approach in Fabric Modeling – Eshelby Inclusion Formalism

With all the limitations, FDM and FEM are currently not the ideal approach for the fabric development problem. Fortunately, a micro-mechanics theory developed several decades

ago is gradually accepted as possessing the potential to implement a new approach in fabric modeling.

The deformation of composite material made of one phase (here called inhomogeneity) dispersed in another continuous phase (called matrix) with mechanical contrast has been researched for over a century in micro-mechanics science and is well understood (Jeffery, 1922; Eshelby, 1957,1959; Bilby, 1975; Freeman, 1987; Mancktelow, 2011). A large number of questions have been addressed. For instance, how the rigid inhomogeneity affects the bulk rheological properties of the matrix (Jeffery, 1922; Samanta, 2002; Jiang, 2007); how the motion of an inhomogeneity is related to the bulk deformation kinematics and strain in 3D deformation (Jeffery, 1922; Eshelby, 1957, 1959; Bilby et al., 1975); and what the rotation and interaction are between the inhomogeneities (Ferguson, 1981; Mandal et al., 2005) etc.

Among these theories, Jeffery's and Eshelby's theories are most widely used. Jeffery's theory mainly deals with the deformation of a system of rigid inhomogeneities surrounded by a matrix and Eshelby theory focuses on a more general situation in which the inhomogeneities are also deformable. Since Eshelby theory is more general and converges to Jeffery's theory when the inhomogeneity is set to be close to a rigid body, I mainly utilize Eshelby theory in this project.

#### 1.4.1 The 'Inhomogeneity-Matrix' System in Eshelby theory

Eshelby theory (1957) is a set of equations (hereafter called 'Eshelby Formalism') originally developed to investigate the deformation of an ellipsoidal inclusion whose

mechanical properties are the same as the surrounding matrix. Eshelby further discovered that inhomogeneity in a matrix can in fact be regarded as an equivalent inclusion. In the following context, the term ‘inclusion’ will be denoted by ‘inhomogeneity’. The deforming system, where an isolated deformable inhomogeneity disperses in a surrounding deformable matrix, is called the ‘inhomogeneity-matrix’ system in this project (Figure 1.1). Eshelby’s (1957,1959) work does not just provide a solution to a specific elasticity problem. Far more significantly, he pioneered an approach to relate the local deformation field to the whole deformation field. This approach has since been developed into a powerful field of continuum mechanics called “micromechanics” (Mura, 1987; Nemat-Nasser and Hori, 1999). Micromechanics has the great potential for numerical simulation of multi-scale fabric development in Earth’s lithosphere (Jiang, 2012, in review) because it has some major advantages over the computational geodynamic approach.



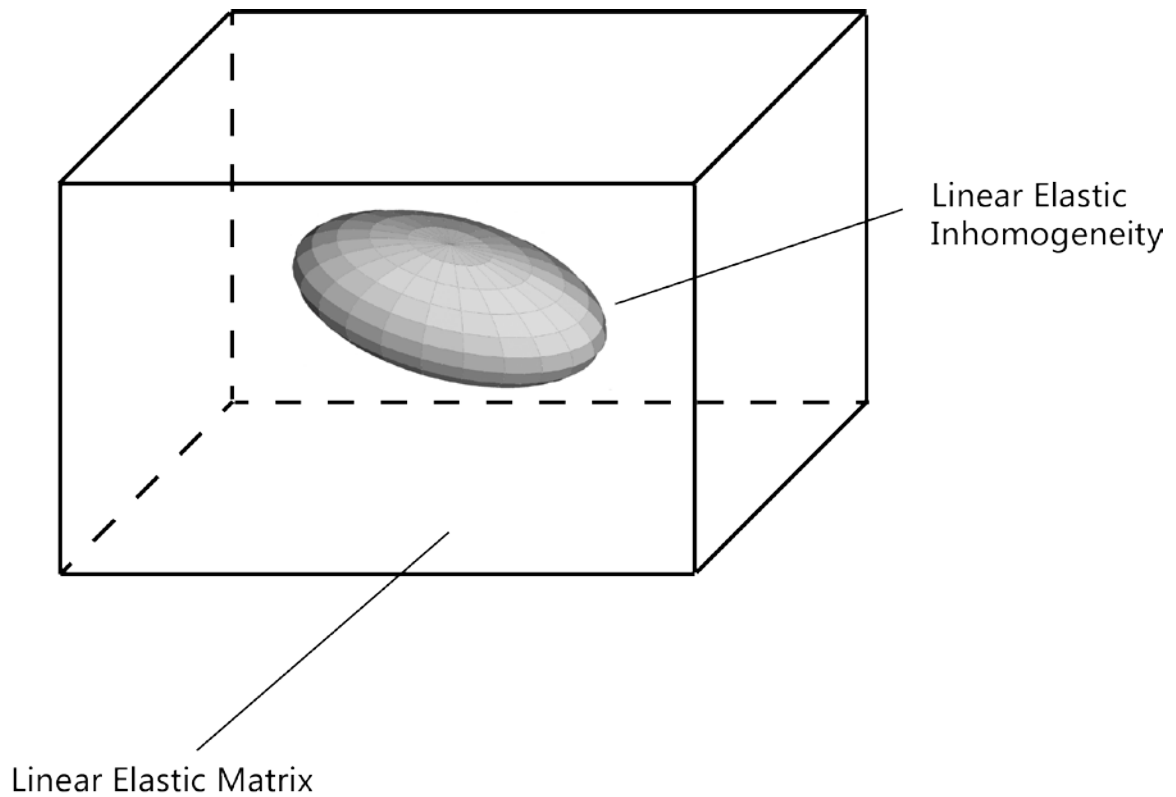


**Figure 1-2 'Inhomogeneity-Matrix' System in Eshelby Formalism**

*The 'inhomogeneity-matrix' system is a deformation system where an elliptical inhomogeneity embedded in a surrounding matrix. Both the inhomogeneity and the matrix are deformable.*

## 1.4.2 Advantages of the Eshelby Formalism

Eshelby Formalism is the main focus of this project because of its great potential to be applied to natural fabric deformation problems. First of all, it relates the local deformation field to the whole deformation field, which provides an extrapolation approach for fabric development models. Second of all, it concentrates on the flow field of an element and its surrounding matrix, which allows flow partitioning in the ‘inhomogeneity-matrix’ system. Third of all, it is mesh-free, making it exempt from the multi-scale limitations that lie in meshes. Last but not the least, Eshelby Formalism has been applied to a number of material science problems such as metal deformation (Withers, 1989; Roatta, 1997) and the crystalline texture development problems (Lebensohn and Tomé, 1993). In this literature, the fabrics of the metal and the textures are well predicted and reproduced by the Eshelby Formalism. Indeed, given the mechanical difference between metal and natural rocks, the applicability of Eshelby theory to deformation fabric development still remains to be validated. However, Eshelby Formalism has great potential in tackling the geology fabric problems.

To sum up, the advantages of Eshelby Formalism mainly lie in the following three aspects:

1. It is not mesh-based. Its mesh-free environment enables it to tackle multi-scale problems without running into computational difficulties.
2. It only focuses on the flow characteristics in deformation, unlike the typical modeling approaches which take into account all the kinematic, mechanical and even thermal properties. Therefore, it is way more computationally efficient, especially in history tracking.

3. The ability to solve the ‘multiple inhomogeneities’ problem shows Eshelby theory’s potential to tackle heterogeneous geological problems. Moreover, non-steady deformation can also be addressed by changing the initial velocity settings.

These three advantages of Eshelby Formalism highlight its importance when applied to tackle the heterogeneous, large strain and multi-scale deformation of rocks and the accompanying fabric development.

## 1.5 Extension of Eshelby Formalism to Power-Law Materials

Eshelby Formalism (1957) is originally developed to investigate the ‘inhomogeneity-matrix’ system where both the matrix and the inhomogeneity are linearly elastic materials (mechanical rheology will be further discussed in Chapter 2). Bilby et al. (1975) later extended the Eshelby Formalism to perfectly linear viscous materials (the so-called Newtonian materials) using the equivalence between the theory of linear elasticity and the theory of linear viscosity.

However, Newtonian material applicability is not enough for geologists because of the fact that the majority of natural rocks are Non-Newtonian, to be more specific, power-law materials (e.g., Karato, 2008). Since Eshelby Formalism was developed to tackle linear elastic and linear viscous materials, when it comes to power-law material situation where the constitutive equation is not linear, Eshelby Formalism can no longer be directly applied.

This incompatibility problem between Eshelby Formalism and power-law material deformation is also addressed in a number of material science literature (Molinari et al., 1987; Lebensohn and Tomé, 1993). Molinari et al. give a solution to the incompatibility problem by proposing the ‘*Tangent Linearization Scheme*’ which uses a Taylor series to approximate the power law materials by linear rheology. Several years later Lebensohn and Tomé incorporated the Eshelby Formalism with the ‘*Tangent Linearization Scheme*’ (hereafter called the *EFTL*). By means of the Tangent Linearization Scheme, Eshelby Formalism is extended to power-law materials eventually.

Yet as known to all, Taylor series, the essentials of the Tangent Linearization Scheme, is an approximation method that will inevitably bring in errors. Hence, the applicability of *EFTL* to geological long-term deformations still needs to be validated. This validation is the main investigation object of this project.

## 1.6 Objectives and Methodology of this Project

As mentioned above, the applicability of *EFTL* to power-law materials remains uncertain, which is the main concern of this project. The potential that the Eshelby Formalism might be applied to the power-law material deformation is so important in geology modeling that, if *EFTL* can be validated to be reliable, then it will open a door to a brand new world in geological modeling. By reliability of *EFTL*, I imply the following:

1. Generally, how well can *EFTL* be used to model the power-law deformations? This general question consists of the following aspects: How do I use quantitative terms to scale the degree of applicability? What assumptions or mechanical condition

- requirements should be met when apply *EFTL* to fabric modeling? What appropriate adjustments can be performed to better adjust the *EFTL* to fabric modeling?
2. Given that the applicability of *EFTL* is determined, what are the geological implications of these results?

Answers to the above two questions are of crucial importance in fabrics modeling in structural geology. If *EFTL* can be validated in my project, not only fabric development problems, but other related problems like lattice preferred orientations development in rocks can also be simulated using the Eshelby Formalism. In fact, Jiang (2012) has already taken advantage of the *EFTL* and gained a brand new view on fabrics in crustal scale shear zones. Therefore, validation of *EFTL* is a milestone step in geology field and is what I aim to accomplish in this project.

In order to achieve such a goal, an approach to compare the *EFTL* results with results based on computational geodynamics is followed. To perform such a comparison, I design two types of computations, with one calculating the results of the *EFTL*, and the other simulating the power-law behavior using a finite difference method. Since *EFTL* is formulated in closed mathematical forms, it can be efficiently calculated in all present mainstream mathematical calculation codes such as Matlab, Mathcad, or Mathematica. Recently, Jiang (2007, 2012 in review) has already developed Mathcad worksheets to yield solutions of *EFTL*. I therefore directly employ them to perform the *EFTL* computation in this project. On the other hand, in order to simulate the power-law behavior in nature, I choose one of the conventional geodynamics approach, the finite difference code FLAC2D from Itasca Corporation. Introductions about Mathcad as well as finite difference method will be given in the following chapter.

To sum up, the procedure of the methodology is illustrated in Figure 1.2. First, I use the algorithm and implementation in Mathcad of Jiang (2012, in review) for the *EFTL* computation. The physical model of the ‘inhomogeneity-matrix’ system in the *EFTL* computation is illustrated in Figure 1.3. Second, I simulate the deformation of the same system using a traditional FDM code FLAC2D. This process is called the ‘FLAC simulation’ in the following context. Finally, I compare the results from the *EFTL* computation and the FLAC simulation, respectively, to evaluate the applicability of the *EFTL* to natural power-law materials.

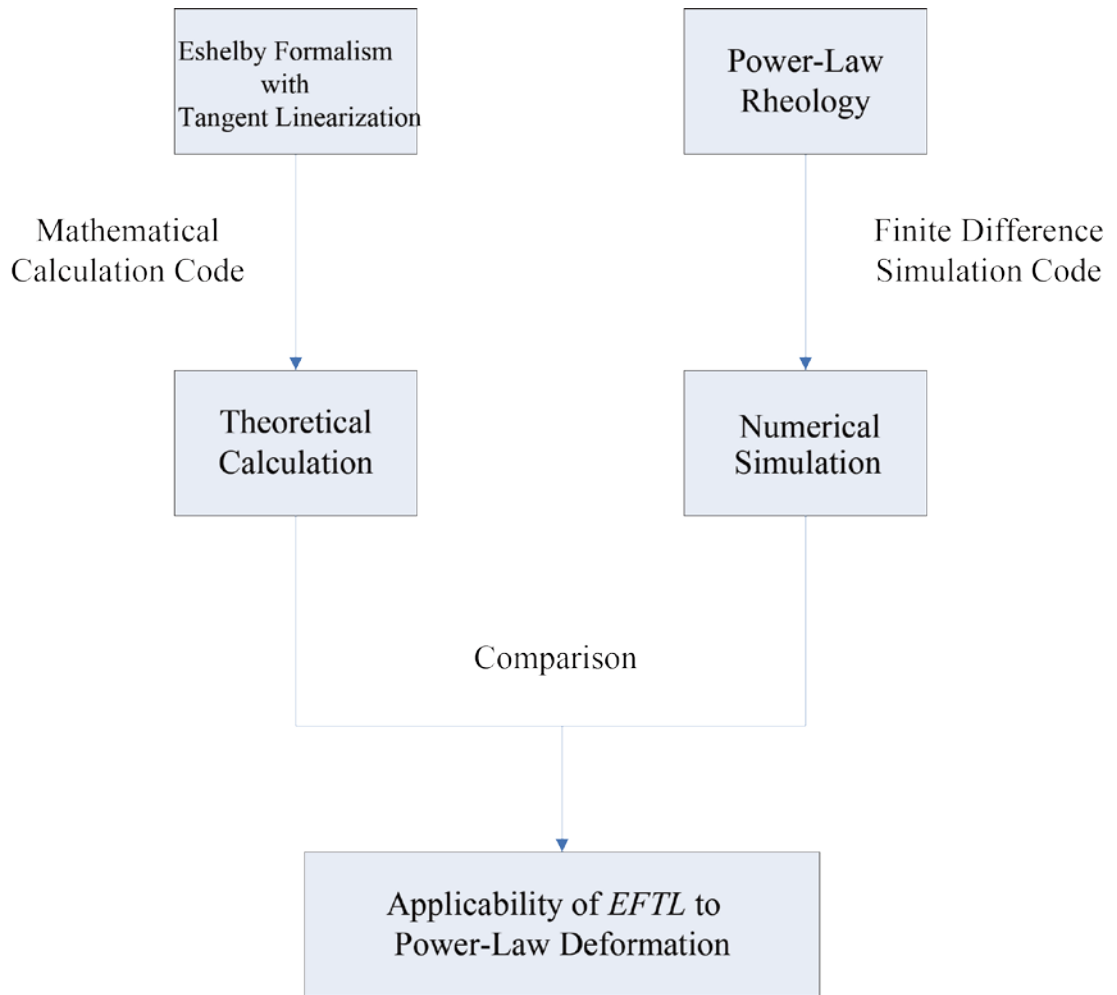


**Figure 1-3 Procedure of the methodology in this project.**

*EFTL will be carried out in a mathematical code and power-law rheological behavior will be simulated in a finite difference program. Through comparisons between the solutions from the two can yield the results of the applicability of the EFTL to power-law material deformations.*

## Theoretical Modeling Design based on Eshelby Formalism

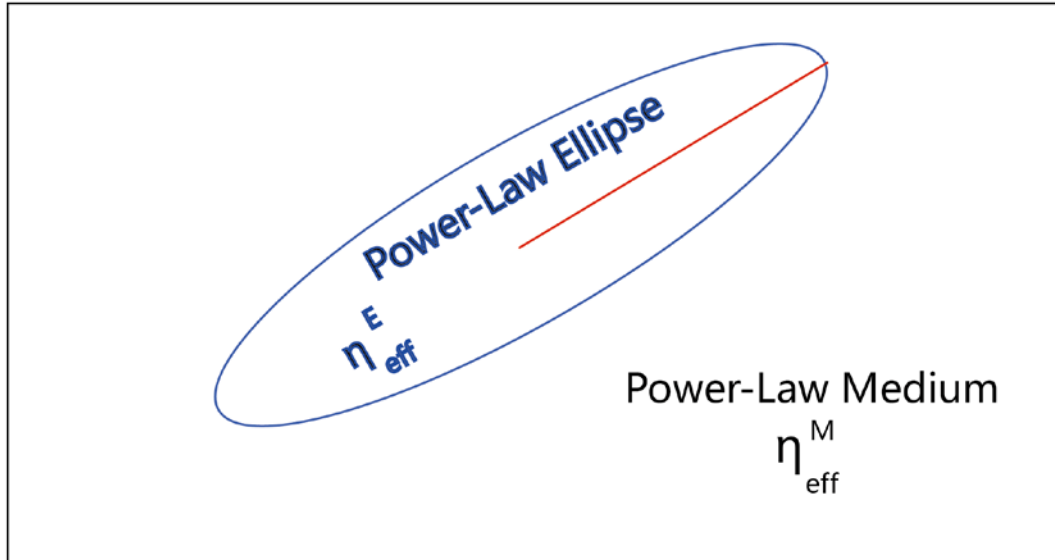


**Figure 1-4 EFTL Computation design in Mathcad.**

*In the EFTL computation, a power-law ellipse is embedded in a power-law matrix. Both of them are deformable but have difference in mechanical parameters. Materials of the ellipse and the matrix are assigned by the effective viscosity ratio at the reference state (usually the initial state where the strain rates of the inhomogeneity and the matrix are*

*set equal):  $r_{eff} = \frac{\eta_{eff}^E}{\eta_{eff}^M}$ , where  $\eta_{eff}^E$  is the effective viscosity of the ellipse while  $\eta_{eff}^M$*

*is the effective viscosity of the matrix. Deformation evolution of the ellipse is determined by two parameters: the axial ratio and the long-axis orientation. Long axis of the ellipse is illustrated as a red line in the figure.*



## 1.7 Thesis Outline

In this thesis, I have now introduced the background of my project, presented the objectives and illustrated the methodology as well as the procedure that I am going to perform towards my goal. In the next chapter, basic terms and theory background will be presented, followed by the modeling designs and simulation setup descriptions in Chapter 3. After all simulations being introduced, Chapter 4 will analyze the results from these simulations, aiming to unveil the implications behind the results. In the final chapter, conclusion will be made and suggestion on how to apply my conclusion to geological problems will be provided.

## Chapter 2

### 2 Theoretical Background

Theory background and modeling design involved in this project are introduced in this chapter, followed by a detailed discussion on the two types of simulation settings in the next chapter.

#### 2.1 Terminology of Continuum Mechanics

In this section, some basic terms of continuum mechanics are introduced and explained before we proceed to the details of the theory using these terms.

##### 2.1.1 Flow Kinematics

Flow is defined by the velocity field of all material particles within the deforming body.

The Eulerian velocity gradient tensor  $\mathbf{L}$  is defined in terms of its components:

$$L_{ij} = \frac{\partial v_i}{\partial x_j} \quad (i, j = 1, 2, 3) \quad (2-1)$$

where  $\mathbf{v}$  is the velocity vector field of the particles and  $\mathbf{x}$  is the coordinate position of the particles. Equation (2-1) can be resolved into a symmetric stretching tensor  $\mathbf{D}$  and an antisymmetric vorticity tensor  $\mathbf{W}$  (Truesdell, 1965; Jiang, 1994a, 1994b, 1999, 2010; Lin et al, 1998).

$$\mathbf{L} = \mathbf{W} + \mathbf{D} \quad (2-2)$$

where  $\mathbf{D} = \frac{1}{2}(\mathbf{L} + \mathbf{L}^T)$ ,  $\mathbf{W} = \frac{1}{2}(\mathbf{L} - \mathbf{L}^T)$  and  $\mathbf{L}^T$  is the transpose of  $\mathbf{L}$ .

Note that if  $\mathbf{L}$  changes with time, the flow is non-steady, otherwise it is steady flow. Furthermore, if  $\mathbf{L}$  changes in space from particle to particle, the flow is heterogeneous, otherwise it is homogeneous. The stretching tensor,  $\mathbf{D}$  is used to describe the change in shape of the deforming body, while the vorticity tensor  $\mathbf{W}$  denotes the rotation that the flow possesses (Means et al., 1980).

To perform a 2D general shear in this project, the velocity gradient tensor  $\mathbf{L}$  is designed as follows (more details will be given in Chapter 2.1.3):

$$L_{ij} = \begin{bmatrix} \dot{\varepsilon} & \dot{\gamma} \\ 0 & -\dot{\varepsilon} \end{bmatrix} \quad (2-3)$$

where  $\dot{\varepsilon}$  is the stretching rate of the deforming body along the  $x$  direction (illustrated in Figure 2.1),  $\dot{\gamma}$  is the shear strain rate parallel to the  $x$  axis.

In addition to the vorticity tensor  $\mathbf{W}$ , Truesdell (1953) proposed the kinematic vorticity number  $W_k$  as a measure of degree of instantaneous rotation. In this project where the 2D general deformation problem is addressed,  $W_k$  is defined by the following equation:

$$W_k = \frac{\dot{\gamma}}{\sqrt{4\dot{\varepsilon}^2 + \dot{\gamma}^2}} \quad (2-4)$$

$W_k$  is commonly used as an indicator for pure shear flow ( $W_k = 0$ ), simple shear flow ( $W_k = 1$ ) and the general sub-simple shear flow ( $0 < W_k < 1$ ). These three flow types will be further discussed in the next section.

Note that the velocity gradient tensor  $\mathbf{L}$  and the kinematic vorticity number  $W_k$  are two important quantities in determining flow types:  $\mathbf{L}$  is used to control how fast the deformation of flow is, while  $W_k$  constrains the type of the flow.

## 2D General Shear In this Project

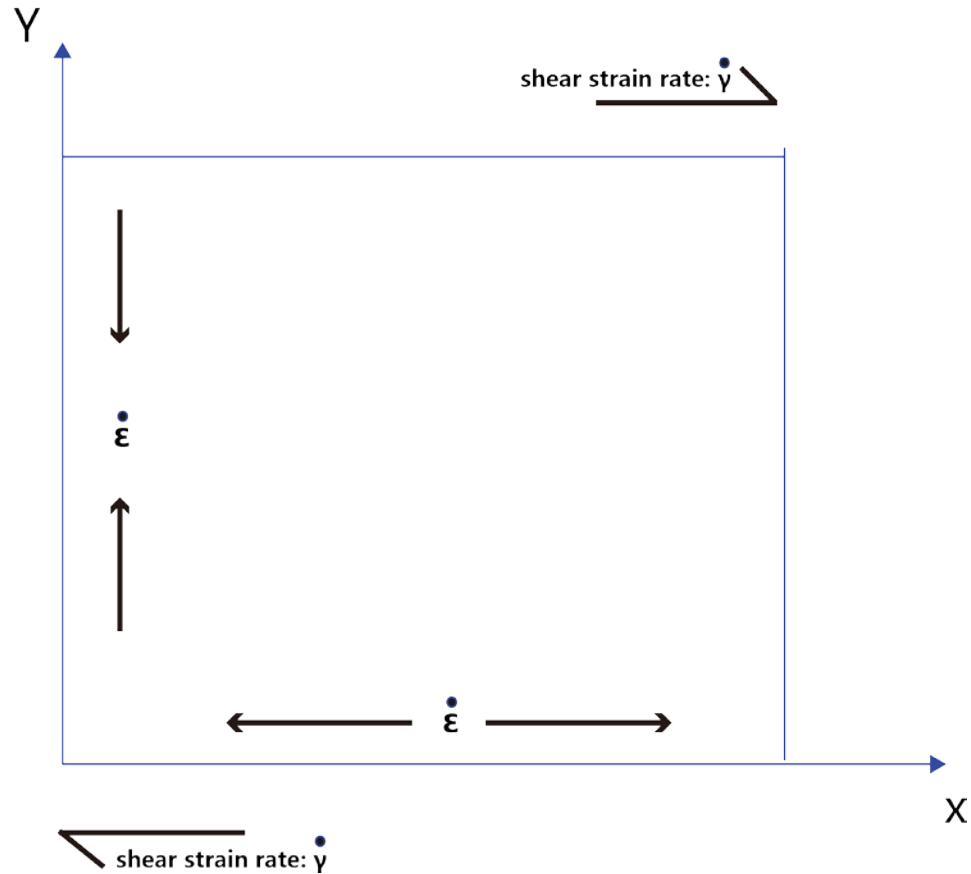


**Figure 2-1 A homogenous domain of 2D general shear used as the flow field in this project.**

*The figure shows a 2D general shear. The boundaries of the domain are being biaxially stretched with stretching rate  $\dot{\epsilon}$  while  $\dot{\gamma}$  is the shear strain rate. These two parameters are necessary in calculating the value of  $W_k$ . An elliptical inhomogeneity of power-law is embedded in the flow field. The deformation history of the inhomogeneity is modeled both by FLAC2D and through EFTL. Comparison of the two sets of results is used to evaluate the applicability of the EFTL.*

### 2.1.2 Strain Ellipsoid and Strain Ellipse

Strain in three-dimension can be completely described by the strain ellipsoid. The strain ellipsoid is the deformed shape of an imaginary sphere with unit radius that is deformed along with the rock volume under consideration (Fossen, 2010).

The strain ellipsoid has three mutually orthogonal planes of symmetry, the principal planes of strain, which intersect along three orthogonal axes that are referred to as the principal strain axes. Their lengths (values) are called the principal stretches (Figure 2.2).

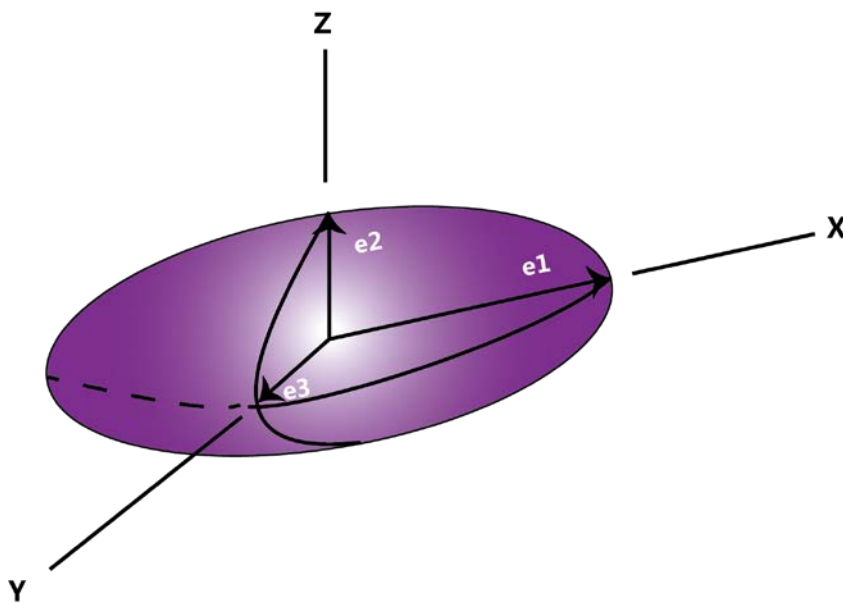


**Figure 2-2 Strain ellipsoid and its three principal axes.**

*The strain ellipsoid in the figure is an imaginary sphere that has been deformed along with the rock. It is described by three vectors,  $\mathbf{e1}$ ,  $\mathbf{e2}$  and  $\mathbf{e3}$ , which defines the principal axes of strain (X, Y and Z) and the orientation of the ellipsoid.*

Since the flow in this project is 2D, instead of strain ellipsoid, strain ellipse is used to describe strains in two dimensions. The strain ellipse represents the deformed shape of an imaginary circle, which is described by a long axis (X) and a short axis (Y).

### 2.1.3 Flow Types

Generally, there are three types of shear flows: pure shear, simple shear and sub-simple shear (also called general shear).

Pure shear ( $W_k = 0$ ) is a perfect coaxial deformation (Figure 2.3). Coaxial deformation means that lines along the principal strain axes have the same orientation as they had in the undeformed state. Pure shear is a plane strain (2D strain) with no volume change. The velocity gradient tensor  $\mathbf{L}$  of pure shear can be expressed as follows:

$$\begin{bmatrix} \dot{\epsilon} & 0 \\ 0 & -\dot{\epsilon} \end{bmatrix} \quad (2-5)$$

where  $\dot{\epsilon}$  is the stretching rate along the x and  $-\dot{\epsilon}$  is the stretching rate along y coordinate axis, respectively. Since the total of the diagonal components of  $\mathbf{L}$  is 0, a constant volume deformation is achieved.

Simple shear ( $W_k = 1$ ) is another type of constant-volume plane strain deformation (Figure 2.3). Unlike pure shear, it is non-coaxial deformation, implying that lines parallel to the principal strain axes have rotated away from their initial positions.  $\mathbf{L}$  for simple shear is:

$$\begin{bmatrix} 0 & \dot{\gamma} \\ 0 & 0 \end{bmatrix} \quad (2-6)$$

where  $\dot{\gamma}$  is called the shear strain rate, indicating the strain rate of the *internal rotation* component in the shear.

Sub-simple shear ( $0 < W_k < 1$ ), also referred to as general shear, is a type of planar deformation between pure shear and simple shear (Figure 2.3). General shear can be regarded as a mix of pure shear and simple shear, with less internal rotation involved than simple shear. The velocity gradient tensor  $\mathbf{L}$  for the general shear can be written as a combination of the ones for the pure shear and simple shear (see equation (2-3)):

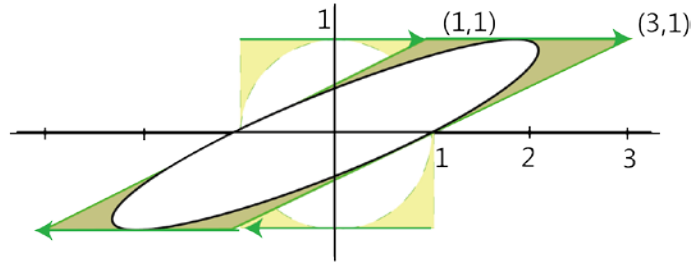
$$\begin{bmatrix} \dot{\epsilon} & \dot{\gamma} \\ 0 & -\dot{\epsilon} \end{bmatrix}$$

where  $\dot{\epsilon}$  and  $\dot{\gamma}$  are already defined above.

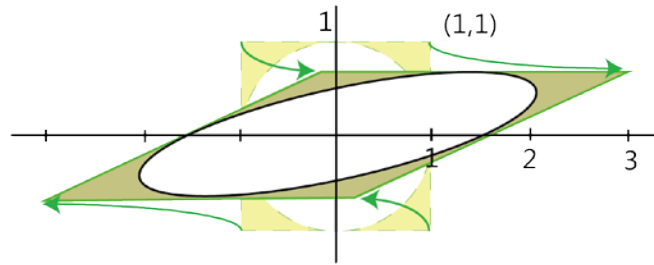
Equation (2-3) explains the reason this format of the velocity gradient tensor is used in this project which aims to perform a 2D general shear.



Simple Shear



General Shear



Pure Shear

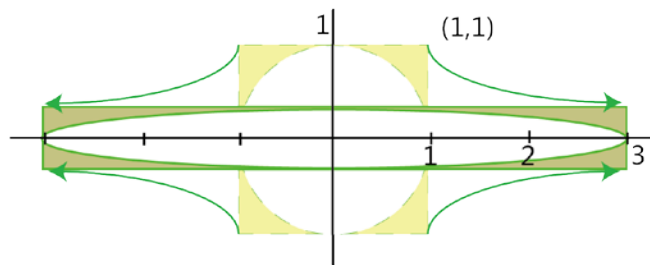


**Figure 2-3 Strain resulting from simple shear, general shear and pure shear.**

**Modified from (Fossen, 2010).**

*This figure illustrates the strain resulting from simple shear, general shear and pure shear. It can be seen from the figure that simple shear is a non-coaxial deformation, pure shear is a perfect coaxial deformation and general shear is a deformation between pure shear and simple shear.*

## 2.1.4 Rheology

Rocks deform in a brittle or a ductile way, where the latter one usually takes place when the temperature and the pressure are relatively higher than the former one. When discussing rock deformation behaviors, it is necessary to discuss the rheology of materials where ideal mechanical behaviors are defined (e.g. elastic, Newtonian, power-law) and the corresponding relationships between stress and strain (or strain rate) are given. This relationship is called *rheology* and the equations that mathematically describe the relationship are called *constitutive laws* or *constitutive equations* (e.g., Ranalli, 1986; Karato, 2008).

### 2.1.4.1 Elastic and Newtonian Materials

Generally, elasticity is the simplest and idealized rheological behavior. When the stress is rather small in low temperature and low pressure environment, all rocks deform in this manner, where the strain is linearly proportional to the stress applied to the deforming body. Ideally, the body returns to its original shape once the applied stress is removed. Mathematically, homogeneous isotropic linear elastic materials have constitutive equations as follows:

$$\sigma_0 = k \varepsilon_{kk} \quad (2-7)$$

$$\sigma'_{ij} = 2\mu \varepsilon'_{ij} \quad (2-8)$$

In equation (2-7),  $\sigma_0$  is the mean normal stress deriving from  $\frac{1}{3}\sigma_{ii}$ ,  $\epsilon_{kk}$  is the volumetric deformation and  $k$  is the bulk modulus. In equation (2-8),  $\sigma'_{ij}$  and  $\epsilon'_{ij}$  are the components of the deviatoric stress tensor and the strain tensor;  $\mu$  is the shear modulus.

While elastic behavior only applies to very small strains that are common in the upper crust rocks, heated rocks under higher pressure in a long-term geologic time tend to flow in a ductile way and accumulate permanent strains. In this situation, rheology of rocks is described in terms of differential stresses and strain rates. One simple material of this kind are the Newtonian fluids whose constitutive equations can be written as:

$$\sigma_{ij} = 2\eta\dot{\epsilon}_{ij} \quad (2-9)$$

where  $\sigma_{ij}$  is the component of the deviatoric stress tensor,  $\dot{\epsilon}_{ij}$  is the component of the strain rate tensor, and  $\eta$  is a mechanical constant called viscosity for isotropic materials. Viscosity is of great importance to indicate Newtonian material's resistance to deformation.

Both elastic and Newtonian materials have linear rheological relationships. It is also important to point out that rheology discussed in this section applies to isotropic elasticity and viscosity only.

#### 2.1.4.2 Power-Law Materials

Other than Newtonian materials, there exist other types of behaviors in which the material flows steadily under small stresses, and the constitutive equations are non-linear. These are called non-Newtonian materials. Among all non-Newtonian materials, power-

law creep (slow and continuous flow) is typical in natural rocks (e.g., Ranalli, 1986; Karato, 2008). A large number of laboratory experiments have been performed to investigate the mechanical properties of rocks and have demonstrated that they behave like power law materials (Gleason and Tullis, 1995; Kohlstedt et al., 1995; Behr and Platt, 2011). Results of these experiments show that the basic form of the constitutive equation for power law is written as follows:

$$\dot{\epsilon}_2 = A_1 \cdot \exp\left(-\frac{Q}{RT}\right) \cdot \sigma_2^n \quad (2-10)$$

where  $\dot{\epsilon}_2$  is the second invariant of the strain rate tensor,  $A_1$  is the material constant,  $Q$  is the activation energy per mole for the creep process,  $R$  is the gas constant,  $\sigma_2$  is second variant of the deviatoric stress tensor.

In my program, this basic form is rewritten as follows to simplify the parameters in use:

$$\dot{\epsilon}_2 = A \sigma_2^n \quad (2-11)$$

where  $A$  is a parameter equal to  $A_1 \cdot \exp\left(-\frac{Q}{RT}\right)$ .

## 2.2 Eshelby Formalism and Tangent Linearization Scheme

In this section, the theory of Eshelby Formalism and its extension to viscous power-law materials using the ‘Tangent Linearization Scheme’ are presented.

### 2.2.1 Eshelby Formalism for linear elastic and viscous materials

Eshelby Formalism (1957) is a theory to study the flow field and progressive deformation of an elliptical inhomogeneity embedded in an infinite elastic matrix. Both the inhomogeneity and the encompassing matrix are isotropic and linearly elastic (Figure 1.1). Eshelby discovered that although the elastic field in the vicinity outside the inhomogeneity is heterogeneous, the elastic field within the inhomogeneity is perfectly homogeneous as long as the inhomogeneity is ellipsoidal.

The theory was then extended by Bilby et al. (1975) to Newtonian materials due to the equivalence between the theory of linear elasticity and the theory of Newtonian fluids. The essential contribution of the Eshelby theory is the discovery that, as long as the element is ellipsoidal, the elastic field within the element remains perfectly homogeneous despite that the one in the vicinity outside the element is heterogeneous.

In the case of isotropic, incompressible Newtonian fluids, the Eshelby Formalism can be written into the following equation such that the flow inside the inhomogeneity is related with the bulk flow (Jiang, 2012 in review):

$$\boldsymbol{\varepsilon}_i = [\boldsymbol{J} + (r - 1)\boldsymbol{S}]^{-1} : \boldsymbol{\varepsilon}_m \quad (2-12)$$

Where  $\boldsymbol{S}$  is the Eshelby tensor that relates the flow inside the ellipsoidal inhomogeneity with the flow of the matrix; ‘:’ is the colon product of dyads; and  $\boldsymbol{J}$  is the fourth order unit tensor, which is defined as:

$$\boldsymbol{J} = \frac{1}{2} (\delta_{ij}\delta_{kl} + \delta_{ik}\delta_{jl}) \quad (2-13)$$

where  $\delta_{ij} = 1$  if  $i = j$ ;  $\delta_{ij} = 0$  if  $i \neq j$ ;

$\boldsymbol{\varepsilon}_i$  and  $\boldsymbol{\varepsilon}_m$  are the strain rate tensor of the inhomogeneity and the matrix, respectively; and

$r$  is the ratio of the viscosity of the inhomogeneity to the viscosity of the matrix.

Equation (2-12) is the explicit form used by Freeman (1987) and Jiang (2007, 2012 in review) in their numerical modeling.

## 2.2.2 Extension of Eshelby Formalism to Power-Law Materials – Tangent Linearization Scheme

The limitation that Eshelby Formalism can only be directly applied to materials with linear constitutive relationship is addressed in a number of micro-mechanics literature.

The formalism has been extended to power-law rheology by the so-called Tangent Linearization Scheme (Molinari et al., 1987; Lebensohn and Tomé, 1993). Here the essential theory of two linearization schemes is first introduced so that their applicability can be analyzed more clearly in the simulations to follow.

### 2.2.2.1 A Pseudo-Linearization Scheme: the Secant Linearization

The solution to apply Eshelby Formalism to power-law material deformation in fact lies in finding a linearization scheme.

It has long been proposed that the constitutive equation of a power-law material can be written in a pseudo-linear form as follows (Hutchinson, 1976):

$$\boldsymbol{\varepsilon}(\boldsymbol{\sigma}) = \mathbf{M}^{(S)}(\boldsymbol{\sigma}) : \boldsymbol{\sigma} \quad (2-14)$$

where  $\mathbf{M}^{(S)}(\boldsymbol{\sigma})$  is the so-called ‘secant viscous compliances’.

Equation (2-14) can be written in a scalar form as follows:

$$\dot{\varepsilon}_2 = A\sigma_2^{n-1}\sigma_2 \quad (2-15)$$

where all parameters have been defined in equation (2-11).

The inverse of  $A\sigma_2^{n-1}$  is the well-known effective viscosity  $\eta_{eff}$  defined in geology literature (e.g., Ranalli, 1986, p79).

Equation (2-15) suggests that in a certain state, the relation between shear stress and the shear strain rate may be approximately linear under some stress systems (Ranalli, 1986, p78). Therefore, a pseudo-linearization scheme can be developed on the basis of equation (2-15). In such a linearization scheme, the rheology of the material will be calculated by equation (2-15) in every single state of stress and strain rate with a certain value of  $\eta_{eff}$ , while in the next state,  $\eta_{eff}$  will be updated before equation (2-15) is applied. This linearization scheme is called the *Secant Linearization* in this project, and the Eshelby Formalism with the Secant Linearization will be denoted by *EFSL*. Computation on *EFSL* will also be performed in the following computation process to investigate its applicability to power-law materials.

### 2.2.2.2 An Approximation Scheme : the Tangent Linearization

The pseudo-linear form of power-law constitutive equation is the early try of linearization, however, writing the power-law constitutive equation in a pseudo-linear form does not actually make it linear. The  $\mathbf{M}^{(s)}$  in equation (2-14) only applies to the exact state of stress and strain rate, which makes the equation always remain non-linear no matter how small an increment of deformation could be. A linear relation in the vicinity of a stress-strain rate state is obtained by doing a Taylor expansion of equation (2-14), which defines the *tangent compliances*:

$$\begin{aligned}\boldsymbol{\varepsilon}(\boldsymbol{\sigma}) &= \boldsymbol{\varepsilon}(\boldsymbol{\sigma}_0) + \left. \frac{\partial \boldsymbol{\varepsilon}}{\partial \boldsymbol{\sigma}} \right|_{\boldsymbol{\sigma}=\boldsymbol{\sigma}_0} : (\boldsymbol{\sigma} - \boldsymbol{\sigma}_0) \\ &= n\mathbf{M}^{(s)}(\boldsymbol{\sigma}_0) : \boldsymbol{\sigma} + (1-n)\boldsymbol{\varepsilon}(\boldsymbol{\sigma}_0) \\ &= \mathbf{M}^{(t)}(\boldsymbol{\sigma}_0) : \boldsymbol{\sigma} + \boldsymbol{\varepsilon}^0\end{aligned}\tag{2-16}$$

where  $\mathbf{M}^{(t)}$  is the tangent compliances tensor with the value of  $n\mathbf{M}^{(s)}$ ;  $\boldsymbol{\varepsilon}^0$  is the back extrapolated term and  $\boldsymbol{\varepsilon}^0 = (1-n)\boldsymbol{\varepsilon}(\boldsymbol{\sigma}_0)$ ;  $n$  is the power-law stress exponent for the material (Molinari et al., 1987; Lebensohn and Tomé, 1993).

Taylor approximation is only valid in a small increment of deformation. In such an increment, the linear form equation (2-16) can be used as the constitutive equation. In the process of computation, a certain step length is assigned, within which both the secant and the tangent compliances are determined by the stress state of the certain time duration and should be updated at every step when applied. After Molinari et al. propose the *tangent compliances*, Lebensohn and Tomé accomplish a significant achievement to



incorporate the tangent linearization scheme with the Eshelby Formalism, which extends the Eshelby Formalism to power-law materials (what I call *EFTL*). In *EFTL* where both the matrix and the inhomogeneity are incompressible isotropic power-law materials, equation (2-16), i.e. the linearization scheme, is applied to Eshelby Formalism and yield the following equation for the flow relationship between the inhomogeneity and the matrix (Jiang, 2012 in review):

$$\boldsymbol{\varepsilon}_i = [\mathbf{J} + (n_m r_{eff} - 1)\mathbf{S}]^{-1} : [\mathbf{J} + (n_m - 1)] : \boldsymbol{\varepsilon}_m \quad (2-17)$$

where  $r_{eff}$  is the effective viscosity ratio of the inhomogeneity to that of the matrix (see Ranalli, 1986 for definition of effective viscosity ratio);  $n_m$  is the power-law stress exponent for the matrix.

Note that only  $n_m$ , the power-law stress exponent for the matrix is included in equation (2-17); while  $n_c$ , the stress exponent for the inhomogeneity, is only used in the iteration process to yield the value of  $r_{eff}$ .

Special cases exist when  $n_m = 1$ , i.e. the matrix is Newtonian. In these cases, if the inhomogeneity is also Newtonian, then  $r_{eff}$  only needs to be replaced by a constant  $r$ .

Otherwise, if the inhomogeneity is power-law material, equation (2-17) is altered into:

$$\boldsymbol{\varepsilon}_i = [\mathbf{J} + (r_{eff} - 1)\mathbf{S}]^{-1} : \boldsymbol{\varepsilon}_m \quad (2-18)$$

It is obvious that equation (2-18) has the same form as the equation (2-17), only with the difference that in the power-law-inhomogeneity situation,  $r$  needs to be replaced by the  $r_{eff}$  and should be updated in every incremental deformation step.

In summary, the general power-law ‘matrix-inhomogeneity’ system deformation can now be solved by the means of the *EFTL*. It should be emphasized that though the Tangent Linearization Scheme linearizes the power-law rheology for the use of Eshelby Formalism, the scheme is only an approximation. The reasons are as follows. For one thing, Taylor Series, which is the essence of the linearization scheme, is an approximation itself. For another, during the deformation, the heterogeneous finite strain near the inhomogeneity will result in the non-uniform viscous compliances in the matrix material (Jiang, 2012 in review). This non-uniformness in the matrix is against the assumption of the Eshelby Formalism and further results in errors in the *EFTL* computation. Therefore, the *EFTL* is yet to be validated when applied to power-law materials’ behavior in geological long-term deformations. By applicability validation, I imply:

1. To investigate the extent to which the *EFTL* can be applied to power-law materials.
2. To find out what are the influencing factors for the applicability.

## 2.3 Mathcad Program

To perform the *EFTL* and *EFSL* computations, a mathematical code is needed. Jiang (2007, 2012 in review) successfully developed an algorithm to yield the closed form solution based on Eshelby Formalism and implement it in the mathematical program Mathcad. In this paper, Jiang’s algorithm and Mathcad worksheet are used. The following paragraph will give a brief description of the Mathcad program, while the details of the algorithm in the program will further be discussed in the next chapter.

Mathcad, Parametric Technology Corporation's (<http://www.ptc.com/products/mathcad/>) engineering calculation program, is primarily intended for the verification, validation, documentation and re-use of engineering calculations and now has been developed to meet the needs of numerical engineering applications in various disciplines. Mathcad is oriented around a worksheet in which equations and expressions are created and manipulated in explicit graphical format, basically the same with hand-writing style. In the calculation process, data can be displayed, manipulated, analyzed and plotted simultaneously. By this means, results accounting for various situations can be instantly obtained merely by making minor changes to the input variables.

## 2.4 Finite Difference Simulations in FLAC

To validate the applicability of the *EFTL* and *EFSL*, it is necessary to seek a reliable simulation of power-law material deformation for reference and a comparison between the two computations should be performed. What I use in this project is a conventional geodynamics approach: the finite difference method. One of the most well-known program codes in the market based on this method is called FLAC, short form from Itasca (<http://www.itascacg.com>) for “Fast Lagrangian Analysis of Continua”. I choose this program code because FLAC2D (the 2D simulation code of FLAC) has been used in structural geology field to solve geological problems (Hobbs et al., 1989; Ord, 1990; McKinnon and Barra, 1998) and has shown great accuracy and reliability. Therefore, it is believed that FLAC2D can perform a reliable simulation to represent the natural behavior of power-law material deformations.

The following few paragraphs will provide necessary theoretical background of the finite difference method and the FLAC2D program. Such background is discussed for the reason that they will better illustrates the potentials of FLAC2D as a reference simulation method, and more importantly, to give an explanation of the cause of the technical problems I encounter in the simulation process.

### 2.4.1 Finite Difference

Together with finite element method, finite difference method is one of the two oldest geodynamic techniques used for solving sets of differential equations when given initial values and/or boundary conditions (Cundall, P.A., 1976, 1987; Desai, 1977). Both of the methods produce a set of algebraic equations to solve, yet they are different in deriving the equations. Finite difference method use field variables (e.g. stress) at discrete points to take the place of every derivative in the equation set, and these field variables are undefined within elements; while finite element method prescribes a central requirement that controls the variation of the field variables throughout each element, using specific functions controlled by parameters (Nagtegaal et al., 1974).

### 2.4.2 Grid and Zone Generation

As mentioned in the first chapter, finite difference is a mesh-based modeling method. In FLAC, mesh is described as *zone*. Hence I adopt this term in the following context.

In order to perform simulations in FLAC2D, shapes and properties of materials must be assigned at the very beginning. Materials are represented by elements, or zones, which

form a grid that is adjusted by the user to fit the shape of the object to be modeled (Figure 2.5). A grid, which is designed in row-column fashion, is defined by specifying the number of zones “ $i$ ” desired in the horizontal ( $x$ ) direction, and the number of zones “ $j$ ” in the vertical ( $y$ ) direction. Each zone is further defined by four grid points, which serve as the outer boundary points. Any zone in the grid is uniquely identified by a pair of  $i, j$  indices, so is the case with gridpoints. Note that if there are  $p$  zones in the  $x$  direction and  $q$  zones in the  $y$  direction, the number of gridpoints should be  $(p+1)$  in  $x$  and  $(q+1)$  in  $y$ , respectively. Zones can be modified to different shapes by adding a circle (element 1 in Figure 2.5), a line (element 2), an arc (element 3) and simply by adjusting the positions of certain grid points to create irregular patterns (elements 4).

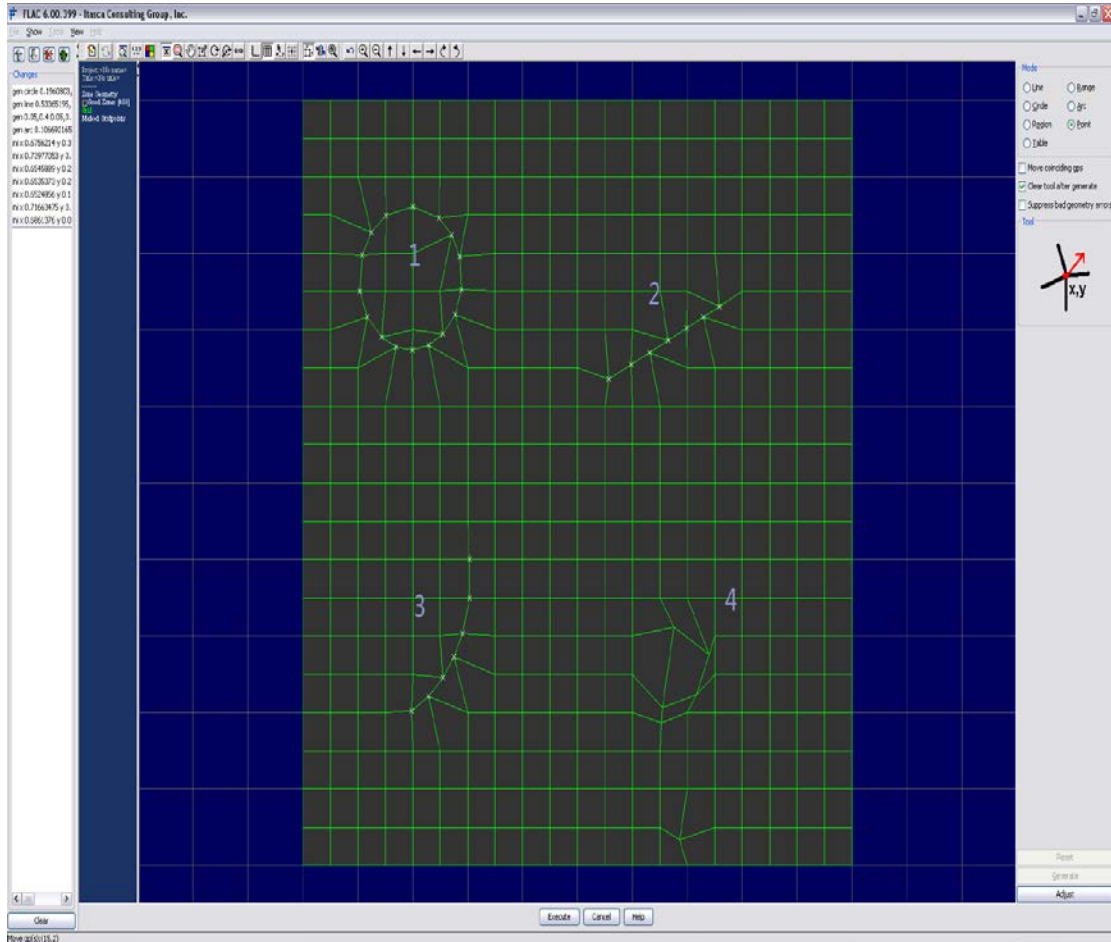


**Figure 2-4 Grid generation in FLAC.**

*Zones can be modified to different shapes in order to fit the shape of the model object and geometry.*

### 2.4.3 FISH Programming Language

Though FLAC was originally developed for geotechnical and mining engineers, the program offers a wide range of capacities to solve complex problems with two useful tools. One of them is the built-in constitutive models that permit the simulation of highly nonlinear materials to become available. The other one is the programming language embedded within FLAC called FISH (*FLACish*).

FISH enables the user to define new variables and functions, which can be used to extend FLAC's usefulness or add user-defined features. For example, new variables may be plotted or history-tracked, special grid generators may be implemented, self-control may be applied to a numerical test, unusual distributions of properties may be specified, and user-written constitutive models can also be created.

FISH programs are written in a typical programming format and embedded in a normal FLAC data file, which can be called and invoked during any time period of the modeling process.

In summary, FISH offers a unique capacity to FLAC users who want to tailor their analysis to meet specific individual needs. In my project, FISH helps to create grid of shape that is not prescribed in FLAC, as well as to specify flexible boundary conditions which are modified every  $n$  steps during the calculation process. This would be discussed later.

## Chapter 3

### 3 Simulation Designs

With all the related theory background having been discussed, I can proceed to my designs for the two simulations: the computations on *EFTL* and *EFSL*, and the finite difference simulation, respectively.

#### 3.1 Simulation Design for *EFTL* and *EFSL*

As mentioned in the previous chapter, Mathcad is the mathematical program that is applied in this project. Since Jiang (2012 in review) has already successfully developed a Mathcad worksheet for the *EFTL*, only a few inputs need to be changed to perform different initial settings in the *EFTL* computation. Such initial settings include the initial state of the ellipsoid (orientation and shape) and the material properties. The core algorithm to calculate the *EFTL* solution is mainly based on equation (2-17) in Chapter 2. However, since no *EFSL* worksheet is developed, the *EFSL* computation will be performed on Jiang's worksheet (2007) with the added adjustment of Secant Linearization Module.

##### 3.1.1 Step Length Settings

In this chapter, the algorithm in the Mathcad worksheet is not given in detail (can be viewed in Jiang, 2007, 2012 in review. Added adjustment commands are presented in Appendix A), but one critical matter mentioned in Jiang (2012 in review) needs to be



mentioned. In the Mathcad worksheet,  $\delta t$  is the step length for computation. According to Jiang, the choice of  $\delta t$  must ensure that each step of the computation represents an *infinitesimal* deformation process, which requires that the following equation be satisfied:

$$\|L_{ij}\|\delta_t \ll 1 \quad (3-1)$$

where  $\|L_{ij}\|$  is the Euclidean norm of the flow velocity gradient tensor.

According to Jiang (2012 in review), all computations demands that the equation (3-1) is satisfied, so that the local step is small enough to yield a precise result after many thousand steps of computation. After a number of experiments, Jiang (2012 in review) also proposes that when the value of  $\|L_{ij}\|\delta_t$  is less than 0.1, the result is reliable. In my project, the value of  $\|L_{ij}\|\delta_t$  is of the magnitude of  $10^{-2}$  and overall computation steps are only 400. Both of the  $\|L_{ij}\|\delta_t$  value and the total amount of step can guarantee that the requirement proposed by Jiang (2012, in review) is met.

### 3.1.2 2D Plane Strain Deformation Settings

The code in Jiang's (2012 in review) worksheet based on *EFTL* is originally implemented for general ellipsoid in 3D flow field. To use it for a 2D planar strain deformation to compare with FLAC2D simulation, I use a significantly elongated ellipsoid aligned with the z-axis to approximate the elliptical cylinder of a 2D deformation. Test computations show that when the relative length parallel to z is over 10 times more than the semi-axis lengths in the xy-plane, the strain along the z-axis is negligible. Therefore, I choose a

sufficiently large relative length along z-axis (2:1:100) so that there is no significant effect of 3D deformation existing in the computations (Figure 3.1).

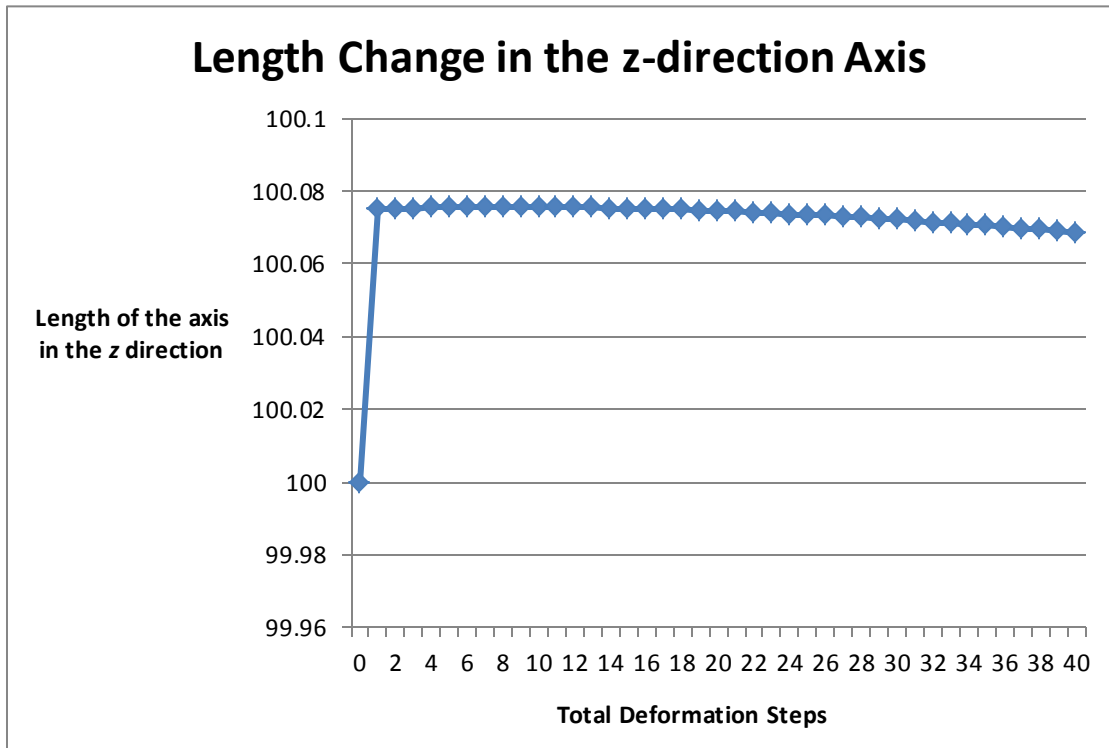


**Figure 3-1 Length change in the z-axis of the elongated ellipsoid during a complete computation.**

*In this test computation, the strain of the z-axis of the ellipsoid is only  $8 \times 10^{-4}$  during the whole deformation. This strain is so infinitesimal that the effect of 3D deformation can be neglected.*

## 3.2 Design for Finite Difference Simulation

As mentioned before, FLAC2D has been successfully applied to various geological problems. Thus, I will carry out the finite difference simulation in 2D with the FLAC2D program in this project. In such a case, it is assumed that there is no deformation in the  $z$ -direction. Also, I use standard unit system in all simulation settings in this project, more specifically, meter (m) for length, second (s) for time, mega Pascal (MPa) for stress.

The general idea of the finite difference simulation in this project is to embed an elliptical inhomogeneity in a matrix in FLAC2D. The matrix is assigned properties as a uniform material, while the inhomogeneity is assigned as another material with rheological contrast to the matrix (Figure 3.1). Then velocity boundary conditions are imposed on the ‘inhomogeneity-matrix’ system boundaries to form a 2D general deformation. Flow characteristics inside the inhomogeneity are the most crucial focus because they determine the deformation history and the final state of the inhomogeneity. The evolution of the deformation state of the elliptical inhomogeneity is represented by two parameters: the orientation and the shape of the ellipse. Orientation of the ellipse is denoted by the orientation of the long axis with respect to the  $x$ -axis, while the shape is denoted by the ratio of the length of the long axis to the length of the short axis. The evolution of the state of the inhomogeneity is calculated using *EFTL* and *EFSL*. The evolution of the elliptical inhomogeneity can also be obtained from the finite difference simulation in FLAC2D. By comparing the results, I can draw conclusions on the applicability of *EFTL* / *EFSL* to the power-law materials.

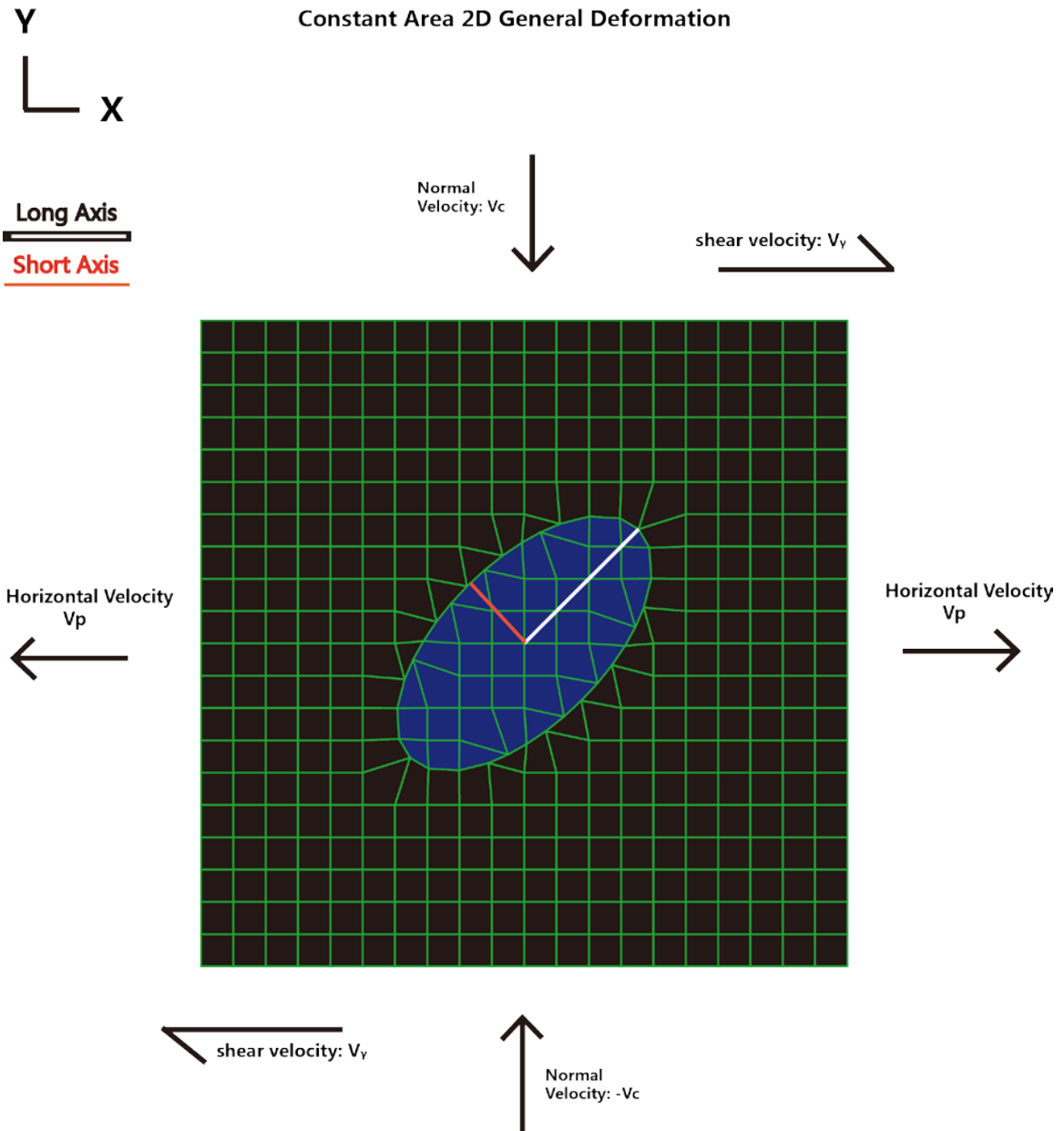


**Figure 3-2 Simulation Design in FLAC.**

*An elliptical inhomogeneity embedded in a 2D general shear deformation modeled by FLAC2D. Boundaries are assigned with velocity conditions which together with the width of the body set up the strain rates. The velocity in x direction is updated continually to ensure that constant area is satisfied and the strain rates remain as constant as possible. For better visual aid, I greatly lower the density of the grid in this figure, where in my actual model, grid density will be 10 times and therefore the ellipse will be smoother.*

### 3.2.1 Grid Generation

Due to the fact that FLAC uses ‘weighted averaging algorithm’ to yield the grid mechanical solution from each single zones and gridpoints, it is inevitable that residual exists. When the grid is denser, the residual caused by averaging is smaller and the solution is more reliable. However, doubling the number of the grid density may cause tens or even hundreds of times of the calculation time because all the single properties within the zones and the gridpoints are doubled, let alone the user-defined variables and the history tracking properties. Therefore, for a given problem, it is of great necessity to seek for a best grid density, which will make the residual small enough to be neglected, as well as not introduce a computational challenge. I perform a series of test simulations to find such an appropriate grid density. These simulations will be elaborated in the next chapter when I discuss the simulation process.

Once the matrix grid is established, I proceed to build the ellipse geometry in FLAC. As mentioned earlier in this chapter, FLAC only predefines geometry like square, line, circle and arc, which is not sufficient for my need to build an elliptical inhomogeneity. Therefore, FISH is adopted to adjust the positions of certain gridpoints to make an ellipse. The ellipse boundary is separated into 1000 portions which is necessary to make the ellipse as smooth as possible, and assign the positions of each portion in polar coordinate system with a loop command (See Appendix B).

Ellipse equations in the polar coordinate system used in this project are:

$$x = a*\cos(\theta)*\cos(\psi)+b*\sin(\theta)*\sin(\psi)$$

$$y = -a*\sin(\theta)*\cos(\psi)+b*\cos(\theta)*\sin(\psi) \quad (3-2)$$

where  $\theta$  is the initial orientation of the ellipse measured by the angle between the long axis of the ellipse and the x-axis,  $\psi$  is the angle between a certain point on the ellipse boundary and the x axis, and  $a$  and  $b$  are the length of the long axis and the short axis respectively.

These ellipse equations are implemented in a loop command in the FISH. In the loop, every polar coordinate system position of the points on the ellipse boundary is stored in a TABLE, a specific type of data structure in FLAC. Simply by generating the table, the ellipse can be immediately built. Once the ellipse is generated, the whole grid can be automatically built as shown in Figure 3.2.

### 3.2.2 Material Property Assignment

Given that simulations are focusing on power-law materials, power-law rheological properties are therefore assigned to both the matrix and the inhomogeneity, but with competence contrasts. As mentioned in the previous chapter, FLAC has a number of built-in creep modules comprising the power-law module, making the material property assignment highly straightforward. In the built-in power law module, five parameters are needed, which are the density, the bulk modulus, the shear modulus, material constant A and stress power exponent n (see in Appendix C).

It is important to mention that, for one thing, material constant A is composed of the influences by the certain material's activation energy, water fugacity, flow temperature etc.; for another, power-law stress exponent n can usually vary from 1 to 7.6 in natural rocks (Twiss and Moores, 1992, p383). As I am particularly concerned with the

applicability of the *EFTL* to natural deformation of rocks, I wish to assign material properties that are as close to natural rocks under natural deformation conditions as much as possible so that the rheology of the materials will not be unrealistic or too far from the rheology we now know of rocks. Therefore, I assign both the matrix and the inhomogeneity with properties of natural rocks references: the matrix being the wet quartzite (Gleason and Tullis, 1995) while the inhomogeneity being the dry Maryland diabase (Mackwell et al., 1988). Note that using rheology of real material reference is not compulsory in this project for the reason that if *EFTL* can be validated, this validation should apply to all material properties as long as the *EFTL* assumptions are met. In the simulation process which will be discussed in the next chapter, the values of  $A$  and  $n$  will be altered to perform a more comprehensive investigation into the subject.

### 3.2.3 Boundary Conditions

Once the grid for the simulation is built and material properties are assigned, boundary conditions can be set. In order to simulate a steady 2D general shear deformation of the matrix, velocity boundary condition is preferable to the stress condition. As shown in Figure 3.2, four boundaries are all assigned with initial velocities, where the normal velocity, horizontal velocity and the shear velocity together constrain the matrix to perform a 2D general shear deformation. As mentioned above, Truesdell's kinematic vorticity number  $W_k$  is used to characterize the deformation type of the system. In particular, I choose four  $W_k$  values to indicate different type of shear deformation, which are 0.1, 0.3, 0.6 and 0.9. With  $W_k = 0.1$  being almost pure shear and  $W_k = 0.9$  being

almost simple shear, this four values of  $W_k$  are able to take into account all typical general shear situations in the nature.

Note that for each experiment with a specific  $W_k$  value,  $W_k$  needs to stay constant during the deformation to maintain the same shear type of deformation.  $W_k$  can be calculated as follows as mentioned in Chapter 1:

$$W_k = \frac{\dot{\gamma}}{\sqrt{4\dot{\epsilon}^2 + \dot{\gamma}^2}} \quad (3-3)$$

where  $\dot{\epsilon}$  is the stretching rate,  $\dot{\gamma}$  is the shear strain rate as shown in Figure 2.1.

Hence,  $W_k$  remains constant when  $\dot{\epsilon}$  and  $\dot{\gamma}$  keep unchanged. Furthermore, since both  $\dot{\epsilon}$  and  $\dot{\gamma}$  are defined by the velocity gradient tensor  $\mathbf{L}$ , thus simply keeping  $\mathbf{L}$  unchanged during the whole simulation process can guarantee the constant value of  $W_k$ .

In addition,  $\dot{\epsilon}$  and  $\dot{\gamma}$  can be described in the following velocity terms:

$$\dot{\epsilon} = \frac{V_n}{H(t)}$$

$$\dot{\gamma} = \frac{V_y}{K(t)} \quad (3-4)$$

where  $V_n$  is the vertical velocity in y direction and  $V_y$  is the shear velocity in x direction. Consider the horizontal width of the grid as K and the vertical height as H. During the deformation, K will be broadened and H will be shortened. Therefore, these two lengths are denoted as K(t) and H(t), indicating that their values keep changing with time (Figure 3.3).



$W_k$  is able to remain constant when both  $\dot{\epsilon}$  and  $\dot{\gamma}$  are kept unchanged throughout the whole deformation. In order to keep  $\dot{\epsilon}$  and  $\dot{\gamma}$  constant while  $K(t)$  and  $H(t)$  are changing along with time,  $V_n$  and  $V_\gamma$  must also change with time correspondingly. This demands that boundary conditions be updated to meet the need of the constant velocity field (See Appendix D).

### Constant Area 2D General Deformation

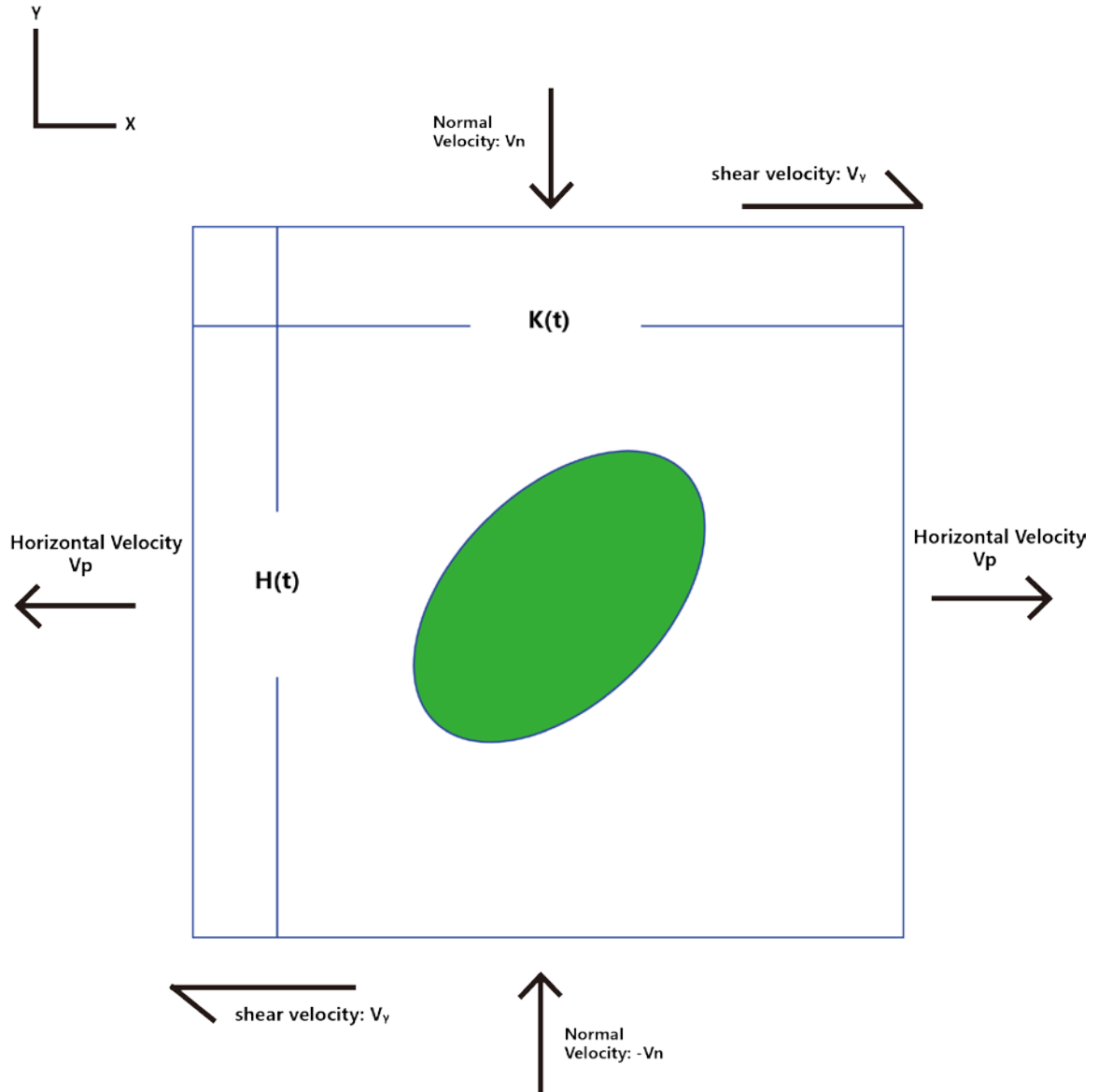


**Figure 3-3 Velocity boundary conditions of the FLAC model.**

*$K(t)$  and  $H(t)$  are respectively the horizontal width and the vertical height of the model that changes along with time.  $V_n$  is the normal velocity, while the combination of the horizontal velocity  $V_p$  and the shear velocity  $V_\gamma$  constitute the total velocity in  $x$  direction.*

### 3.2.4 Timestep Selection for FLAC modeling

FLAC allows the user to define a timestep in creep simulation, if the user skips it, then the default value for timestep is zero, in which case the program treats the material as linearly elastic or elasto-plastic as appropriate. Although the user has this option, the setting of timestep is not arbitrary. If the user wants a system to always be in mechanical equilibrium in the creep simulation, the time-dependent stress changes produced by the constitutive law must not be large compared to the strain-dependent stress changes. Otherwise, out-of-balance forces will be large, and inertial effects will affect the solution. Therefore, timestep setting should draw more of user's attention in response to the specific creep problem he/she wants to perform. In my project, in order to keep the system creeping steadily and the unbalanced force low to maintain system stability, the timestep should not exceed the recommended maximum value defined in FLAC. The method to find the appropriate timestep is presented below.

Creep processes are governed by the deviatoric stress state. An estimate for the maximum creep timestep for numerical accuracy can be expressed as the ratio of the material viscosity to the shear modulus as follows:

$$\Delta t_{max}^{cr} = \frac{\eta}{G} \quad (3-7)$$

where  $\eta$  is the material viscosity and the  $G$  is the shear modulus.

For power law rheology, viscosity can be estimated as the ratio of the stress magnitude,  $\bar{\sigma}$ , to the creep rate,  $\dot{\epsilon}_{cr}$ , therefore the equation above becomes:

$$\Delta t_{max}^{cr} = \frac{\bar{\sigma}^{1-n}}{AG} \quad (3-8)$$

where the stress magnitude  $\bar{\sigma}$ , also known as the Von Mises stress invariant, can be determined by the initial stress state before the creep process begins by using the FISH function in FLAC (see Appendix E). The maximum  $\bar{\sigma}$  yielded from the function should be used to calculate the maximum timestep  $\Delta t_{max}^{cr}$ .

In my simulation, the value of  $\Delta t_{max}^{cr}$  is calculated as  $10^7$  s/step, hence I set the appropriate timestep to  $10^5$  s/step, which is two orders of magnitude lower than the maximum value so as to guarantee the system stability.

In addition to the appropriate timestep, creep problem time in FLAC represents real time, which prompts us to assign velocity conditions in accordance with nature. It is generally thought that the strain rate in rock flow is approximately  $10^{-13} \sim 10^{-14} \text{ s}^{-1}$  (e.g., Karato, 2008). In my model, if strain rate is with magnitude of  $10^{-14} \text{ s}^{-1}$  and the timestep is set as  $10^5$ , it takes  $10^9$  steps to perform a 1 m displacement. Given that one step takes about 1s to calculate, in this case it takes over 30 years to perform a small displacement of 1m. This is unbearably time-consuming. Therefore, when assigning the velocities, I assign the magnitude to be  $10^{-10}$ , in which case the calculation time can be significantly reduced to dozens of hours. Meanwhile, the strain rate in a step is now  $10^{-10} \times 10^5 = 10^{-5} \text{ s}^{-1}$ , which is an infinitesimal deformation compared to tectonic deformations. Therefore the result will still be reliable.

### 3.2.5 Obtaining Results in FLAC

Generally, to compare the flow characteristics inside the inhomogeneity between *EFTL*, *EFSL* and the FLAC simulation, two indicators are chosen. One of them is the orientation of the inhomogeneity represented by the orientation of the long axis. The other is the axial ratio, to be specific, ratio of the length of the long axis to the length of the short axis. The former indicator serves as the orientation change while the latter one indicates the shape change of the inhomogeneity.

Note that both the orientation and the axial ratio can be retrieved. On the one hand, orientation of the ellipse is represented by the orientation of the long axis. Since the orientation of the long axis can be achieved by locating the position of the long axis and applying the trigonometric functions, the orientation seeking problem can be ultimately transferred into seeking the position of the two endpoints of the long axis. On the other hand, as long as the endpoints of both the long axis and the short axis in the coordinate system are obtained, then the lengths of the two axes can be obtained from the distance calculating equations. Therefore, both of the two indicators can be retrieved when the coordinate position of the endpoints of both the long axis and the short axis are constrained. The following paragraph will specify the process to seek for such endpoints in FLAC2D.

First of all, it is necessary to develop an algorithm to distinguish all the gridpoints that are on the boundary of the ellipse in FLAC2D. Since I used the data type *TABLE* to construct the boundary of the ellipse, all the points on it has been marked by FLAC. In FISH, a simple selection statement can help sort out all the marked points without difficulty. Once

all the points on the ellipse boundary are sorted out and stored, distance between the origin and each stored point can be calculated by using the distance equations:

$$d = \sqrt{x^2 + y^2} \quad (3-9)$$

where  $d$  is the distance,  $(x,y)$  is the coordinate position of the stored point.

When all  $d$  with respect to each point on the ellipse are calculated, the long axis point  $\mathbf{P}_L$   $(x_L, y_L)$  and the short axis point  $\mathbf{P}_S$   $(x_S, y_S)$  can be located by finding the largest  $d$  and the shortest  $d$ . Therefore, the two indicators are ready to be obtained when  $\mathbf{P}_L$  and  $\mathbf{P}_S$  are constrained.

For the orientation of the long axis, the angle  $\theta$  between the long axis and the  $x$  coordinate axis can be calculated by:

$$\theta = \arctan \frac{y_L}{x_L} \quad (3-10)$$

By this means, the orientation of the long axis is found, which is represented by the angle  $\theta$  (Figure 3.4).

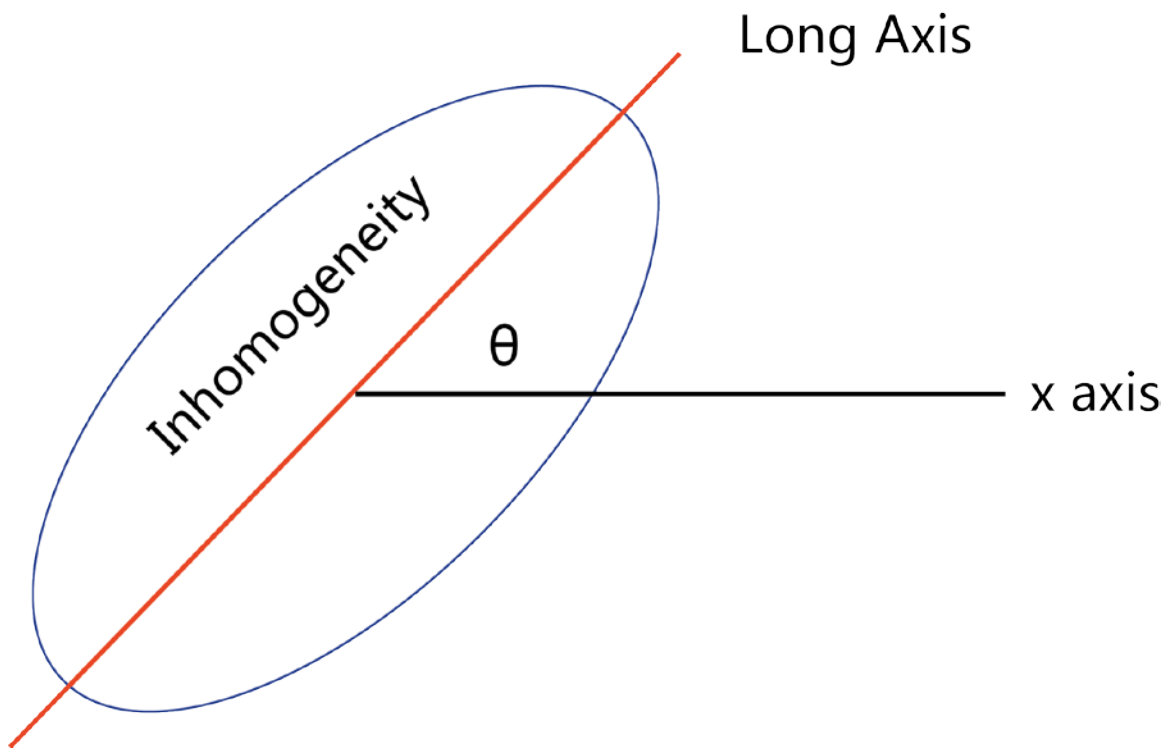


**Figure 3-4 Orientation of the elliptical inhomogeneity.**

*Initial orientation is defined by the angle ( $\theta$ ) between the long axis and the x axis.*

Moreover, again by using the distance equation, the axial ratio can be obtained by using the following equation:

$$R = \frac{\sqrt{X_L^2 + Y_L^2}}{\sqrt{X_S^2 + Y_S^2}} \quad (3-11)$$

where R is the ratio and the other coefficients have been defined before.

In FLAC, the three equations from above are also implemented in FISH (See Appendix F). *FLAGS* in the FISH programming language helps to identify the marked gridpoints. Then distance between each marked gridpoint on the boundary of the ellipse and the origin is calculated. Then loop command is used to compare each two of such distances, and iterate the distance comparisons to yield the minimum and the maximum values of these distances. This being done, the long axis and the short axis are found, thus the orientation and the axial ratio are obtained.

The histories of the two indicators are tracked throughout the whole process of the simulation and can be plotted as curves (Figure 3.5).



FLAC (Version 6.00)

LEGEND

17-Aug-11 23:13  
step 40002  
Creep Time 4.0000E+09

HISTORY PLOT  
Y-axis :  
2 ratio1 (FISH)  
X-axis :  
Number of steps

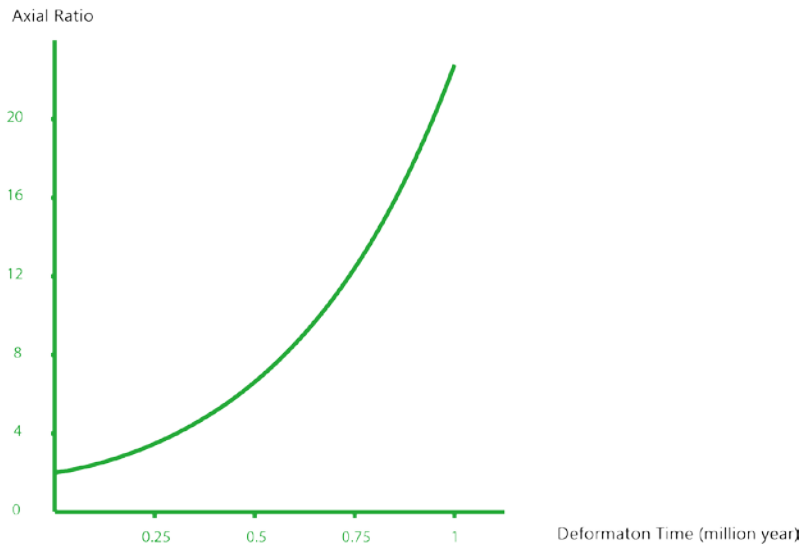
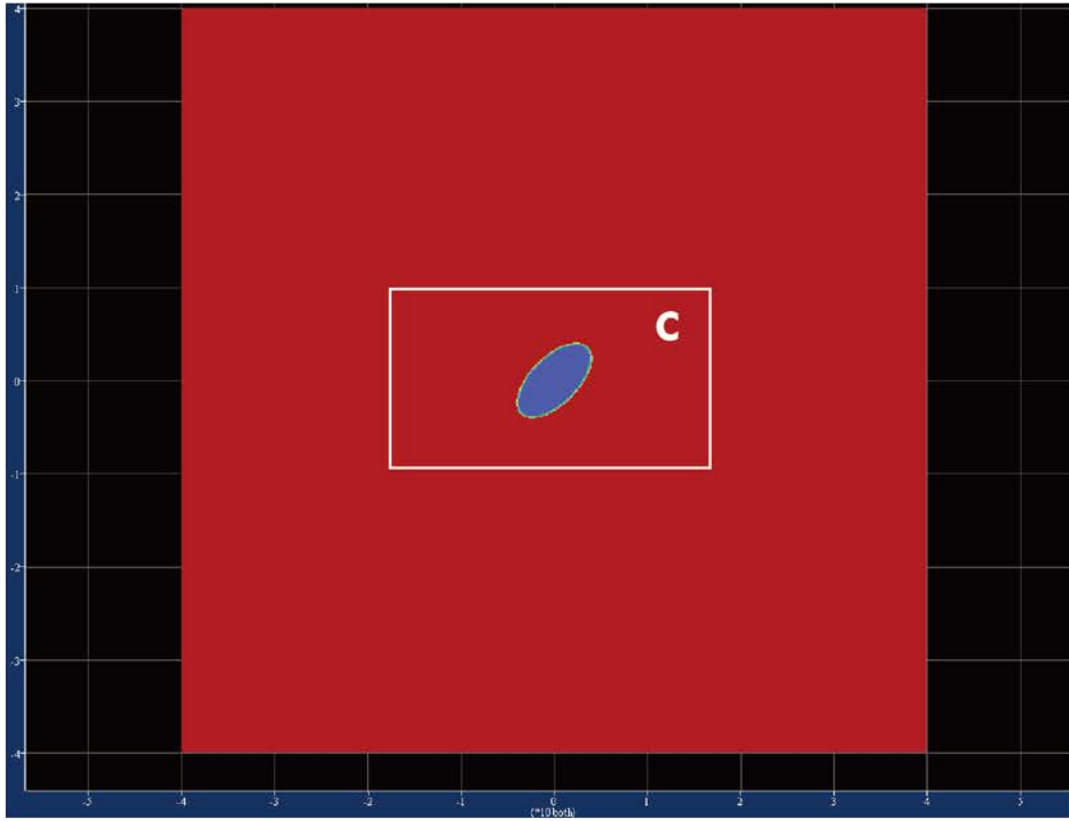


**Figure 3-5 Axial ratio history of an elliptical inhomogeneity modeled in FLAC.**

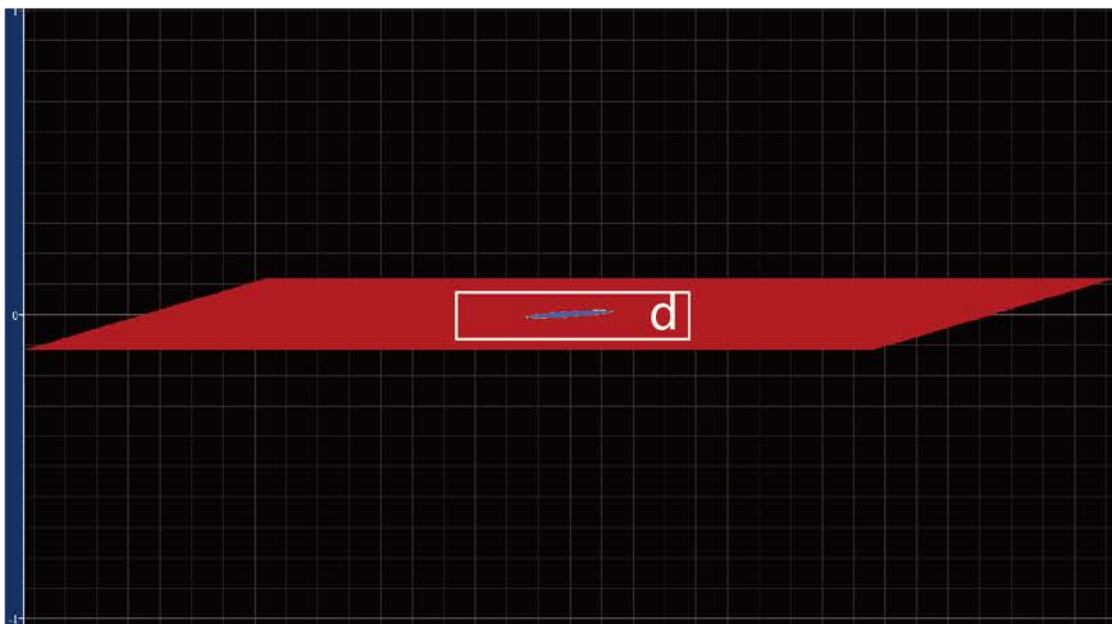
*X axis indicates the total deformation time while y axis is the axial ratio of the elliptical inhomogeneity. In this simulation, axial ratio is originally set to be 2, i.e., the length of the long axis is twice of the short axis. After 1 million years of deformation, the ellipse has been elongated along the long-axis direction and the final-state axial ratio is around 24 (See Figure 3.6).*

# Initial State and Final State of the Matrix

a)



b)



## Initial State and Final State of Elliptical Inhomogeneity

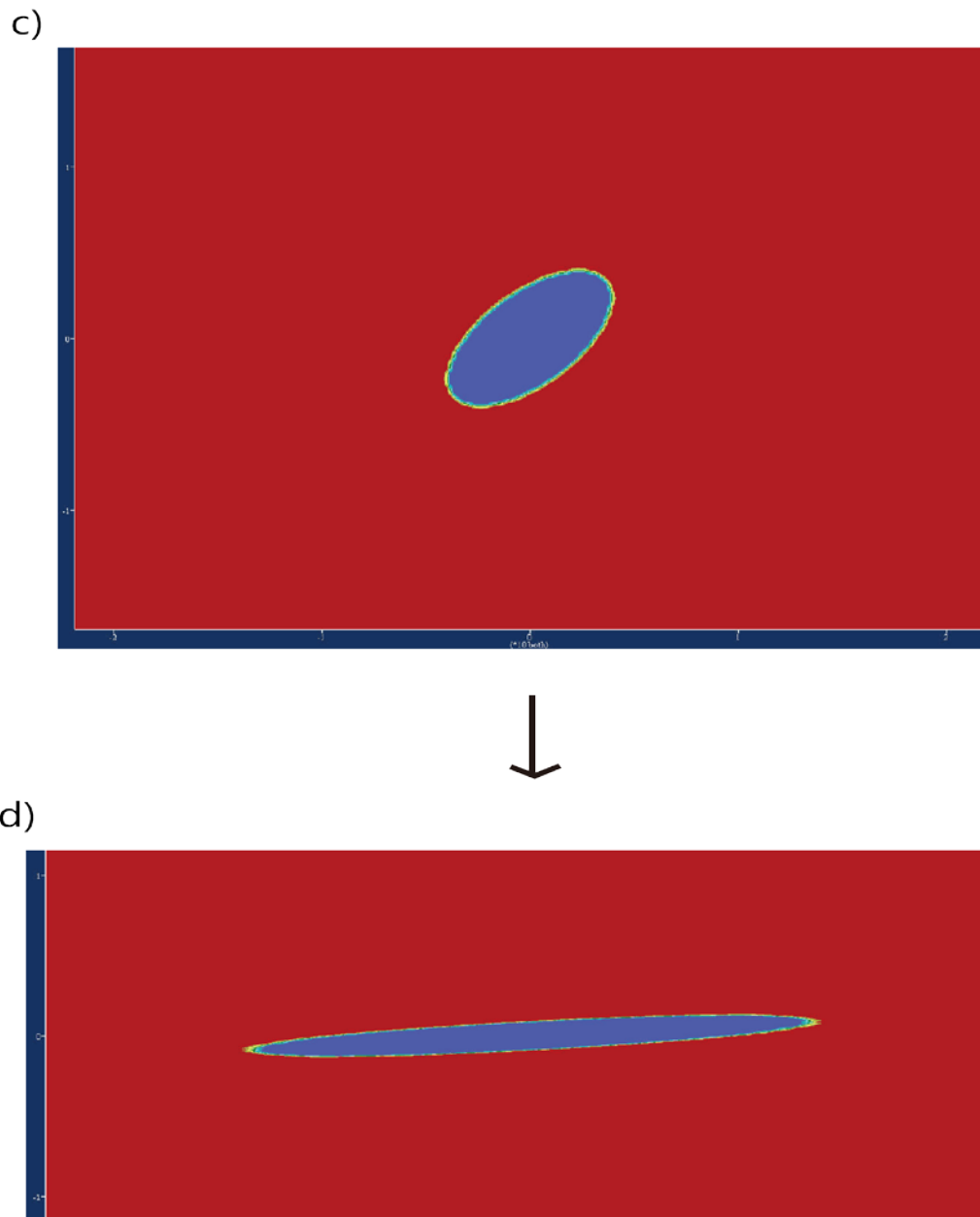


**Figure 3-6 Initial state and final state of the matrix and the elliptical inhomogeneity.**

*Figure a) and b) are the initial state and the final state of the matrix. After 1 million years of deformation, the model has deformed to 25% of its original height. Figure c) and d) are the initial and final state of the inhomogeneity. In figure c), axial ratio of the elliptical inhomogeneity is 2 while in the final state the axial ratio is 24.*

### 3.3 Optimization in Finite Difference Simulation

In order to minimize computational time consumption, optimization should first be applied before prudently jumping into the process of simulation in FLAC. By optimization, I imply that the best parameter selections need to be determined. Such settings are designed to be able to guarantee the precision of the solution and take up the least computational time cost. Computational time is one of the major concerns in this project because some simulations with non-optimized parameters will take over a year to complete while some of them will even terminate just after a few steps. These situations will be detailed in the following paragraphs.

In the following few paragraphs, several aspects of optimization are discussed and testing simulations on the optimized parameter selections are performed.

#### 3.3.1 Elastic Relaxation Time

Since the built-in power-law constitutive module in FLAC is the viscoelastic module, which takes into account both the power-law viscous behavior and the elastic behavior, it is necessary to minimize the elasticity effect when it is used to simulate pure viscous deformations. This elasticity effect issue is also addressed by Zhang et al. (2000) who discovered that when the strain rate is around  $10^{-14} \text{ s}^{-1}$  the deforming body will behave as perfect viscous material, while with the strain rate being  $10^{-6} \text{ s}^{-1}$  the body poses a great tendency to act like pure elastic materials. In addition, Shaw (2004) proposed that the elastic relaxation time is the key to minimize the elasticity effect. The viscoelastic body will have perfect viscous behavior when the overall evolution time is significantly

larger than the relaxation time, otherwise the elasticity effect may be large or even dominant. The elastic relaxation time is given by:

$$T_{relax} = \frac{\eta}{G} \quad (3-12)$$

where  $\eta$  is the viscosity and  $G$  is the shear modulus.

Since the material properties in my simulation is power-law,  $\eta$  here will be replaced by the effective viscosity, which is derived from the second invariant of the strain rate tensor and the second invariant of the stress tensor calculated in the flow. Take the material properties from one of my simulations as an example to test the elastic relaxation time.

The material properties are as follows:

**Table 3-1 Material properties Assignment in FLAC2D in one experiment.**

*Bulk modulus and shear modulus are in unit of mega Parscal, A is the overall mechanical parameter that equals  $A_1 \cdot \exp(-\frac{Q}{RT})$ ; n is the stress exponent. The material property assignment is based on the data of the wet quartzite when deformed in 573K (Gleason and Tullis, 1995).*

Bulk Modulus (MPa)	Shear Modulus (Mpa)	A (MPa <sup>-n</sup> · s <sup>-1</sup> )	n
$3 \times 10^6$	$2.25 \times 10^6$	$4.5466 \times 10^{-21}$	4

**Table 3-2 Material property of wet quartzite (Gleason and Tullis, 1995)**

*A1 in the table is the material constant, Q is the activation energy, R is the gas constant and T is the temperature. Material property data is based on wet quartzite.*

<b>A1 (MPa<sup>-n</sup> · s<sup>-1</sup>)</b>	<b>Q (J/mol)</b>	<b>R (<math>\frac{J}{mol K}</math>)</b>	<b>T (K)</b>
<b>1.40296 × 10<sup>-8</sup></b>	137000	8.314	573

Calculation yields that, where  $L_{ij} = \begin{bmatrix} 3 \times 10^{-10} & 6.03 \times 10^{-11} & 0 \\ 0 & -3 \times 10^{-10} & 0 \\ 0 & 0 & 0 \end{bmatrix}$ , the effective

viscosity is  $1.216 \times 10^{12}$  MPa · s, therefore the relaxation time is about  $4.053 \times 10^5$ s.

On the other hand, the total deformation time in this experiment is set to be one million year, about  $1.4 \times 10^{14}$ s, which considerably exceeds the value of the relaxation time  $10^5$ .

Consequently, the elasticity effect in my finite difference model is small enough to avoid exerting noticeable impact on the viscous behavior.

### 3.3.2 Grid Density Selection

As briefed in the previous chapter, grid density can largely affect the solution and the computational efficiency of simulations. On the one hand, higher density leads to higher precision in the simulation result. One explanation is that with denser grid, there will be more zones to form the inhomogeneity ellipse and more gridpoints on the boundary, which will guarantee the long/short axis endpoints a more precise position when being

calculated. However on the other hand, denser grid will consequently result in more computational time. Therefore, it is of great necessity to seek for the best grid density, which is able make the residual small enough to be neglected, as well as not introduce a computational challenge.

I used bracketing to find the optimum grid density as follows: I gradually increase the grid density, and plot the results graphically of all simulations. When the results converge, the density in the converging result will be the optimum density.

In my simulations, the matrix area is designed to be 80m×80m, the long axis of the inhomogeneity is 5m and the short one is 2.5m. After dozens of attempts, it comes to the result that the whole matrix area needs 460×460 zones to make the results reproducible. That is to say, the zone density is required to be at least 31.36 zones/ $m^2$  to meet the needs of the solution precision. This density allows the inhomogeneity ellipse boundary to be formed by at least 180 gridpoints, guaranteeing the reliability of the result when the endpoints of the axes are calculated. Meanwhile, it takes about 10 hours for a single simulation, which is acceptable.

To further ensure that this density is the optimum one, another extremely time-consuming simulation is performed by assigning a grid density to be four times of the resulted optimum density. In this grid density, it takes nearly a week for a single simulation to complete. Simulation results of both inhomogeneity orientation and in axial ratio are perfectly identical (See figure 3.7 and figure 3.8), meaning that the optimum grid density is reliable.

### Orientation Plot with Different Density

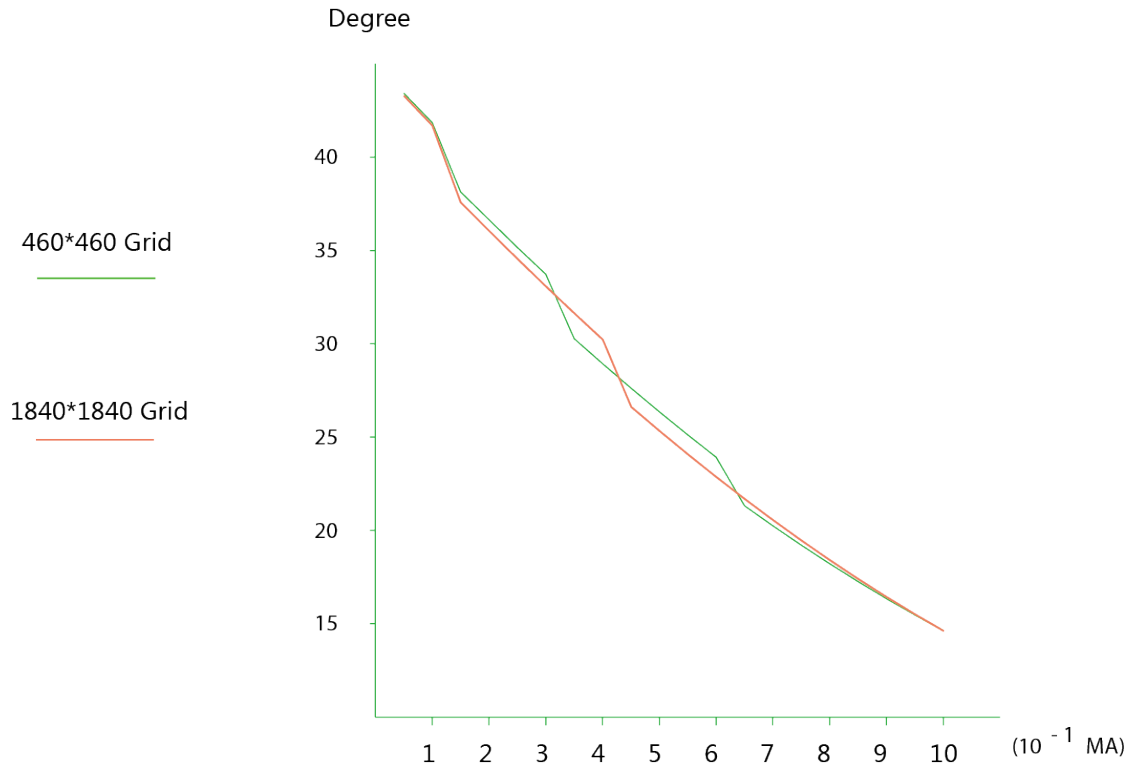


**Figure 3-7 History of the Inhomogeneity orientation for two different grid densities.**

*The green curve is the result from the mesh with 460×460 zones and the red one is from a mesh with 4 times denser zones. The y axis is the orientation in degree (original orientation being 45 ° ) and the x axis represents the deformation time in  $10^{-1}$  MA. The two curves are practically the same. There is no noticeable gain in using the denser grid. The ‘steps’ in the curves are errors caused by using the line segment joining the two farthest significant points on the ellipse to represent the long axis (See Figure 3.9). This type of errors is unavoidable because of discretization of the ellipse. Fortunately these errors are always bounded between two pairs of nearby significant points and never accumulate.*



### Ratio Plot with Different Density

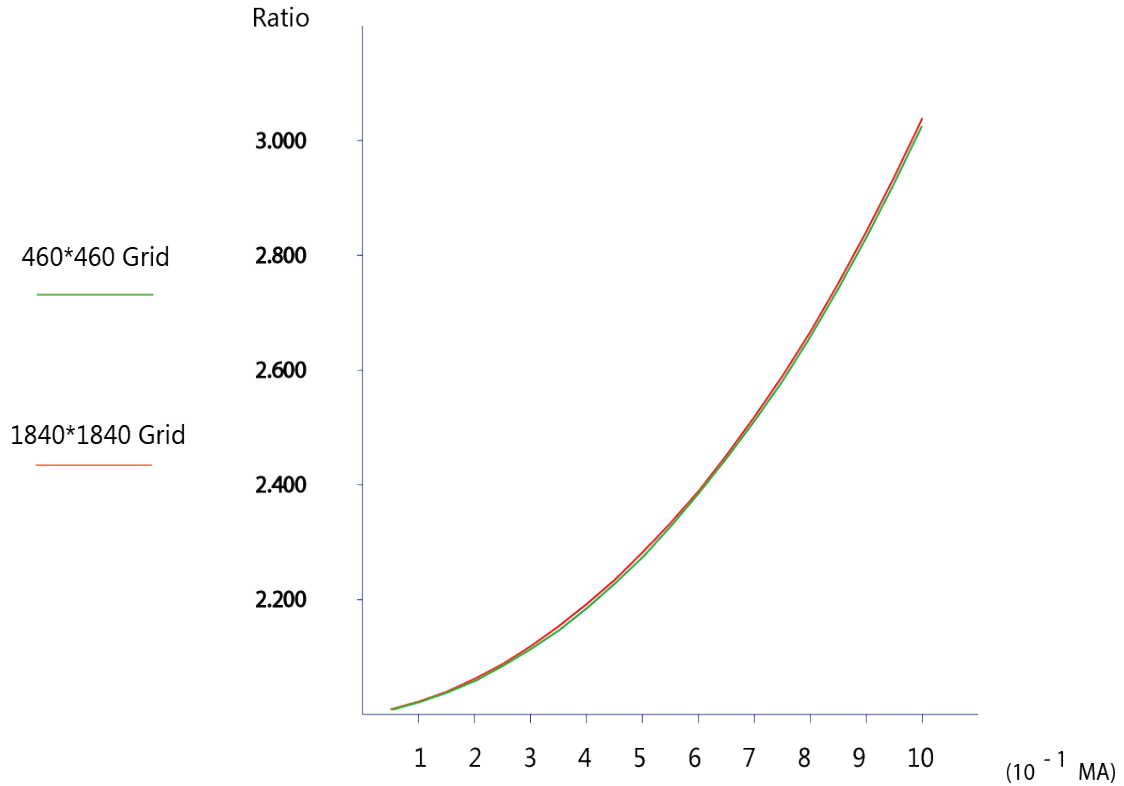


**Figure 3-8 Inhomogeneity axial ratio plot with different grid densities.**

*Green curve is the solution from the grid with lower density like in the former figure. Initial axial ratio is set to be 2, which means the long axis is 2 times of the short axis. In this figure, the two curves once again show perfect identity, implying that the two grid density models yield the same solutions. Therefore, grid with 460×460 zones is the optimum grid for future experiments.*

# Errors Between True Long Axis and Calculated Long Axis

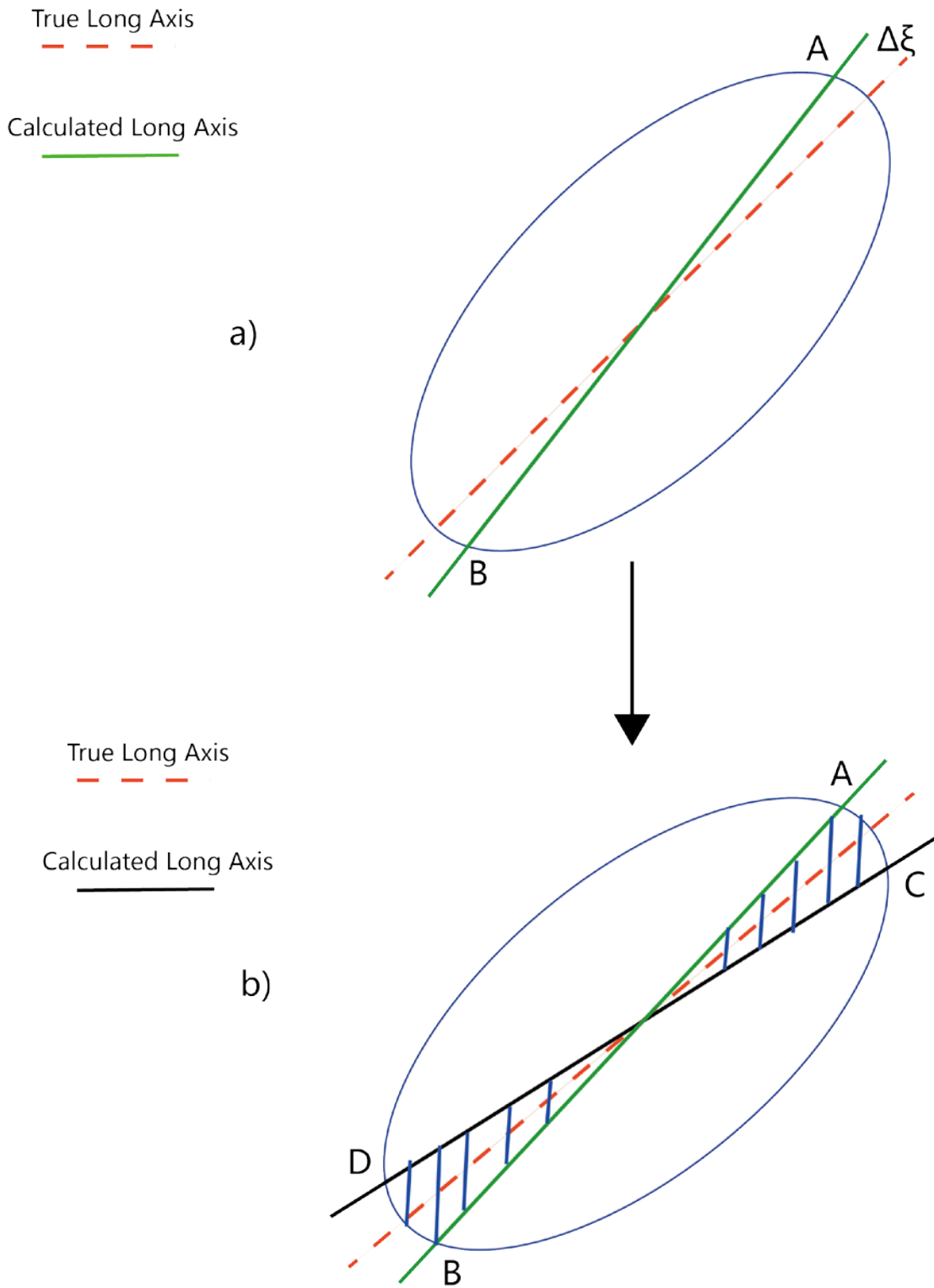


**Figure 3-9 Error in the calculated long axis.**

- a) *The red line is the true long axis and the green line is the long axis calculated in FISH. However, because the long axis is taken in the computation as the line joining two farthest significant points A and B (gridpoints), there will be an inevitable error  $\Delta\xi$ .*
- b) *In a subsequent step of computation, the red line is still the true long axis while the farthest gridpoints switch from AB to the nearby pair CD. Consequently the calculated long axis will 'jump' to the line connecting the new farthest gridpoints and a 'step' will result in the orientation history curve. However, these errors are always bounded between two pairs of nearby significant points (the shady area) and therefore never accumulate. The actual evolution curve should pass nearly through the mid points at the steps (Figure 3.10).*

# Actual Evolution Curve

Evolution Curve Output in FLAC

Actual Evolution Curve

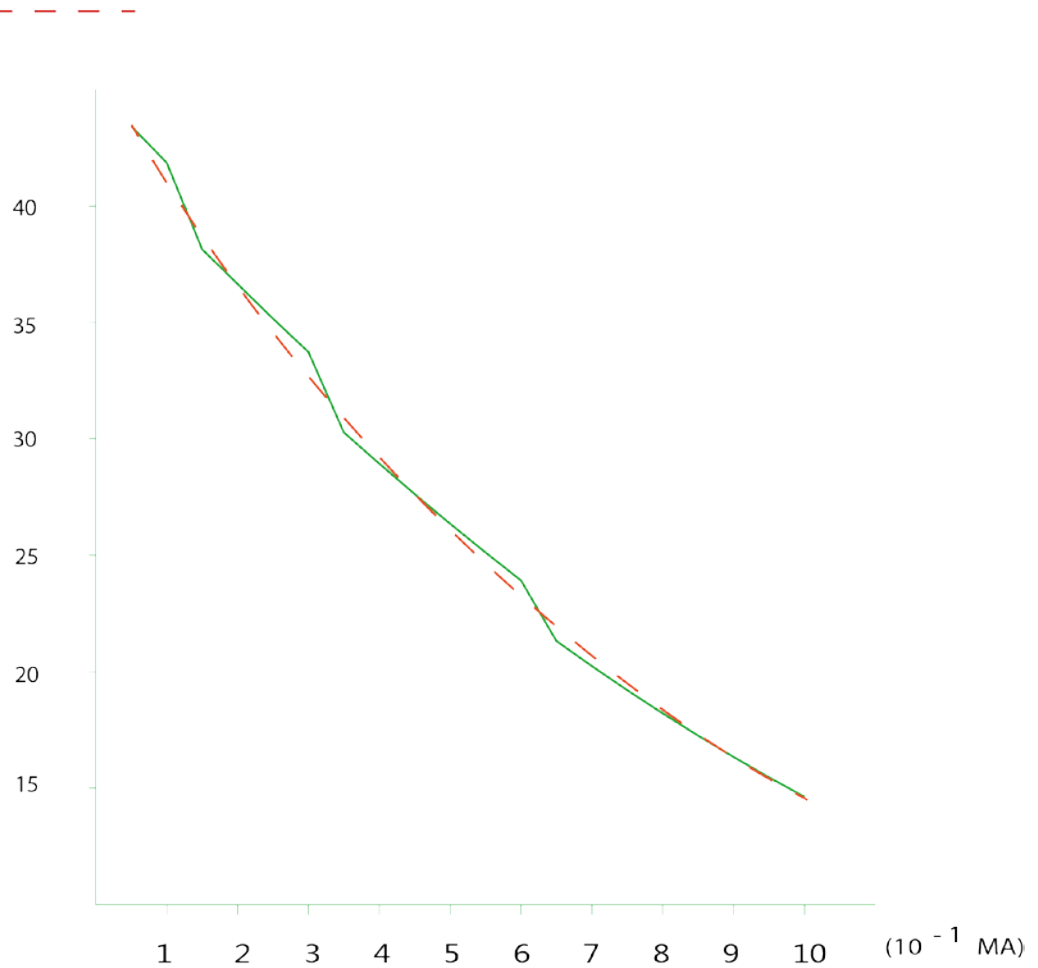


**Figure 3-10 Actual Evolution Curve in FLAC simulation.**

*The actual evolution curve should pass nearly through the mid points at the steps.*

### 3.3.3 The Finite Model Size Effect

In *EFTL* and *EFSL* computations, the matrix is assumed to extend infinitely. However, this is not the case in *FLAC* simulation. Because of the finite size, there will be inevitably boundary effects, especially when the strain is large. While we strive to make the model large compared to the embedded elliptical inhomogeneity, there is a limit to do so to keep the problem a single-scale one with reasonable number of zones manageable by *FLAC*. Therefore, grid area setting and the corresponding boundary effects in *FLAC* must be considered when the grid is generated.

Mandal (2003) discovered that the inhomogeneity can only interact with the matrix in its vicinity area which is within the size of the inhomogeneity itself. That is to say, the inhomogeneity cannot ‘feel’ the influence of the matrix that is farther than one inhomogeneity’s area. Note that this argument is based on the condition that the materials are Newtonian. When it comes to power-law materials, the applicability of Mandal’s theory remains unknown and needs to be tested.

Undoubtedly if the model is extremely large relative to the inhomogeneity, the boundary effect will be negligible. However, this will also evoke the computational time cost problem. It is already demonstrated in the previous experiments that the grid density should be at least 31.36 zones/m<sup>2</sup>, which is rather high. Under such a grid density, a 100m increase in the grid area (rather small in tectonic problems) will cause a million more zones, making the computation time last for more than several weeks for a single simulation. On the contrary, even if the grid area is only a bit smaller than what it needs to be to avoid the boundary effect, with the 2D general deformation going on and the vertical boundary being shortened, the negative impacts on the inhomogeneity will

considerably accumulate and eventually make the results totally useless. Therefore, it is even more crucial to seek for the best grid area value than optimizations on any other aspects because of the more significant sensitivity of the system to the grid area setting.

A series of testing simulations with varying model size are designed. Deformation time is assigned to be one million years, same as all the following experiments to be performed. Grid area is first set to be 2 times of the inhomogeneity ellipse. Then the area is set to increase gradually until the solutions from two contiguous greatly converge. The converging grid area  $A_c$  implies that any area value larger than  $A_c$  will not change the solutions of the simulations, i.e., the boundary effect can be minimized in such a situation.

Results from the series of simulations show that the area ratio of the matrix to the inhomogeneity should at least be 650:1 to yield consistent results. Particularly in numerical models in this project, as the inhomogeneity is 5m long and 2.5m short, the matrix is designed to be 80m×80m. In such an area size, the boundary effect is mostly minimized and more importantly, each simulation only takes up an acceptable computational time (around 2 days).

### 3.3.4 Boundary Velocity Updating

As deformation advances, the lengths of the model in both x-direction and y-direction change. This implies the strain rates will change with time unless the imposed boundary velocities are changed correspondingly. In addition, the area of the deforming body will not be constant unless boundary velocities change with time. For this, the boundary

velocities are continuously updated every few steps of computation through a FISH function (See Chapter 3.2.3).

The reason that the boundary velocities are updated every few steps rather than every step is that with a total of 211600 zones, updating at every single step is a big challenge for both the computational efficiency and the memory capacity of the computer.

Through a series of simulations, it is confirmed that when velocity is updated every 20 steps of computation, the duration of one experiment will be around 40 hours, which is an acceptable amount of computational time. Most importantly, compared to a simulation where the boundary velocities are updated at every step, the orientation solution variation is only approximately  $1^\circ$  after 0.25 million years of deformation. Such a variation is so small that it will not change the pattern the result curve.

### 3.4 Result Post-Processing and Comparisons

When the *EFTL*, *EFSL* computations and the FLAC simulations have been conducted, they should each have two sets of curve figures: the first set being for the history of the long axis orientation and the second set being for the history of the ellipse's shape (axial ratio). Post-processing work on these curve figures are performed in a vector artwork processing software Illustrator from Adobe Corporation (<http://www.adobe.com>). The main work is to merge all the figures from 3 models into one figure, where all three curves can be visualized and compared. By this means, the variances between the three models can be determined.

In each composite comparison figure, the green curve is from FLAC simulations (indicated by 'FLAC'); the blue curve is from *EFTL* (indicated by 'TL') and the red curve is from *EFSL* (indicated by 'SL') (Figure 3.10). The candidate curve that lies closer to the FLAC curve shows better applicability to power-law material deformations.



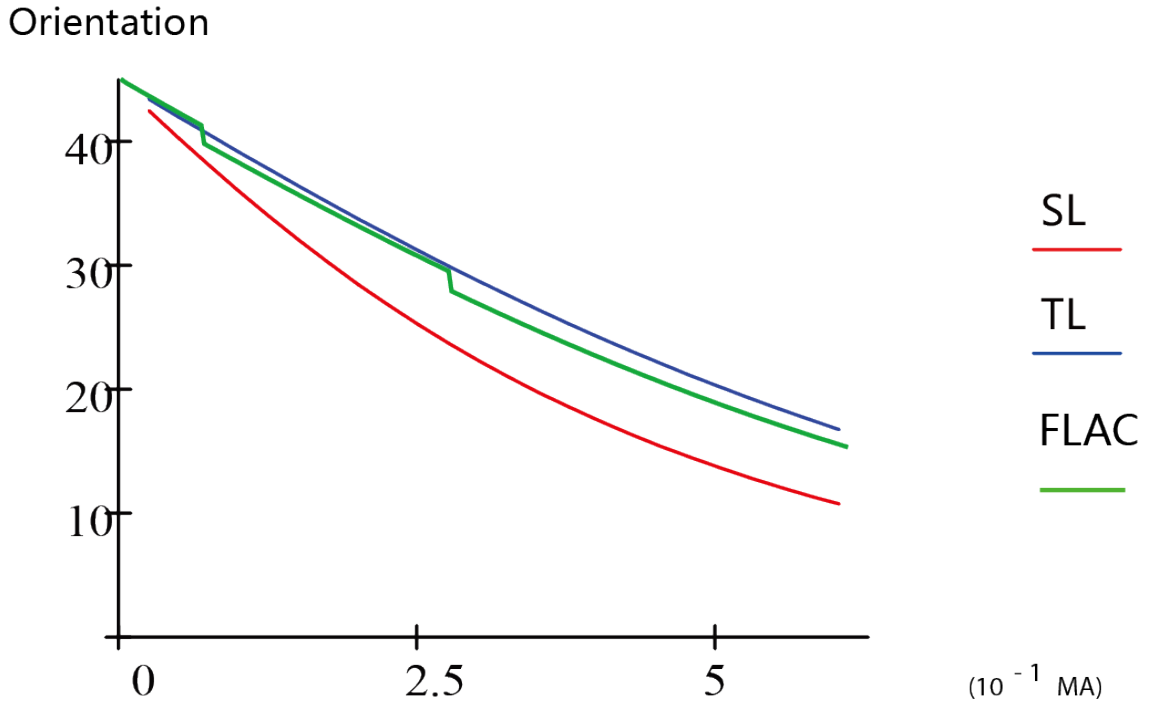


**Figure 3-11 Result curve figure for comparisons.**

*An example of simulation results for the orientation history of the long axis orientation. Simulation inputs are as follows:  $Wk = 0.1$ , normal strain rate is  $3 \times 10^{-10} \text{ s}^{-1}$ , shear strain rate is  $6.03 \times 10^{-11} \text{ s}^{-1}$ , initial orientation of the elliptical inhomogeneity is  $45^\circ$ , and the initial axial ratio of the ellipse is 2. Details about the mechanical properties in this simulation can be viewed in Section 4.1.3. Comparison indicates that EFTL is close to the FLAC simulation, suggesting that EFTL is more applicable than EFSL in the certain situation.*

## Chapter 4

### 4 Simulations and Results

In this chapter, simulation procedure and results will be presented. By comparing the results from the *EFTL*, *EFSL* computations with the results from the finite difference simulation in *FLAC*, one is able to shed light on the applicability of the *EFTL* and *EFSL* as well as to conclude which one is better for the power-law behavior in nature.

#### 4.1 Verification Simulations

Before running simulations and comparisons for the most general situation of a power law inhomogeneity embedded in a power law matrix, it is necessary to run a few benchmark simulations to test both the simulation methods and the setups. I will start with the simplest situation of a Newtonian inhomogeneity in a Newtonian matrix, move to a power law inhomogeneity in a Newtonian matrix, a Newtonian inhomogeneity in a power law matrix, and eventually a power law inhomogeneity in a power law matrix.

##### 4.1.1 A Newtonian Inhomogeneity in a Newtonian Matrix

The simplest and special situation in my project is that both the matrix and the inhomogeneity are Newtonian materials. Given the objective of the project being an investigation on power-law materials, one may question the necessity of doing such a Newtonian simulation. However, in fact, this is a foremost step in my project, which benchmarks on the solution precision of the Eshelby Formalism code in *Mathcad* as well

as the simulation setup in FLAC, the efficiency of the FISH operations and even the feasibility of the essential comparison paradigm of the project. If the solutions from the *EFTL*, *EFSL* computations and the FLAC simulations do not converge in the simplest situation, then the code or the program will be inadequate for investigating more complex and more general situations.

Therefore, the verification simulation where a Newtonian inhomogeneity embedded in a Newtonian matrix is performed. Before the results of the simulation are discussed, the initial conditions are first presented. Note that for all simulations in this project, the flow is always 2D general shear and the initial axial ratio of the elliptical inhomogeneity is set at 2. Timestep in both FLAC simulation (  $10^5$  s/step) and Eshelby Formalism computations ( $10^7$  s/step) will also stay constant. Other parameters in this simulation are presented in Table 3 below.

**Table 4-1 Initial Conditions for the verification simulation where a Newtonian inhomogeneity is embedded in a Newtonian matrix.**

$W_k$	$L_{ij}$	Viscosity Ratio (inhomogeneity to matrix)	Initial Orientation of Inhomogeneity
0.3	$\begin{bmatrix} 3 \times 10^{-10} & 1.887 \times 10^{-10} & 0 \\ 0 & -3 \times 10^{-10} & 0 \\ 0 & 0 & 0 \end{bmatrix}$	1.886	45°

As shown in Table 3, matrix and inhomogeneity both are assigned Newtonian materials which show viscosity contrasts of 1.886 (viscosity of inhomogeneity to viscosity of matrix). Initial orientation of the inhomogeneity is defined by the angle between the elliptical long axis and the x axis (See Section 3.2.5). Result curves from the Eshelby Formalism and FLAC simulations are compared on Figure 4.1 through the orientation history and the shape variation history of the inhomogeneity. As shown in Figure 4.1, after a total deformation time of 1 million year, the orientation of the strain ellipse becomes  $1.383^\circ$  while the aspect ratio is 11.932. Both histories from the two simulations show nearly perfect agreement. The result ensures that both the methodology and the simulation setups are reliable, ready for further simulations on power-law materials.

## Newtonian Matrix and Newtonian Inhomogeneity

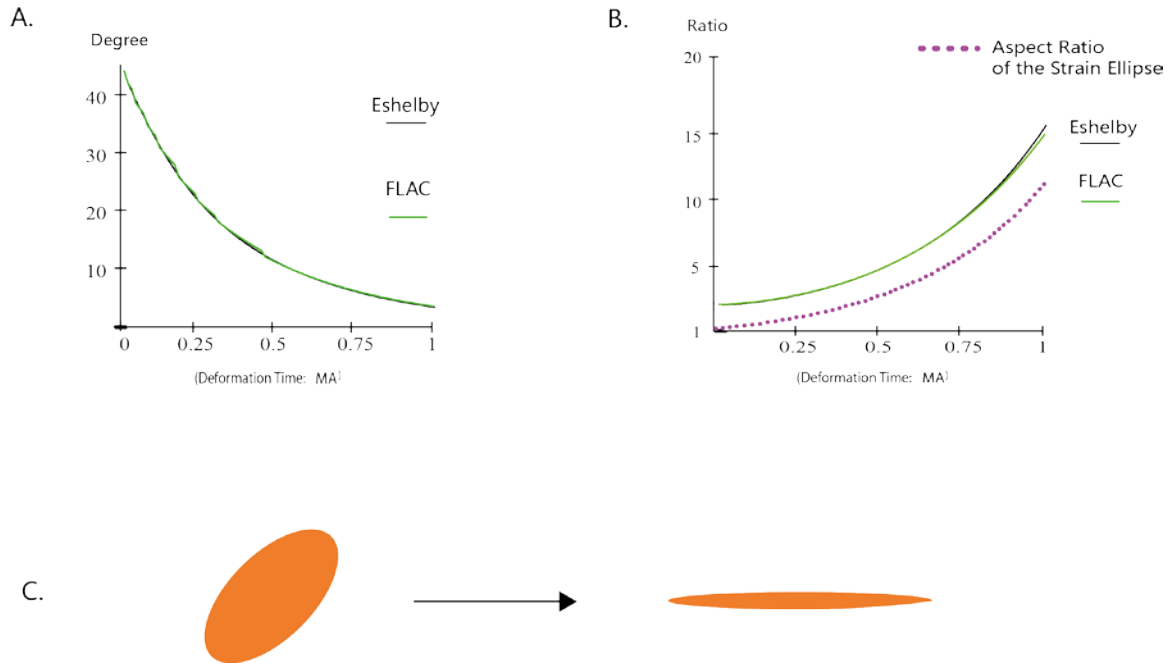


**Figure 4-1 Results from FLAC and Eshelby Formalism for a Newtonian inhomogeneity embedded in a Newtonian matrix.**

*Figure 4.1A is the inhomogeneity orientation evolution history over time while Figure 4.1B is the axial ratio history. Evolution of the aspect ratio of the stain ellipse is illustrated in purple dotted line. Figure 4.1C is the initial state and final state of the inhomogeneity. One can conclude that in both of Figure 4.1A and Figure 4.1B, the results from FLAC and Eshelby Formalism perfectly match each other.*

### 4.1.2 A Power-Law Inhomogeneity in a Newtonian Matrix

In this section, I inspect another special situation in which the inhomogeneity is power-law material while the matrix remains Newtonian material. This simulation is another step to the general situation of a power-law inhomogeneity embedded in a power-law matrix.

The recent work of Mancktelow (2011) was on a power-law inhomogeneity in a Newtonian matrix. By taking into account the variations of two parameters: axial ratio and the power law stress exponent, he calculated the corresponding variations of the effective viscosity ratio in Matlab (<http://www.mathworks.com>), and plot a 3D graph as shown in Figure 4.2.

Such phenomenological results can be further improved in this project. With the assistance of *EFTL*, one is now able to capture the essence of the deforming system where a power-law inhomogeneity embedded in a Newtonian matrix.

Note that when the matrix is a Newtonian material and the inhomogeneity is ellipsoidal, Eshelby Formalism assumptions are completely satisfied regardless of the rheology of the inhomogeneity as long as the matrix is isotropic and incompressible (Chapter 2.2), i.e., in each infinitesimal step, Eshelby Formalism can be directly applied. Therefore, in this case Tangent Linearization Scheme is no longer an approximation.

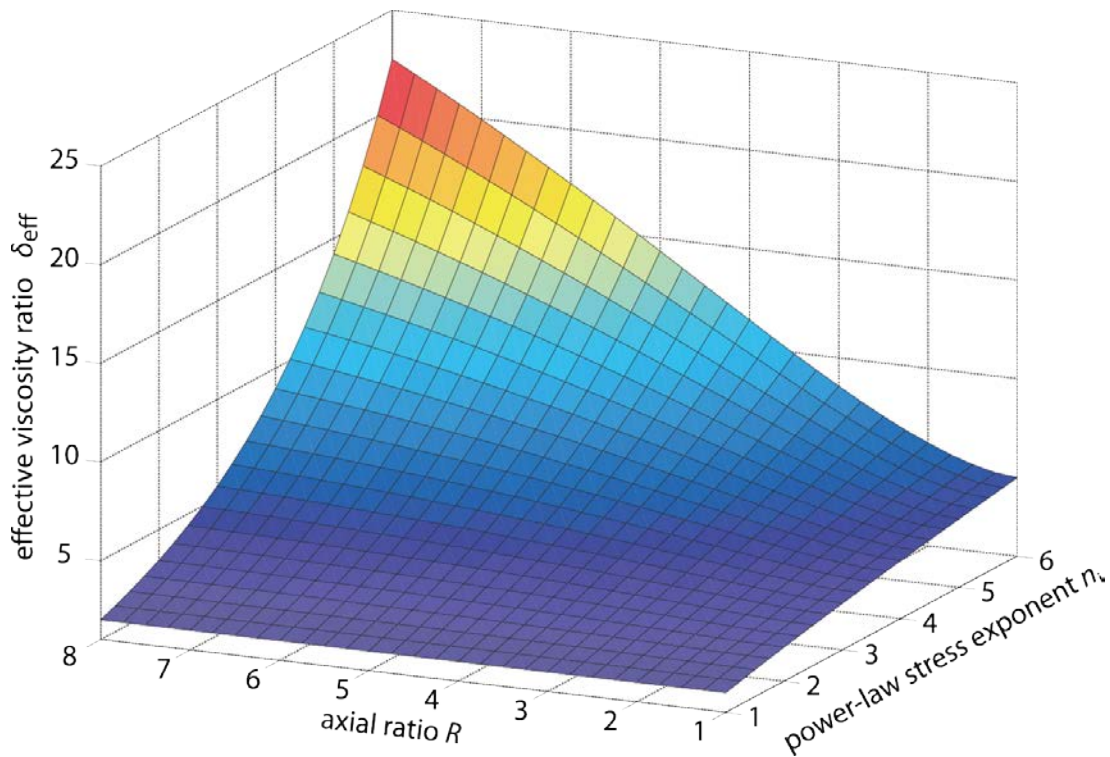


**Figure 4-2 Response of effective viscosity ratio in respect to the variations of axial ratio and power-law stress exponent of the inhomogeneity. Figure modified from Mancktelow (2011).**

*Figure shows the response of effective viscosity ratio to the different settings of axial ratio and power-law stress exponent in the deformation where the inhomogeneity is power-law material while the matrix is Newtonian. The orientation of the inhomogeneity is 0° or 90° with respect to x-axis. Effective viscosity ratio solution is achieved by using Eshelby Formalism. Figure is plotted in Matlab.*

Initial conditions for this simulation are shown in Table 4 below.

**Table 4-2 Initial conditions for the simulation where a power-law inhomogeneity is embedded in a Newtonian matrix.**

$W_k$	$L_{ij}$	Effective Viscosity Ratio (inhomogeneity to matrix)	Initial Orientation of Inhomogeneity (degree)
0.3	$\begin{bmatrix} 3 \times 10^{-10} & 1.887 \times 10^{-10} & 0 \\ 0 & -3 \times 10^{-10} & 0 \\ 0 & 0 & 0 \end{bmatrix}$	0.396	45

As shown in Figure 4.3, after 1 million years deformation, the aspect ratio of the strain ellipse becomes 11.932 and the orientation becomes 1.383°. As expected, result curves from the Eshelby Formalism greatly converge to the ones from the FLAC simulation (Figure 4.3). This result validates the theory of Eshelby Formalism as well as the Tangent theory, and also validates the applicability of my simulation setups in both software programs.

More importantly, this simulation implies that the deforming system where a power-law inhomogeneity embedded in a Newtonian matrix finally has a solution based on



mathematical and physical theories, the *EFTL*. Once the shape, orientation of the inhomogeneity and the material properties for the deforming system are known, all the flow characteristics in this ‘inhomogeneity-matrix’ system are determined and the whole deformation history over an amount of time duration can be obtained.

## Power-Law Inhomogeneity

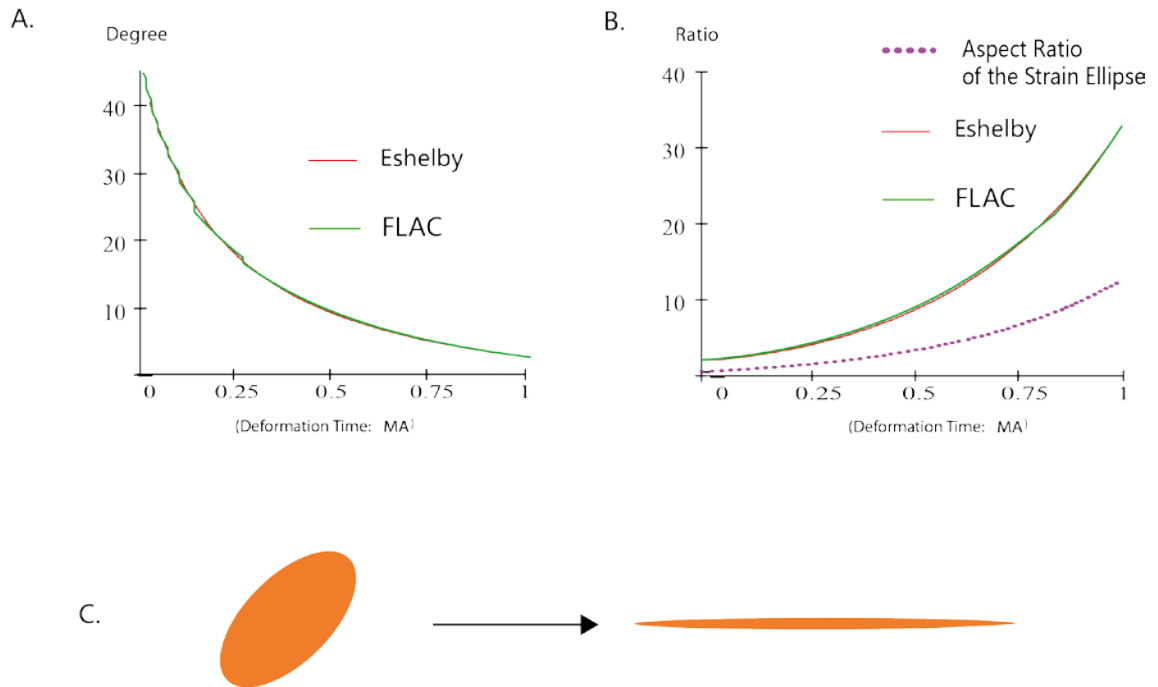


**Figure 4-3 Results from FLAC and Eshelby formalism for a power-law inhomogeneity embedded in a Newtonian matrix.**

Figure 4.3A is the orientation history while Figure 4.3B is the axial ratio evolution of the inhomogeneity. Result curve from Eshelby Formalism is the red one and the green curve is the FLAC result. As usual, the purple dotted line is the aspect ratio history of the strain ellipse, indicating the total strain of the 'inhomogeneity-matrix' system. Figure 4.3C is the initial state and the final state of the inhomogeneity simulated in FLAC model. Comparisons between Eshelby Formalism result and the FLAC result in Figure 4.3A and Figure 4.3B shows that in this simulation, Eshelby Formalism perfectly converges to the FLAC model.

### 4.1.3 A Newtonian Inhomogeneity in a Power-Law Matrix

In this section I proceed to another special case in this project, where the matrix is set to be power-law material while the inhomogeneity is set to be Newtonian.

When the matrix is Newtonian, the viscosity remains constant throughout the matrix and the whole deformation time. Thus in this case, regardless of the rheology of the inhomogeneity, Eshelby theory assumption is always met and Eshelby Formalism can be directly applied. However, it is a completely different situation when the matrix becomes power-law material. During such a deformation, the effective viscosity of the matrix varies with space and time. Hence Eshelby Formalism can no longer be directly applied and the Tangent Linearization Scheme is used as an approximation. Therefore, the simulation in this section is the first one so far to test the Tangent Linearization Scheme.

Initial conditions for this simulation are presented in Table 5 below.

**Table 4-3 Initial conditions for the simulation where a Newtonian inhomogeneity is embedded in a power-law matrix.**

$W_k$	$L_{ij}$	Effective Viscosity Ratio (inhomogeneity to matrix)	Initial Orientation of Inhomogeneity	Stress Exponent of Matrix ( $n_m$ )
0.1	$\begin{bmatrix} 3 \times 10^{-10} & 6.03 \times 10^{-11} & 0 \\ 0 & -3 \times 10^{-10} & 0 \\ 0 & 0 & 0 \end{bmatrix}$	2.439	45°	6

After about 0.5 million years deformation, the aspect ratio of the strain ellipse of the bulk becomes 4.51 and the orientation is  $1.043^\circ$ . Result curves are shown in Figure 4.4. Interpretation from the figure shows that *EFTL* is without any doubt the better model than the *EFSL* in this simulation. This result also suggests two important points:

- 1) Theory on the Secant Scheme is validated. *EFSL* has noticeable difference from the power-law behavior simulated in FLAC in this simulation. The reason is that no matter how small the incremental deformation is, the rheology equation for the matrix remains non-linear.
- 2) *EFTL* to a great extent converges the power-law behavior simulated in FLAC.

Clarification should be made on the deformation time in this experiment. The deformation time in this simulation is only half of the one in other simulations, which leads to the relatively small total strain of the matrix. The cause of this short deformation time is that when the mechanical contrasts between the matrix and the inhomogeneity is significant, the strain will have a strong tendency to localize, which easily causes ‘bad geometry’ in FLAC and terminate the simulations.

## Power-Law Matrix and Newtonian Inhomogeneity

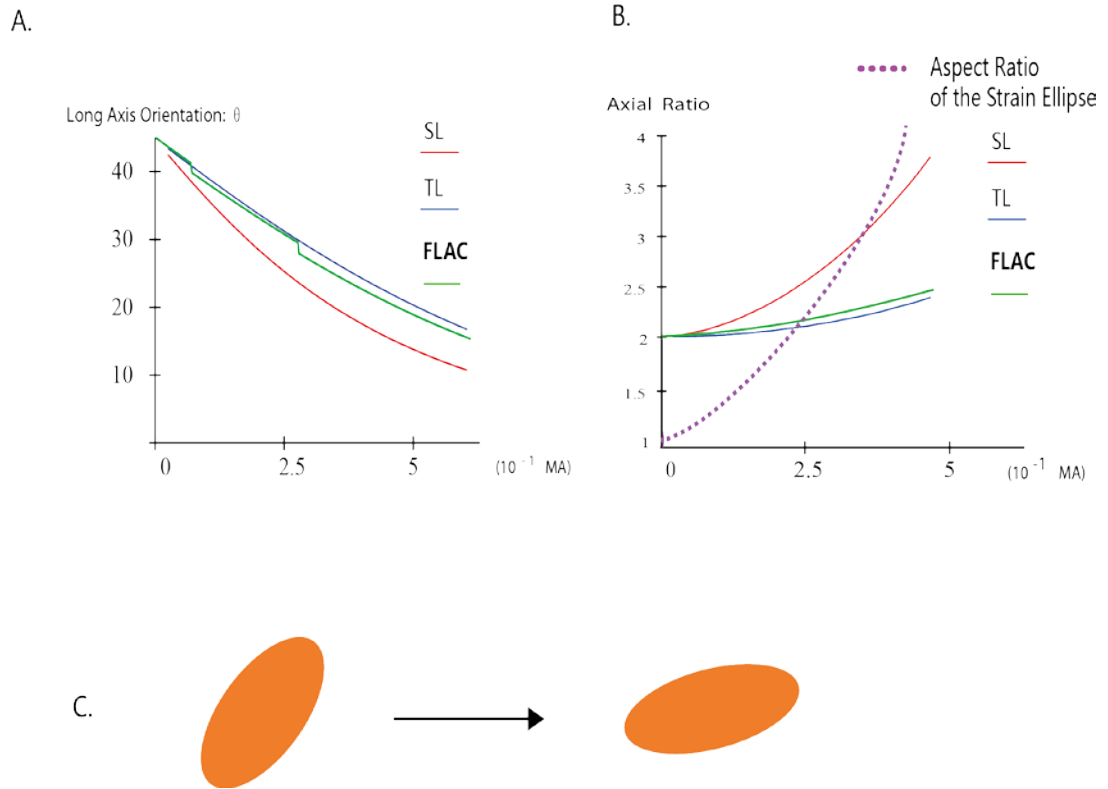


**Figure 4-4 Results from FLAC and Eshelby Formalism for a Newtonian inhomogeneity embedded in a power-law matrix.**

Figure 4.4A and Figure 4.4B are the orientation and the axial ratio evolution history of the inhomogeneity. EFTL is denoted by TL, EFSL by SL and FLAC simulation by FLAC. Figure 4.4C illustrates the deformation evolution of the inhomogeneity simulated in FLAC model. Figure 4.4A and figure 4.4B both show that EFTL has a much closer result to the FLAC simulation than the EFSL. Total bulk strain is only about half of the previous simulations due to the bad geometry existence in FLAC.

## 4.2 Simulations on General Power-law Deformation

Through a series of verification simulations, it is clear that simulation approaches in this project are reliable in both the *EFTL*, *EFSL* computations and the FLAC simulations. On top of that, *EFTL* is validated in special cases of power-law deformations. In the following paragraph, illustrations will be given on the process in which I perform simulations on the general power-law problems, where the matrix and inhomogeneity are both power-law materials and exhibit competence contrasts.

In order to research on this general power-law deformation problem, it is required that all the parameters that are responsible for the results are examined one by one. By this means, one is able to interpret the parameter effect on the applicability of the *EFTL*.

Parameters that have potential influence on the result are listed as follows:

1. Types of the shear deformation represented by the value of the kinematic vorticity number  $W_k$
2. Initial shape and orientation settings for the inhomogeneity ellipse
3. Material properties, which specifically are the material coefficient  $A$  and the stress exponent  $n$

### 4.2.1 Shear Flow Type Variations

It has been discussed in Chapter 2 that the Truesdell's kinematic vorticity number  $W_k$  is a representative measure of the instantaneous non-coaxiality as well as an indicator for the types of the shear flows. For pure shear flow  $W_k = 0$ , for simple shear flow  $W_k = 1$  and for general shear flow  $0 < W_k < 1$ .

In order to account for all the general shear-flow-type situations in nature, four representative  $W_k$  values are chosen: 0.1, 0.3, 0.6 and 0.9, where 0.1 and 0.9 approaches the two end members pure shear flow and simple shear flow, while 0.3 and 0.6 takes into consideration the common sub-simple shear flow in nature.

In the simulation process, both the matrix and the inhomogeneity are assigned to be power-law materials, and four different  $W_k$  values are applied while other parameters are kept unchanged. By this means, one is able to observe the response of the system to  $W_k$  values.

Initial conditions for this series of simulations are listed in Table 6.

**Table 4-4 Initial conditions for simulations with shear flow type variations.**

$W_k$	$L_{ij}$	Effective Viscosity Ratio	Initial Orientation of Inhomogeneity	Stress Exponent of Matrix ( $n_m$ )	Stress Exponent of Inhomogeneity ( $n_i$ )
0.1	$\begin{bmatrix} 3 \times 10^{-10} & 6.03 \times 10^{-11} & 0 \\ 0 & -3 \times 10^{-10} & 0 \\ 0 & 0 & 0 \end{bmatrix}$	1.581	60°	4.7	2.9
0.3	$\begin{bmatrix} 3 \times 10^{-10} & 1.887 \times 10^{-10} & 0 \\ 0 & -3 \times 10^{-10} & 0 \\ 0 & 0 & 0 \end{bmatrix}$	1.59	60°	4.7	2.9
0.6	$\begin{bmatrix} 3 \times 10^{-10} & 4.5 \times 10^{-10} & 0 \\ 0 & -3 \times 10^{-10} & 0 \\ 0 & 0 & 0 \end{bmatrix}$	1.628	60°	4.7	2.9
0.9	$\begin{bmatrix} 3 \times 10^{-10} & 1.239 \times 10^{-9} & 0 \\ 0 & -3 \times 10^{-10} & 0 \\ 0 & 0 & 0 \end{bmatrix}$	1.763	60°	4.7	2.9

A series of four simulations are conducted and results are shown in Figure 4.5. As in the previous experiments and in the following, the green curve represents results from FLAC simulation, as the red and blue ones are the *EFSL* curve and the *EFTL* curve, respectively. All of the four figures are result curve of the inhomogeneity axial ratio. The reason is that the result curves of the ellipse orientation are always consistent with the corresponding axial ratio curves. By ‘consistent’, I mean the relative positions of the *EFTL*, *EFSL* and the FLAC simulation are in great agreement in the orientation evolution curves and in the axial ratio revolution curves. Therefore, the result implication in the two types of curves is practically the same, thus only one of them is needed to be presented here.

One can clearly see several significant points in Figure 4.5:

- 1) In the situation where both the matrix and the inhomogeneity are power-law material, neither *EFSL* nor *EFTL* can perfectly describe the behavior simulated in FLAC simulation. Yet the differences between the three curves are not significant, especially when the strain is large (aspect ratios of the strain ellipse are around 15 in four simulations) and the deformation time is relatively long (1 million years) compared to natural rock deformations.
- 2) In all of the four simulations, the FLAC result lies in between *EFSL* and *EFTL*, where *EFSL* always deforms the fastest and *EFTL* deforms the slowest. Equation (2-17) shows that, in the ‘inhomogeneity-matrix’ deformation system, with higher competence contrast (higher effective viscosity ratio), the deformation strain rate of the inhomogeneity will be lower. Therefore, in the situation where the inhomogeneity is mechanically stronger than the matrix (competence contrast is larger than 1 in



- Table 6), the result curves in fact imply that *EFTL* always over-estimates the effective viscosity ratio while *EFSL* always under-estimates it. When the competence contrast is reversed, i.e., the inhomogeneity is mechanically weak and the matrix is strong, the result will also be reversed (*EFTL* over-estimates the effective viscosity ratio and *EFSL* under-estimates it). Further details will be given in Section 4.2.3 and Chapter 5.
- 3) The fact that all composite curves from the four simulations are in great agreement leads to a conclusion that, for different  $W_k$  values, simulations share consistent results.

### Variation in Shear Flow Type ( $W_k$ )

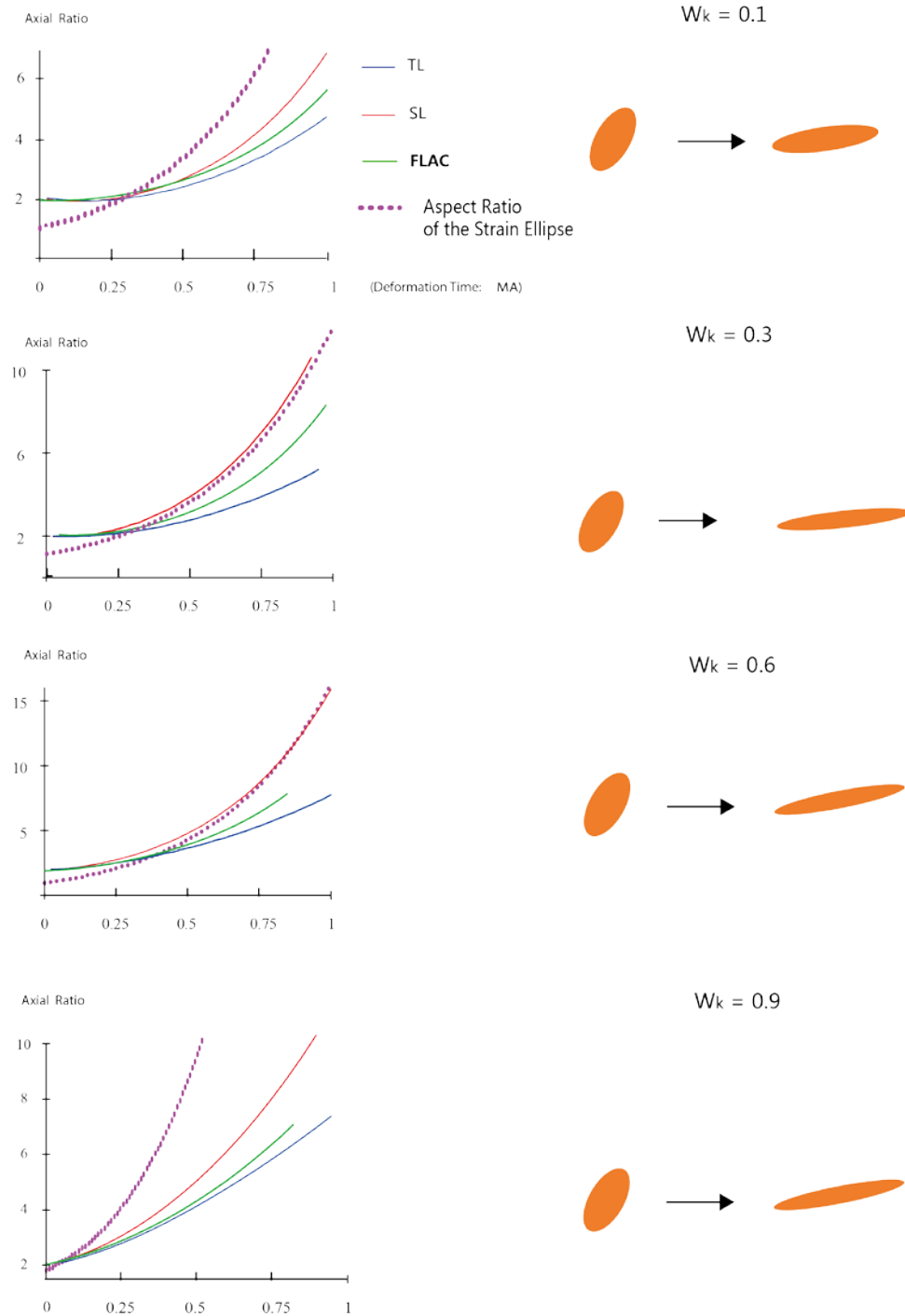


**Figure 4-5 Results from FLAC and Eshelby Formalism for  $W_k$  variation simulations.**

*Four types of shear flow are simulated and they yield consistent results. FLAC model curve always lies between EFTL and EFSL.*

### 4.2.2 Initial Orientation/Shape Variations

It is implied in Eshelby theory (1957) that different initial shapes and orientations will lead to different deformation patterns in shear flow deformation. Simulations with different initial shapes and orientations of the inhomogeneity are presented in this section.

In order to spare some redundant simulations, carrying out simulations on the initial orientation variations alone is believed to be sufficient. The reason is that difference in the initial orientation will lead to different shape evolution of the inhomogeneity even for an identical initial shape. Hence technically, changing the initial orientation of the inhomogeneity already considers the effect of the shape variations during deformation. A series of simulations with different sets of initial orientations are designed. Further, due to the symmetry of the ellipse, one only needs to consider the orientation range between  $0^\circ$  and  $180^\circ$ . I will consider 6 different initial orientations for  $\theta$  to be  $0^\circ$ ,  $30^\circ$ ,  $60^\circ$ ,  $90^\circ$ ,  $120^\circ$  and  $150^\circ$ , to represent all the general situations. Same as the previous series of simulations, value of the initial orientations of the inhomogeneity is the only parameter that changes, while all other parameters remain constant. In this series of simulations,  $W_k$  values are all set to be 0.1 and the initial axial ratios are still 2:1.

Initial conditions for the simulations in this section are presented in Table 7.

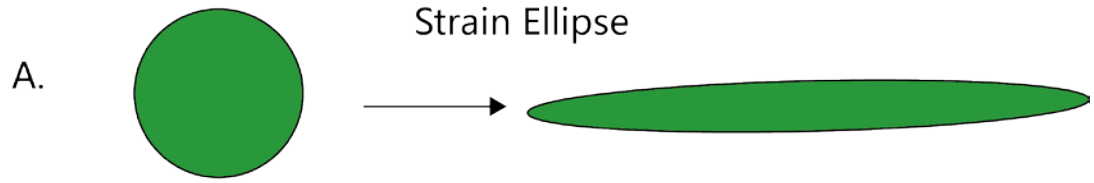
**Table 4-5 Initial conditions for simulations on different initial inhomogeneity orientations.**

$W_k$	$L_{ij}$	Effective Viscosity Ratio	Stress exponent of matrix	Stress exponent of inhomogeneity	Initial inhomogeneity orientation
0.3	$\begin{bmatrix} 3 \times 10^{-10} & 1.887 \times 10^{-10} & 0 \\ 0 & -3 \times 10^{-10} & 0 \\ 0 & 0 & 0 \end{bmatrix}$	1.59	4.7	2.9	0°, 30°, 60°, 90°, 120°, 150°

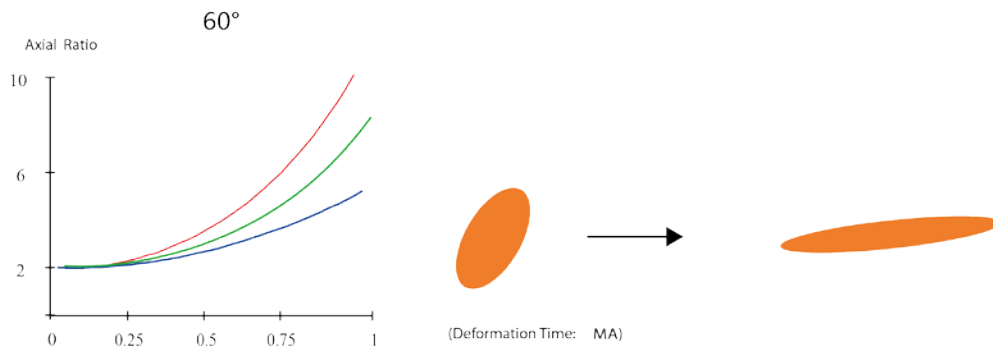
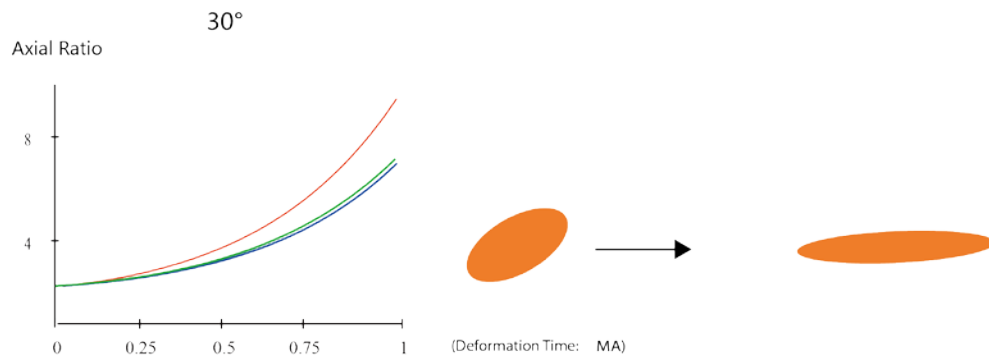
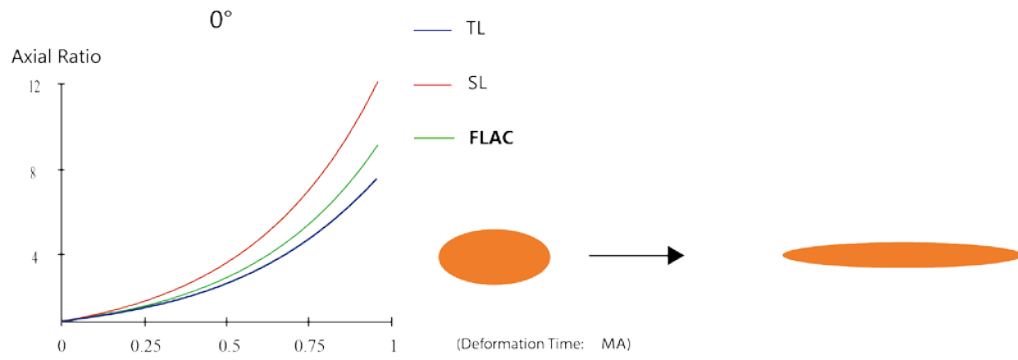
After 1 million years deformation, the aspect ratio of the strain ellipse is 11.932 while the orientation is 1.383°.

Result curves are shown in Figure 4.6. All composite curves again show exact same patterns where *EFTL* deforms the slowest, *EFSL* the fastest and *FLAC* simulation in between. Therefore, a conclusion can be made that simulation results are consistent for all initial inhomogeneity orientations or shapes.

## Axial Ratio Solutions for Experiments with Different Initial Inhomogeneity Orientations



B.



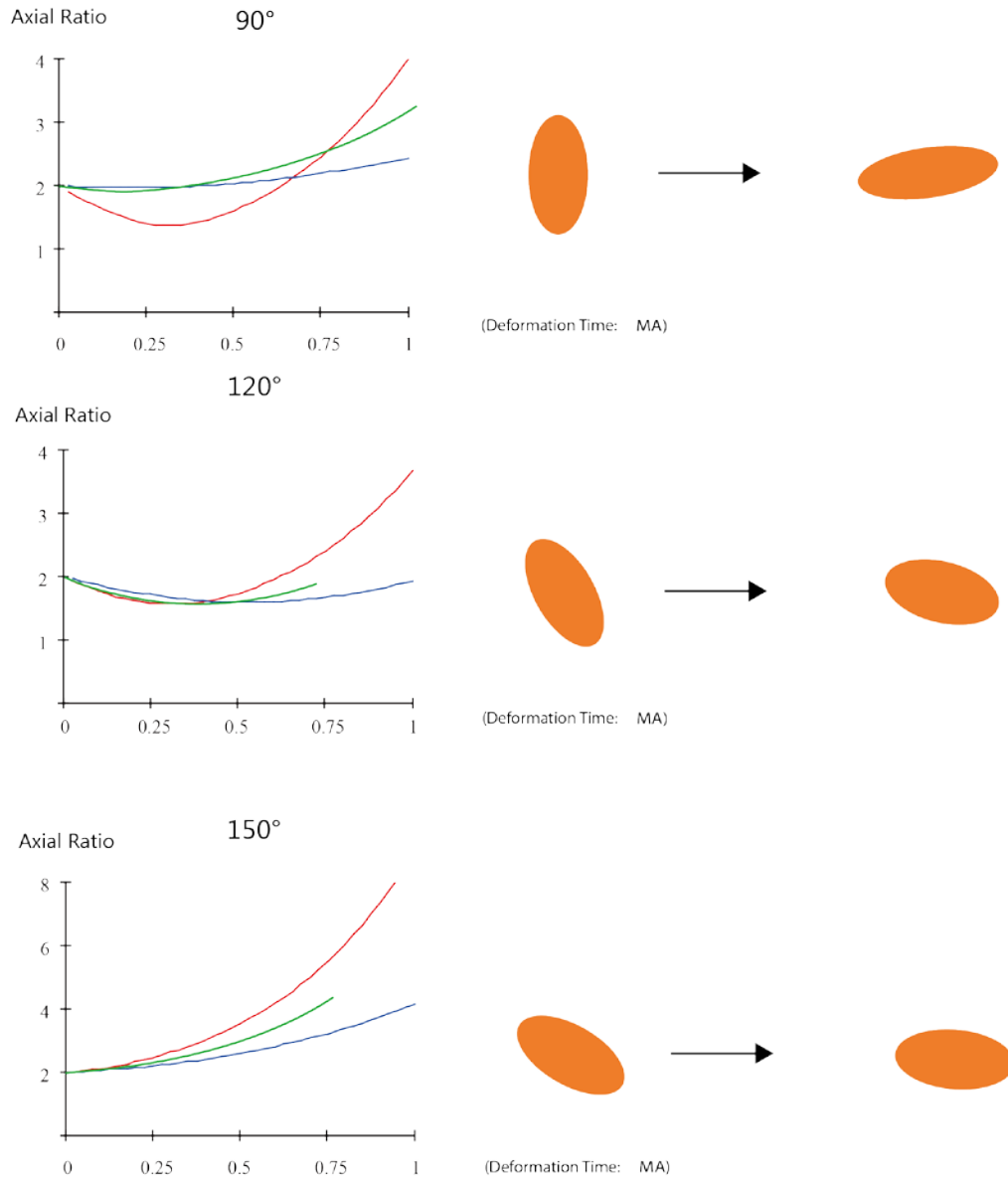


**Figure 4-6 Axial ratio simulation results from FLAC and Eshelby Formalism with initial orientation variations.**

*Initial orientation of the inhomogeneity is set at 0° , 30° , 60° , 90° , 120° and 150° .Figure 4.7A is the evolution of the strain ellipse for all the 6 simulations. Figure 4.6B includes 6 results from simulations with initial orientation variations of the inhomogeneity. The orange ellipses show the initial state and the final state of the inhomogeneity for each FLAC simulation. Conclusion can be made from these simulations that all initial orientations of the inhomogeneity yield consistent results.*

### 4.2.3 Mechanical Property Variations

In this section, how the mechanical property variations influence the deformation history of the ‘inhomogeneity-matrix’ system is investigated, which is one of the major concerns of this project. This topic is of great importance because of it will give an answer to the question that to what extent the *EFTL* / *EFSL* can be applicable to power-law materials. This answer is crucial for one to make appropriate adjustments to the computation and yield results that are more comparable to rock deformation observed in nature.

In power law rheology, materials can be mostly distinguished by two mechanical properties. They are the material parameter  $A$  and the power-law stress exponent  $n$  referring to equation (2-11),  $\dot{\epsilon}_2 = A\sigma_2^n$ . These two properties together define the effective viscosity when the stress or strain rate state is known. Either by changing  $A$  or changing  $n$  can ultimately change the effective viscosity of the material at a given stress or strain rate state. Plus, only the stress exponent  $n$  enters the linearization equation (2-17). Therefore, aiming to validate *EFTL*, only the stress exponent  $n$  needs to be investigated, regardless of the material parameter  $A$ . That is to say, the design of the following simulations is to change the value of the power-law stress exponent  $n$ , through which the deformation evolution response of the ‘inhomogeneity-matrix’ system to the effect of the  $n$  value variations is explored. According to Twiss and Moores (1992, p383), stress exponent only range from 2 to 7.6 in natural rocks. Thus in the following experiments,  $n$  also ranges from 2 to 7.6.

The approach adopted in this project on mechanical property experiments is as follows. First set the stress exponent of the matrix  $n_m$  at 2. Then make the stress exponent of the inhomogeneity  $n_i$  change from 2 to 7.6. While the simulation with the Eshelby

Formalism has no difficulty regardless of the stress exponent, FLAC simulation runs to ‘bad geometry’ at very low finite strains when the stress exponent of the inhomogeneity,  $n_c$ , is increased to only 4. This is because, when the stress exponent of the matrix is kept high, even a moderately high inhomogeneity stress exponent will cause significantly enhanced strain localization in the matrix in the vicinity of the inhomogeneity, thus distorting the zones there to “bad geometries”. To overcome this difficulty, the matrix stress exponent,  $n_m$ , is increased to 3. The simulations run much more smoothly and the system does not come to the unpleasant bad geometry until  $n_c$  reaches 5.5.

In all simulations in this section,  $W_k$  is set at 0.3, the velocity gradient tensor is assigned

as:  $L_{ij} = \begin{bmatrix} 3 \times 10^{-10} & 1.887 \times 10^{-10} & 0 \\ 0 & -3 \times 10^{-10} & 0 \\ 0 & 0 & 0 \end{bmatrix}$  and the initial inhomogeneity orientation is

set at 45°. Other initial conditions for simulations in this section are presented below in Table 8.

**Table 4-6 Initial mechanical conditions for simulations on different mechanical properties.**

Stress Exponent of Inhomogeneity ( $n_i$ )	Stress Exponent of Matrix ( $n_m$ )	Effective Viscosity Ratio ( $r_{eff}$ )
4.7	3	0.824
4.9	3	0.786



5.1	3	0.742
5.4	3	0.725

Result curves are shown in Figure 4.7. Only the results from simulations with  $n_c$  ranging from 4.7 to 5.4 are illustrated in the figure because it is sufficient to draw conclusions. One can observe from the figure that the FLAC curves lie in between the *EFTL* curves and *EFSL* curves in all simulations, indicating that results are consistent for all mechanical properties. Attention should be paid on the deforming strain rate of the three curves in the composite figure. When the inhomogeneity is weaker than the matrix (effective viscosity ratios in Table 8 are less than 1), the relative position of the three curves become reversed of the ones in the previous simulations where the inhomogeneity is stronger than the matrix. More specifically, *EFTL* always deforms the fastest, *EFSL* the slowest and the FLAC simulation in between, implying that *EFTL* over-estimate the compliance of the inhomogeneity while the *EFSL* under-estimate it.

In summary, several observations can be obtained from the simulations on general power-law deformations.

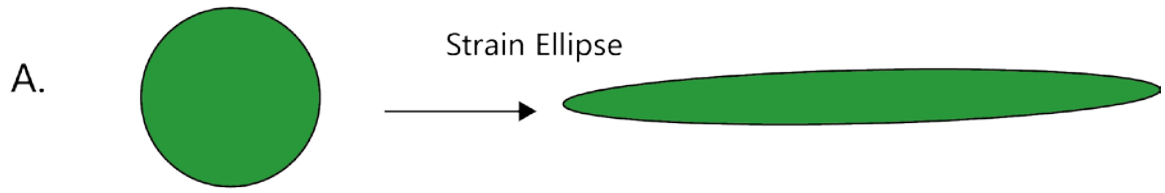
- 1) Result curves from FLAC simulation always lie in between the *EFTL* curves and the *EFSL* curves. When the inhomogeneity is mechanically stronger than the matrix, *EFTL* always over-estimates the ‘strength’ of the inhomogeneity and consequently

uses a higher effective viscosity ratio ( $r_{eff}$ ) than necessary, while *EFSL* underestimates the ‘strength’ and uses a lower  $r_{eff}$ . On contrary, when the inhomogeneity is mechanically weaker than the matrix, *EFTL* will over-estimate this weakness while *EFSL* under-estimates it. Therefore, in general power-law deformations, neither *EFTL* nor *EFSL* can perfectly match FLAC simulations.

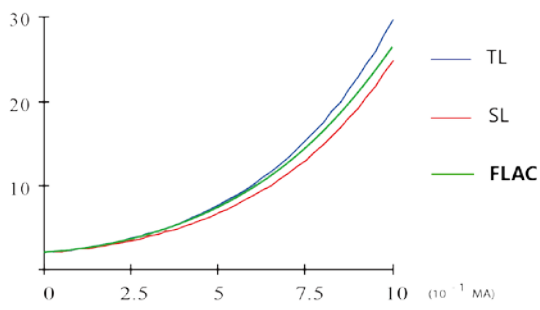
- 2) Consistent results are yielded in all simulations. Such results are independent of the initial settings of shear flow types, initial orientation/shape of the inhomogeneity or mechanical property variations.

These are only observations from the result curves. More insights and how these insights can be applied to future work will be discussed in the following chapter.

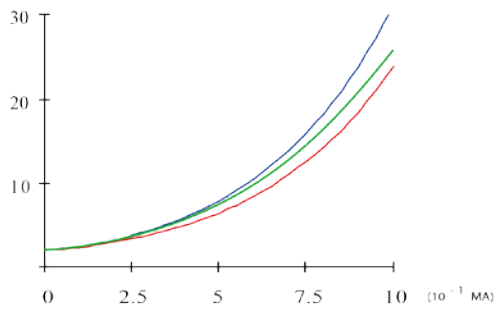
## Experiments on Power-Law Stress Exponent Variation



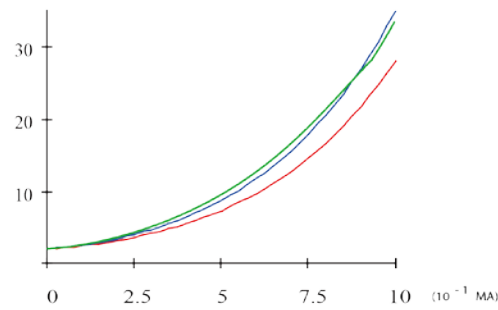
B.



$n(\text{medium})=3, n(\text{inhomogeneity})=4.7$



$n(\text{medium})=3, n(\text{inhomogeneity})=4.9$



$n(\text{medium})=3, n(\text{inhomogeneity})=5.4$



**Figure 4-7 Results from FLAC and Eshelby Formalism on varying power-law stress exponent.**

*Stress exponent for the matrix is kept constant while the one for the inhomogeneity changes from 4.7 to 5.4. Figure A illustrates the initial state and the final state of the strain ellipse. Figure B presents three simulations with different stress exponents of the inhomogeneity, which are 4.7, 4.9 and 5.4. Initial and final states of the inhomogeneity are also illustrated by the orange ellipses. Consistent results are yielded for all settings of the varying stress exponents of the inhomogeneity. In these simulations where the inhomogeneity is mechanically weaker than the matrix, simulated strain rate of the inhomogeneity in EFTL becomes the fastest; the one in EFSL becomes the slowest while the one in FLAC simulation again lies in between the above two.*

## Chapter 5

### 5 Result Discussions and Conclusions

With all simulations having been presented in the previous chapters, it is high time to summarize the results and interpret the profound meanings of these observations. Such interpretations will help one better simulate the deformation fabric development problems.

#### 5.1 Result Summary and Discussions

There are mainly four results that can be observed from all the simulations in Chapter 4. Each of these results is presented and discussed in the following paragraphs.

##### 5.1.1 Newtonian Inhomogeneity in Newtonian Matrix

In Section 4.1.1 a benchmark simulation is performed on the deformation system where a Newtonian inhomogeneity is embedded in a Newtonian matrix. Since Eshelby Formalism originally is competent in tackling the Newtonian deformations, this simulation is in fact performed to benchmark the simulation setups in FLAC2D. Figure 4.1 shows that the result curve of the Eshelby Formalism perfectly matches the one of the FLAC simulation. This successful result suggests the accuracy of the simulation setups in both Mathcad and in FLAC2D, and implies that the *EFTL*, *EFSL* computations and the FLAC simulations are adequate for simulating the following power-law deformations.

### 5.1.2 Power-Law Inhomogeneity in Newtonian Matrix

When the inhomogeneity becomes power-law material and the matrix remains Newtonian, Figure 4.3 shows that result curve of Eshelby Formalism again perfectly converges to the one of FLAC simulation.

Explanation of this result is as follows. When the matrix remains Newtonian, viscosity of the matrix is not affected by the stress / strain rate state and stays constant throughout the deformation. Thus, the assumption of the Eshelby Formalism is met regardless of the inhomogeneity material. Therefore, the linearization equation of the Tangent Scheme and the Secant Scheme is actually the same, which is equation (2-18). Furthermore, Taylor expansion is an exact representation of the rheology of the matrix, not an approximation. Therefore, from the theoretical point of view, the result of Eshelby Formalism should be in agreement with the result of the finite difference simulation.

### 5.1.3 Newtonian Inhomogeneity in Power-Law Matrix

The ‘inhomogeneity-matrix’ system where a Newtonian inhomogeneity is embedded in a power-law matrix is another special case. Figure 4.4 shows that, the results of *EFTL* are in great agreement with the results of the FLAC simulation, while the results of *EFSL* have significant deviations.

In this simulation, when the matrix is no longer linear rheological material, its viscosity is affected by the current stress / strain rate state. In the far-field matrix area, since the velocity gradient tensor  $\mathbf{L}$  stays constant throughout the deformation, the viscosities

remain unchanged. However, the viscosity of the matrix will continuously change in the vicinity of the inhomogeneity because of the heterogeneity caused by the interaction between the inhomogeneity and the surrounding matrix. Thus, when the matrix becomes power-law material, a linearization scheme is needed. Since Tangent Scheme is just an approximation, deviations between the *EFTL* computation and the FLAC simulation are inevitable.

However, being Newtonian, the inhomogeneity has a constant viscosity leading to reduced interaction between the inhomogeneity and the matrix in the vicinity of the inhomogeneity. Consequently, heterogeneity in the vicinity of the inhomogeneity becomes rather small. Therefore, deviation between the *EFTL* computation and the FLAC simulation also becomes insignificant.

On the other hand, since the linearization scheme in *EFSL* is just a pseudo-linear form which only applies to the exact state of stress and strain rate, the power-law constitutive equation will always remain non-linear no matter how small an increment of deformation could be. Therefore, theoretically Secant Scheme is not sufficient to be a good approximation of the power-law rheology. This is validated in the simulation in Section 4.1.3, where the results of *EFSL* have significant deviations from results of the FLAC simulation.

In summary, in the situation where a Newtonian inhomogeneity is embedded in a power-law matrix, Tangent Scheme is much better an approximation of the power-law rheology than the Secant Scheme.

#### 5.1.4 Power-Law Inhomogeneity in Power-Law Matrix

When it comes to the most general situation where both the inhomogeneity and the matrix are power-law materials, neither *EFTL* nor *EFSL* can perfectly match the result simulated in FLAC2D (Figure 4.5, 4.6, 4.7). However, all the result curves show a similar pattern, which is that the curve from FLAC simulation always lies in between the *EFTL* curve and the *EFSL* curve. This pattern can be further sub-categorized into the following two situations:

1. When the effective viscosity ratio ( $r_{eff}$ ) of the inhomogeneity to the matrix is larger than 1 (the inhomogeneity is mechanically stronger than the matrix), *EFTL* always deforms the slowest while *EFSL* consistently deforms the fastest, implying that *EFTL* uses a higher  $r_{eff}$  than necessary while *EFSL* uses a lower one. In other words, the strength of the inhomogeneity is overestimated in *EFTL* and underestimated in *EFSL*.
2. When the competence contrast is reversed (the inhomogeneity is weaker than the matrix), the previous pattern becomes reversed. To be detailed, *EFTL* now consistently deforms the fastest while *EFSL* deforms the slowest. Thus, in this case, the weakness of the inhomogeneity is again magnified in *EFTL* and reduced in *EFSL*.

Explanation of this pattern is presented as follows. First of all, deviations between *EFTL*, *EFSL* computations and FLAC simulations are inevitable because they are all approximations to power-law rheology. Second of all, it has been proved (Lebensohn and Tomé, 1993) that, when the stress exponent of the matrix approaches infinity ( $n_m \rightarrow \infty$ ), the Tangent approximation tends to a uniform stress state (lower-bound approximation)



while the Secant interaction tends to a uniform strain-rate state (upper-bound approximation). However, deformations in natural rocks are neither completely stress uniform nor completely strain-rate uniform. Therefore, the real power-law behavior should lie in between the Tangent Behavior and the Secant Behavior when  $n_m \rightarrow \infty$ . When  $n_m$  is finite, the real power-law behavior should also lie in between the Tangent Behavior and the Secant Behavior because the Tangent approximation is always the lower-bound approximation while the Secant approximation is always the upper-bound one (Figure 5.1).

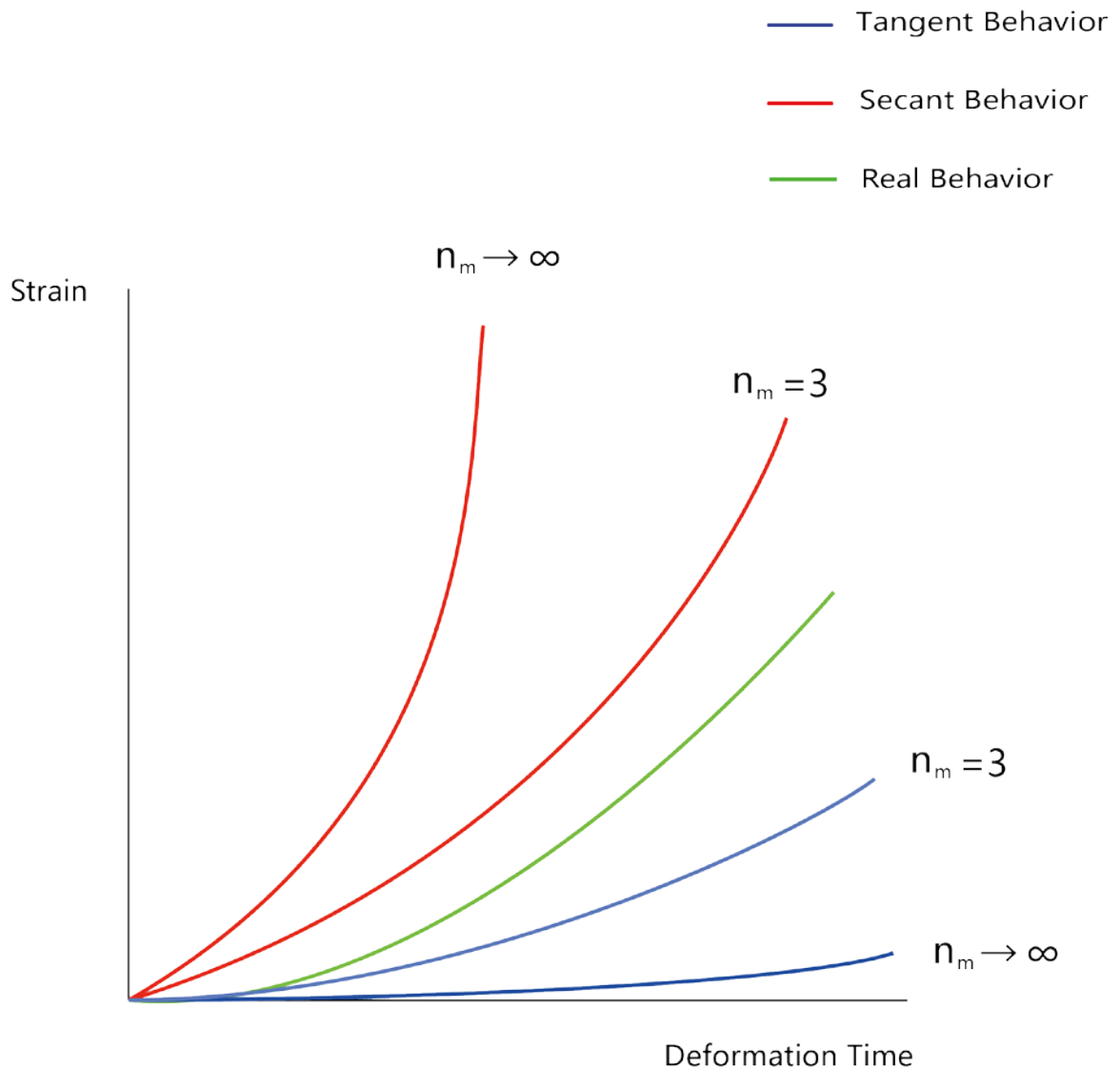


**Figure 5-1 Schematic strain history of an inhomogeneity modeled by the Secant Behavior, Tangent Behavior and the Real Power-law Behavior as  $n_m$  varies.**

*Secant Behaviors are denoted by red curves, Tangent Behavior by blue curves and the real power-law behavior by a green curve. In both situations where  $n_m \rightarrow \infty$  and  $n_m = 3$ , the real power-law behavior should lie in between the Secant Behavior and the Tangent Behavior because the Tangent approximation is always the lower-bound approximation while the Secant approximation is always the upper-bound one. Deviations between the three behaviors will change with respect to different  $n_m$ .*

## 5.2 Applicability of the Eshelby Formalism with Tangent Linearization Scheme

As mentioned in Chapter 1, the validation of the applicability of *EFTL* is the main goal of this project. In this section, the applicability of *EFTL* is discussed and all the questions related to the applicability will be given answers.

### 5.2.1 Applicability Quantification

To summarize the soundness of the applicability of *EFTL* from the simulation observations, some quantitative terms should be employed. Here I focus on the axial ratio evolution and the orientation evolution of the inhomogeneity.

Take one simulation in section 4.2.1 as an example for the applicability quantification. This simulation is chosen because its result figure suggests the largest deviations between *EFTL* and FLAC simulation compared to other simulations. The initial conditions for this simulation are shown in Table 9.

**Table 5-1 Initial conditions for a general power-law simulation.**

$W_k$	$L_{ij}$	Effective Viscosity Ratio	Initial Orientation of Inhomogeneity	Stress Exponent of Matrix ( $n_m$ )	Stress Exponent of Inhomogeneity ( $n_i$ )
0.6	$\begin{bmatrix} 3 \times 10^{-10} & 4.5 \times 10^{-10} & 0 \\ 0 & -3 \times 10^{-10} & 0 \\ 0 & 0 & 0 \end{bmatrix}$	1.628	60°	4.7	2.9

In this simulation, with a relative large  $W_k$ , the aspect ratio of the strain ellipse becomes 9.658 after 0.8 million years of deformations. The height of the ‘inhomogeneity-matrix’ system is shortened from 80m to 2.4m (Figure 5.2). Therefore, the Cauchy strain of the system in the y-direction is -0.97. This strain is large enough when compared to natural rock transpression deformations.

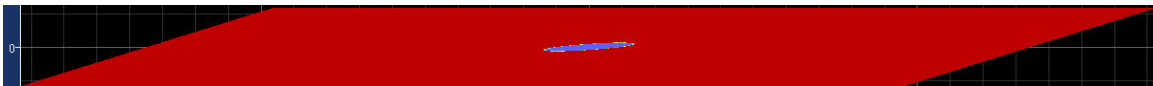


**Figure 5-2 The ‘inhomogeneity-matrix’ system after 1 million years deformation in the example simulation.**

*The height of the system along y-axis direction is 2.4m after deformation. The system has been shortened 97% in y-axis direction.*

Undergone this large strain deformation of the system, the axial ratios / orientations of the inhomogeneity simulated in FLAC2D and computed in *EFTL*, *EFSL* are listed in Table 10 (can also be viewed in Figure 4.5).

**Table 5-2 Resulted axial ratios and orientations of the inhomogeneity**

Ratio in FLAC	Ratio in <i>EFTL</i>	Ratio in <i>EFSL</i>
5.7	4.8	7.3

Orientation in FLAC	Orientation in <i>EFTL</i>	Orientation in <i>EFSL</i>
7.4°	7.8886°	6.9015°

Following observations can be obtained from Table 10. In the computation of the axial ratios, *EFTL* under-estimates the ratio by 15.8%, while *EFSL* over-estimates it by 28%. On the other hand, in the orientation computation, *EFTL* under-estimates the spin angle by 6.6% while *EFSL* over-estimates it by 6.7%.

Note that the deformation time of all the simulations in Chapter 4 is set at 1 million years. This corresponds only to the early increment of a typical tectonic deformation which usually lasts for more than several million years (e.g., Karato, 2008). Thus, the statistics in Table 10 can only represent the deviations in the early period of tectonic deformations. As shown in Figure 5.3, when the general shear deformation proceeds to the late period, orientation of the inhomogeneity will soon approach the shear plane direction and the inhomogeneity will stop spinning. In nature, this phenomenon is in fact the cause of tectonic transposition. This phenomenon is also simulated by one of the simulations in Section 4.2.2, where the initial orientation of the inhomogeneity set at 0°. In the composite curve figures of this simulation, the orientation of the inhomogeneity only varies in a range of  $\pm 0.1^\circ$  which is possibly caused by errors. More importantly, the deviation between the axial ratio simulated in FLAC and the one computed in *EFTL* is only 8.6%. Therefore, it can be concluded that when the deformation proceeds to the late

period, the inhomogeneity will soon approach the shear plane direction and stop spinning, and therefore the deviations between *EFTL* / *EFSL* and FLAC simulations will be smaller in the subsequent deformations.

In the practical fabric-development simulations, since the results are retrieved from the late period of deformations, the deviations on axial ratio of the fabric (inhomogeneity) are supposed to be only less than 10% between the *EFTL* computations and the power-law deformations in nature; while the deviations on the fabric orientation are negligible. In other words, *EFTL* is able to precisely simulate the orientation evolution of the fabrics, and simulate the shape of the fabrics only with a deviation smaller than 10%, which is small enough for the extrapolation of the long-term and large-strain tectonic deformations.

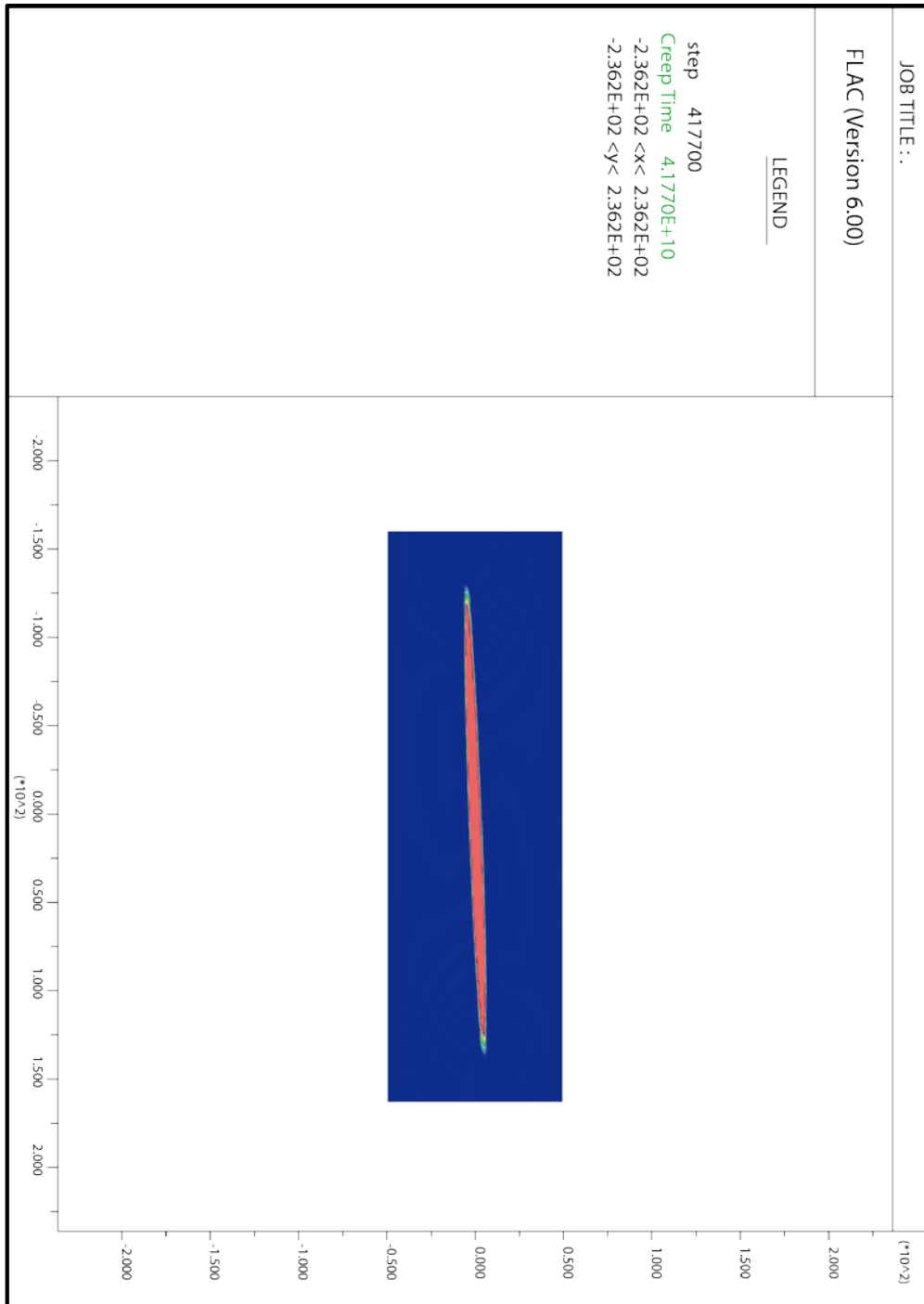


**Figure 5-3 Late-period general shear deformation.**

*In late-period general shear deformation, the inhomogeneity orientation is almost horizontal. In nature, all fabrics will evolve to be transposition foliations.*

## 5.2.2 Mechanical Condition Requirement

Simulations in this project only accounts for the power-law materials whose stress exponent ranges from 2.9 to 5.5. From Section 5.2.1, it is now known that materials within the 2.9-5.5 stress exponent range can be modeled by *EFTL* only with about 10% deviations.

Given that the stress exponents in natural rocks range from 2 to 7.6 according to Twiss and Moores (1992, p.383), there is still some range of stress exponents (2-2.9, 5.5-7.6) that has not entered the simulations in this project. However, it is believed that this leftover range of power-law materials can also be modeled by *EFTL* for the following two reasons:

- 1) *EFTL* has been applied to metal deformations by Lebensohn and Tomé (1993) and has well predicted the metal textures. Metals have stress exponents higher than 7.6, therefore the leftover range in this project also meets the assumption in the Tangent theory.
- 2) It is validated in Section 4.2.3 that the relationship between *EFTL* and FLAC simulation remains consistent regardless of the stress exponent variations. Therefore, as long as the assumptions in *EFTL* are not violated, the leftover range of materials should also yield consistent result.

In conclusion, the applicability of *EFTL* to power-law deformations of natural rocks is validated.



### 5.3 Appropriate Modifications

In order to minimize the inevitable deviations between the Tangent Behavior and the real power-law behavior (see Section 5.1.4), appropriate modifications to *EFFL* can be made.

Lebensohn and Tomé proposed a possible modification in the manual of their VPSC code. The modification is as follows.

It is discussed in Chapter 2 that equation (2-17) is the one to calculate the strain rate tensor of the inhomogeneity in *EFTL*:

$$\boldsymbol{\varepsilon}_i = [\mathbf{J} + (n_m r_{eff} - 1)\mathbf{S}]^{-1} : [\mathbf{J} + (n_m - 1)] : \boldsymbol{\varepsilon}_m \quad (5-1)$$

As the Secant Linearization amounts to setting  $n_m = 1$  in the above equation, and as has been shown in this project, the real power-law behavior as modeled by FLAC always lies between the Secant and Tangent linearizations, a better empirical representation of the power-law behavior, as proposed by Lebensohn and Tomé is to introduce an adjustable parameter  $n^{eff}$  to equation (5-1), such that  $1 < n^{eff} < n_m$  and equation (5-1) becomes:

$$\boldsymbol{\varepsilon}_i = [\mathbf{J} + (n^{eff} r_{eff} - 1)\mathbf{S}]^{-1} : [\mathbf{J} + (n^{eff} - 1)] : \boldsymbol{\varepsilon}_m \quad (5-2)$$

Note that when  $n^{eff} = 1$ , equation (5-2) is in fact equation (2-18), which is the equation adopted by *EFSL*.  $n^{eff}$  value lying between 1 and  $n_m$  in fact implies that the real power-law behavior should lie in between the Secant Behavior and the Tangent Behavior, which agrees with all the simulations in this project and the discussions in Section 5.1.4.

### 5.3.1 Practical Implementations

It is now known that modifications can be made to perfect *EFTL*. In this section, insight into how to make appropriate modifications in practical implementations of *EFTL* is presented.

Simulations of phenomenological analysis are conducted to yield possible range of the  $n^{eff}$  values. Initial conditions for this simulation are in Table 11.

**Table 5-3 Initial conditions for simulation on  $n^{eff}$  value.**

$W_k$	$L_{ij}$	Effective Viscosity Ratio	Initial Orientation of Inhomogeneity	Stress Exponent of Matrix ( $n_m$ )	Stress Exponent of Inhomogeneity ( $n_i$ )
0.3	$\begin{bmatrix} 3 \times 10^{-10} & 1.887 \times 10^{-10} & 0 \\ 0 & -3 \times 10^{-10} & 0 \\ 0 & 0 & 0 \end{bmatrix}$	1.59	60°	4.7	2.9

Results are shown in Figure 5.4. When  $n^{eff}$  equals 1 and 4.7, implying *EFSL* and *EFTL* respectively, the result curves exhibit some deviations from the *FLAC* simulation. After a series of test simulations, result shows that when  $n^{eff}$  equals 1.5, which meets the presumption that  $1 < n^{eff} < n_m$ , the behavior best fits the power-law deformation simulated in *FLAC*. Therefore, in this case of simulation,  $n^{eff}$  should be applied to replace the original  $n_m$  and  $n^{eff}$  should be 1.5.

Note that  $n^{eff} = 1.5$  in the above simulation is only a phenomenological finding. I conduct other simulations with original  $n_m$  set at different values.  $n^{eff}$  values vary in each of these simulations. Thus, the appropriate value of  $n^{eff}$  varies correspondingly when the  $n_m$  as well as the effective viscosity ratio changes. From a phenomenological point of view, the  $n^{eff}$  values are within the range of 1.5-2.

In summary, with the modified  $n^{eff}$  taking the place of the original stress exponent of the matrix ( $n_m$ ), *EFTL* is potentially able to perfectly simulates power-law deformations in nature. However, the determination of the value of  $n^{eff}$  requires more knowledge on the flow evolution of the matrix especially in the vicinity of the inhomogeneity. This kind of knowledge is what we currently lack of thus no further work can be done in this project to give a solution of the  $n^{eff}$  calculation other than phenomenological analysis.

## Simulation on $n_{eff}$

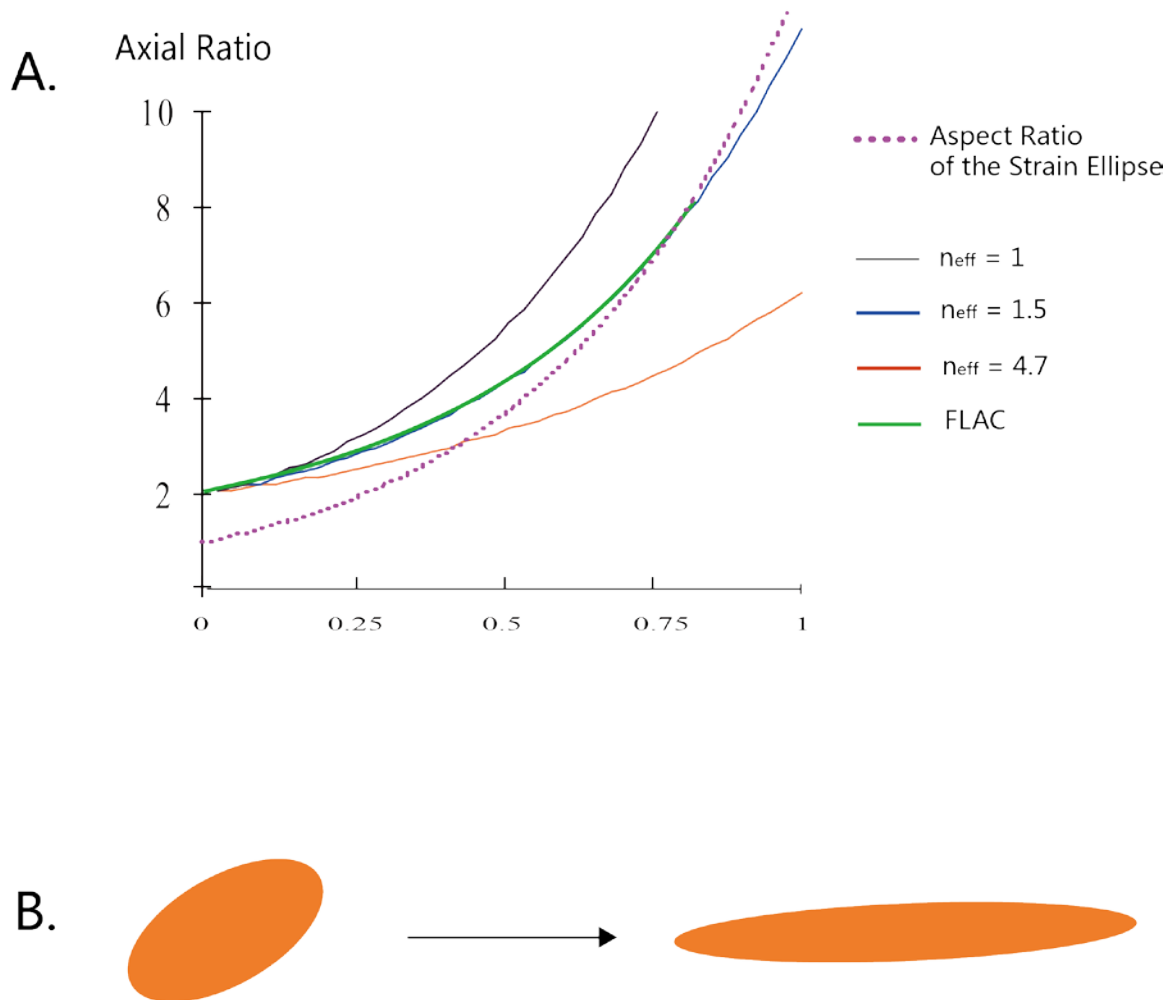


### Figure 5-4 Results from Eshelby Formalism and FLAC on $n^{eff}$ .

Several simulations based on different  $n^{eff}$  values are performed in Eshelby Formalism model and in FLAC model. In figure A, as usual, the green curve is the result from the FLAC model, the purple dotted line is the aspect ratio of the strain ellipse, while the other three curves are results from Eshelby Formalism model. When  $n^{eff}$  equals 1.5, Eshelby Formalism fits the FLAC result best. Figure B shows the evolutions of both the shape and the orientation of the inhomogeneity.

## 5.4 Conclusions and Future Work

The Eshelby Formalism with the Tangent Linearization Scheme (*EFTL*) provides a potentially better framework to simulate fabric development problems compared to the early kinematic models and the computational geodynamics. In this project, I propose a series of simulations on the ‘inhomogeneity-matrix’ deformation system, aiming to validate the applicability of *EFTL*.

Main conclusions of the project are as follows:

- 1) When the matrix is Newtonian and the inhomogeneity is power-law, *EFTL* perfectly simulates the power-law deformations.
- 2) When the matrix is power-law and the inhomogeneity is Newtonian, *EFTL* can simulate the power-law deformations only with slight deviations.
- 3) When in general power-law deformation situations, where both the matrix and the inhomogeneity are power-law, *EFTL* poses some deviations from the power-law behavior. However, such deviations are rather small in natural rock deformations (less than 10% deviations). Therefore, *EFTL* can still simulate the general power-law deformations well enough for long-term geological problems.
- 4) A further empirical improvement of the *EFTL* can be made by using an effective stress exponent for the matrix which lies between 1 and the actual stress exponent. For natural rocks with stress exponents between 3-5, the effective stress exponent is in the range of 1.5-2.

Through this thesis, the Eshelby Formalism with Tangent Linearization is validated to be applicable to power-law materials. By combining the ‘Homogeneous Equivalent Medium’

(HEM) and the ‘self-consistent’ theories (Molinari, 1987; Lebensohn and Tomé, 1993; Jiang, 2012 in review), *EFTL* is now able to tackle the ‘multi-scale’ and ‘multi-inhomogeneities’ problems and simulate the natural rock deformations without being penalized by all the negative effects caused by the conventional mesh-based approaches.

Further work is suggested to focus on the strain/stress field in the vicinity of the inhomogeneity, where the interaction between the inhomogeneity and the matrix is most significant. By gaining more insight into such interaction, one may be able to constrain the value of the  $n^{eff}$  for the appropriate modification to the *EFTL*.

Indeed, *EFTL* is not perfect at this stage, yet it is able to simulate the geological long-term deformations well enough for fabric development modeling.

## References

- Behr, W. M. and J. P. Platt (2011). "A naturally constrained stress profile through the middle crust in an extensional terrane." Earth and Planetary Science Letters **303**(3–4): 181-192.
- Bilby, B. A., J. D. Eshelby, et al. (1975). "The change of shape of a viscous ellipsoidal region embedded in a slowly deforming matrix having a different viscosity." Tectonophysics **28**(4): 265-274.
- Brun, J. P. and P. R. Cobbold (1980). "Strain heating and thermal softening in continental shear zones: a review." Journal of Structural Geology **2**(1-2): 149-158.
- Ferguson, C.C. (1981). "A strain reversal method for estimating extension from fragmented rigid inclusions." Tectonophysics **79**(3–4): T43-T52.
- Cundall, P. (1976). "Explicit finite-difference methods in geomechanics." Numerical methods in Geomechanics, ASCE: 132-150.
- Currie, C. A., R. S. Huisman, et al. (2008). "Thinning of continental backarc lithosphere by flow-induced gravitational instability." Earth and Planetary Science Letters **269**(3-4): 436-447.
- Currie, C. A., K. Wang, et al. (2004). "The thermal effects of steady-state slab-driven mantle flow above a subducting plate: the Cascadia subduction zone and backarc." Earth and Planetary Science Letters **223**(1-2): 35-48.
- Desai, C. S. (1977). "ANALYSIS AND EVALUATION OF SOME FINITE ELEMENT SCHEMES FOR FLOW THROUGH RIGID AND DEFORMABLE MEDIA." 3. 21-23. 45.
- Eshelby, J. D. (1957). "The Determination of the Elastic Field of an Ellipsoidal Inclusion, and Related Problems." Proceedings of the Royal Society of London. Series A. Mathematical and Physical Sciences **241**(1226): 376-396.
- Eshelby, J. D. (1959). "The Elastic Field Outside an Ellipsoidal Inclusion." Proceedings of the Royal Society of London. Series A. Mathematical and Physical Sciences **252**(1271): 561-569.
- Fossen, H. (2010). "Deformation bands formed during soft-sediment deformation: Observations from SE Utah." Marine and Petroleum Geology **27**(1): 215-222.
- Freeman, B. (1987). "The behaviour of deformable ellipsoidal particles in three- dimensional slow flows: implications for geological strain analysis." Tectonophysics **132**(GEOBASE): 297-309.

- Gleason, G. C. and J. Tullis (1995). "A flow law for dislocation creep of quartz aggregates determined with the molten salt cell." Tectonophysics **247**(1-4): 1-23.
- Goodwin, L. B. and B. Tikoff (2002). "Competency contrast, kinematics, and the development of foliations and lineations in the crust." Journal of Structural Geology **24**(6-7): 1065-1085.
- Goodwin, L. B. and B. Tikoff (2002). "Competency contrast, kinematics, and the development of foliations and lineations in the crust." Journal of Structural Geology **24**(6-7): 1065-1085.
- Hans, R. (1975). "Particle paths, displacement and progressive strain applicable to rocks." Tectonophysics **28**(1-2): 1-37.
- Hobbs, B. E., H. B. Muhlhaus, et al. (1990). "Instability, softening and localization of deformation." Deformation mechanisms, rheology and tectonics(GEOBASE): 143-165.
- Hobbs, B. E. and A. Ord (1989). "Numerical simulation of shear band formation in a frictional-dilatational material." Archive of Applied Mechanics **59**(3): 209-220.
- Hutchinson, J. W. (1976). "Bounds and Self-Consistent Estimates for Creep of Polycrystalline Materials." Proceedings of the Royal Society of London. A. Mathematical and Physical Sciences **348**(1652): 101-127.
- Jeffery, G. B. (1922). "The Motion of Ellipsoidal Particles Immersed in a Viscous Fluid." Proceedings of the Royal Society of London. Series A **102**(715): 161-179.
- Jiang, D. (1994a). "Flow variation in layered rocks subjected to bulk flow of various kinematic vorticities: theory and geological implications." Journal of Structural Geology **16**(8): 1159-1172.
- Jiang, D. (1994b). "Vorticity determination, distribution, partitioning and the heterogeneity and non-steadiness of natural deformations." Journal of Structural Geology **16**(1): 121-130.
- Jiang, D. (2007). "Numerical modeling of the motion of rigid ellipsoidal objects in slow viscous flows: A new approach." Journal of Structural Geology **29**(GEOBASE): 189-200.
- Jiang, D. (2010). "Flow and finite deformation of surface elements in three dimensional homogeneous progressive deformations." Tectonophysics **487**(1-4): 85-99.
- Jiang, D. (2012). "A general approach for modeling the motion of rigid and deformable ellipsoids in ductile flows." Computers and Geosciences **38**(1): 52-61.



- Jiang, D. (In review). "Deformable ellipsoids in three-dimensional power-law viscous flow: theoretical formulation, numerical implementation, and potential applications." Journal of Structural Geology
- Jiang, D. and P. F. Williams (1998). "High-strain zones: a unified model." Journal of Structural Geology **20**(8): 1105-1120.
- Karato S (2008) Deformation of Earth materials: an introduction to the rheology of the solid Earth. Cambridge University Press, Cambridge..
- Kohlstedt, D. L., B. Evans, et al. (1995). "Strength of the lithosphere: constraints imposed by laboratory experiments." Journal of Geophysical Research **100**(B9): 17,587-517,602.
- Lebensohn, R. A. and C. N. Tomé (1993). "A self-consistent anisotropic approach for the simulation of plastic deformation and texture development of polycrystals: Application to zirconium alloys." Acta Metallurgica et Materialia **41**(9): 2611-2624.
- Li, Changcheng, "An Investigation of Deformation Structures and Their Tectonic Significance Across the Grenville Front Tectonic Zone in the Vicinity of Sudbury, Ontario, Canada" (2012). Electronic Thesis and Dissertation Repository. Paper 464.
- Lister, G. S. and P. F. Williams (1983). "The partitioning of deformation in flowing rock masses." Tectonophysics **92**(1-3): 1-33.
- Mancktelow, N. S. (2011). "Deformation of an elliptical inclusion in two-dimensional incompressible power-law viscous flow." Journal of Structural Geology **33**(9): 1378-1393.
- Mackwell, S. J., D. Dimos, et al. (1988). "Transient creep of olivine: point-defect relaxation times." Philosophical Magazine A (Physics of Condensed Matter, Defects and Mechanical Properties) **57**(5): 779-789.
- Mandal, N., S. Kumar Samanta, et al. (2005). "Rotation behaviour of rigid inclusions in multiple association: Insights from experimental and theoretical models." Journal of Structural Geology **27**(GEOBASE): 679-692.
- McKinnon, S. D. and I. Garrido de la Barra (1998). "Fracture initiation, growth and effect on stress field: a numerical investigation." Journal of Structural Geology **20**(12): 1673-1689.
- Molinari, A., G. R. Canova, et al. (1987). "A self consistent approach of the large deformation polycrystal viscoplasticity." Acta Metallurgica **35**(12): 2983-2994.
- Mura, T. Micromechanics of Defects in Solids 2nd edn (Kluwer Academic, New York, 1987).

- Nagtegaal, J. C., D. M. Parks, et al. (1974). "On numerically accurate finite element solutions in the fully plastic range." Computer Methods in Applied Mechanics and Engineering **4**(2): 153-177.
- Nemat-Nasser, S., and Hori, M., *Micromechanics: Overall Properties of Heterogeneous Materials*, Amsterdam: Elsevier, 1993; Second Edition, 1999.
- Ord, A. (1990). "Mechanical controls on dilatant shear zones." Geological Society, London, Special Publications **54**(1): 183-192.
- Passchier, C. W. (1991). "The classification of dilatant flow types." Journal of Structural Geology **13**(1): 101-104.
- Passchier, C. W. (1998). "Monoclinic model shear zones." Journal of Structural Geology **20**(8): 1121-1137.
- Passchier, C. W., J. D. Hoek, et al. (1990). "Ductile reactivation of Proterozoic brittle fault rocks; an example from the Vestfold Hills, East Antarctica." Precambrian Research **47**(1-2): 3-16.
- Ramsay, J. G. and R. H. Graham (1970). "Strain variation in shear belts." Canadian Journal of Earth Sciences **7**(3): 786-813.
- Riggs, E. M. and H. W. Green (2001). "Shear localization in transformation-induced faulting: first-order similarities to brittle shear failure." Tectonophysics **340**(1-2): 95-107.
- Robin, P.-Y. F. and A. R. Cruden (1994). "Strain and vorticity patterns in ideally ductile transpression zones." Journal of Structural Geology **16**(4): 447-466.
- Ranalli, G. (1986). *Rheology of the Earth*. Chapman & Hall. New York..
- Samanta, S. K., N. Mandal, et al. (2002). "Development of structures under the influence of heterogeneous flow field around rigid inclusions: Insights from theoretical and numerical models." Earth-Science Reviews **58**(GEOBASE): 85-119.
- Sanderson, D. J. and W. R. D. Marchini (1984). "Transpression." Journal of Structural Geology **6**(5): 449-458.
- Segurado, J., R. A. Lebensohn, et al. (2012). "Multiscale modeling of plasticity based on embedding the viscoplastic self-consistent formulation in implicit finite elements." International Journal of Plasticity **28**(1): 124-140.
- Shaw, T., M. Winston, et al. (2004). "Commonality of Elastic Relaxation Times in Biofilms." Physical Review Letters **93**(9): 098102.

- Simpson, C. and D. G. De Paor (1993). "Strain and kinematic analysis in general shear zones." Journal of Structural Geology **15**(1): 1-20.
- Truesdell, C. (1953). "Two measures of vorticity." Journal of Rational Mechanics and Analysis **2**(2): 173-217.
- Truesdell, C. (1965). Rational mechanics of deformation and flow. Proceedings of the 4th International Congress on Rheology, 1965.
- Twiss, R. J. and Moores, E. M. (1992). Structural geology. W. H. Freeman and Company. New York.
- Williams, P. F. and D. Jiang (2005). "An investigation of lower crustal deformation: Evidence for channel flow and its implications for tectonics and structural studies." Journal of Structural Geology **27**(8): 1486-1504.
- Zhang, Y., N. S. Mancktelow, et al. (2000). "Numerical modeling of single-layer folding: Clarification of an issue regarding the possible effect of computer codes and the influence of initial irregularities." Journal of Structural Geology **22**(10): 1511-1522.

## Appendices

**Appendix A: Added adjustment command to Jiang's (2012) worksheet in Mathcad to assign initial material settings. Through this algorithm the initial effective viscosity is calculated.**

$$\begin{aligned}
 \text{visratio} := & \left. \begin{aligned}
 e0 & \leftarrow \frac{1}{2}(L + L^T) \\
 I0 & \leftarrow \sqrt{\frac{1}{2}[(e0_{1,1})^2 + (e0_{2,2})^2 + (e0_{3,3})^2] + (e0_{1,2})^2 + (e0_{1,3})^2 + (e0_{2,3})^2} \\
 B0 & \leftarrow 7.6226 \cdot 10^{-26} \\
 \sigma0 & \leftarrow \left(\frac{I0}{B0}\right)^{\frac{1}{n0}} \\
 \text{eff0} & \leftarrow \frac{\sigma0}{I0} \\
 B & \leftarrow 1.8982 \cdot 10^{-20} \\
 \sigma & \leftarrow \left(\frac{I0}{B}\right)^{\frac{1}{n}} \\
 \text{eff} & \leftarrow \frac{\sigma}{I0} \\
 \text{vr} & \leftarrow \frac{\text{eff}}{\text{eff0}} \\
 \text{vr} &
 \end{aligned} \right|
 \end{aligned}$$

$$A \equiv 7.925 \quad A0 \equiv 3910$$

$$q \equiv 385000 \quad q0 \equiv 348000$$

$$n \equiv 2.9 \quad n0 \equiv 4.7$$

$$\text{visratio} = 1.581$$

## Appendix B: FISH commands to generate ellipse geometry in FLAC2D

*def elli*

*ntab = 1*

*np=1000*

*d\_theta=2.0\*pi/np*

*fi = 45\*pi/180*

*loop n(1,np)*

*xtable(ntab,n) = 5\*cos(fi)\*cos(theta)+2.5\*sin(fi)\*sin(theta)*

*ytable(ntab,n) = -5\*sin(fi)\*cos(theta)+2.5\*cos(fi)\*sin(theta)*

*theta=theta+d\_theta*

*endloop*

*end*

*elli*

*gen table 1*

## Appendix C: Mechanical Property Assignment in Power-Law Model in FLAC2D

*group 'matrix' notnull*

*group 'inhomogeneity' region 75 75*

*model power group 'matrix'*

*prop dens 2.95e-5 bulk 4.63e6 shear 3.05e6 a\_1=1.8982e-20 n\_1=3.0 group 'matrix'*

*model power group 'clast'*

*prop dens 2.65e-5 bulk 3e6 shear 2.25e6 a\_1=7.6226e-26 n\_1=5 group  
'inhomogeneity'*

## Appendix D: Velocity Boundary Condition Updating FISH in FLAC2D

*def velstep*

*loop n(1,40000)*

*command*

*step 1*

*end\_command*

*; initial\_co*

$$vx1 = 0.15e-4*x(1,1) + 0.09435e-4*y(1,1)$$

$$vxvar1 = 0.15e-4*(x(461,1)-x(1,1))$$

$$vx2 = 0.15e-4*x(1,461) + 0.09435e-4*y(1,461)$$

$$vxvar2 = 0.15e-4*(x(461,461)-x(1,461))$$

$$vx3 = 0.15e-4*x(461,1) + 0.09435e-4*y(461,1)$$

$$vxvar3 = vx2-vx1$$

$$vxvar4 = 0.15e-4*x(461,461) + 0.09435e-4*y(461,461) - vx3$$

$$vy1 = -0.15e-4*y(1,1)$$

$$vy2 = -0.15e-4*y(1,461)$$

$$vyvar = vy2 - vy1$$

*command*

*apply xvel vx1 var vxvar1,0 from 1,1 to 461,1*

*apply xvel vx2 var vxvar2,0 from 1,461 to 461,461*

*apply xvel vx1 var 0,vxvar3 from 1,1 to 1,461*

*apply xvel vx3 var 0,vxvar4 from 461,1 to 461,461*

*apply yvel vy1 from 1,1 to 461,1*

*apply yvel vy2 from 1,461 to 461,461*

*apply yvel vy1 var 0,vyvar from 1,1 to 1,461*

*apply yvel vy1 var 0,vyvar from 461,1 to 461,461*

*end\_command*

*end\_loop*

*end*



## Appendix E: Von Mises Stress Invariant Calculation in FISH command by ITASCA

```
config extra 1
def mises
; --- calculate and store Von Mises stress in extra variable 1 ---
max_mises = 0.0
loop i (1,izones)
loop j (1,jzones)

mstr = (sxx(i,j) + syy(i,j) + szz(i,j)) / 3.
dsxx = sxx(i,j) - mstr
dsyy = syy(i,j) - mstr
dszz = szz(i,j) - mstr
dsxy = sxy(i,j)

vmstr2 = 1.5 * (dsxx*dsxx + dsyy*dsyy + dszz*dszz)
vmstr2 = vmstr2 + 3. * (dsxy*dsxy)

if vmstr2 > 0.0 then
ex_1(i,j) = sqrt(vmstr2)
else
ex_1(i,j) = 0.0
endif
```

```
max_mises = max(max_mises,ex_1(i,j))  
endloop  
endloop  
end  
  
mises  
  
plot hold ex_1 zone fill alias 'Von Mises Stress'  
print max_mises
```

## Appendix F: Fish Command to Obtain and History-Tracked Ellipse Orientation and Axial Ratio

```
def results
  loop i (1,461)
  loop j (1,461)

    if and(flags(i,j), 128) = 128
      ltemp = sqrt(x(i,j)*x(i,j)+y(i,j)*y(i,j))

      if ltemp >= length
        length = ltemp
        xtemp = i
        ytemp = j
      endif

      if ltemp < lshort
        lshort = ltemp
      endif

    endif

  end_loop
end_loop
```

*longaxis = length*

*degree = atan(y(xtemp,ytemp)/x(xtemp,ytemp))/pi\*180*

*shortaxis = lshort*

*ratio = longaxis/shortaxis*

*end*

*history degree*

*history ratio*

*history unbalance*

# Curriculum Vitae

**Name:** Zhenyu Zhong

**Post-secondary Education and Degrees:** University of Western Ontario  
London, Ontario, Canada  
2009-2012  
Master of Science (M.Sc.)

Nanjing University  
Nanjing, Jiangsu, China  
2005-2009.  
Honor Bachelor of Science (H.B.Sc.)

**Honours and Awards:** International Graduate Student Scholarship  
University of Western Ontario  
2009-2011

Academic and Physical Scholarship  
Nanjing University  
2005-2009

**Related Work Experience** Teaching Assistant  
University of Western Ontario  
1999-2011

Research Assistant  
University of Western Ontario  
2009-2012

## Publications:

Zhang, Y., Gao, X., **Zhong, Z.**, Deng, X., Peng, B.  
Comprehensive evaluation of heavy metal contamination of sediment in Lake Dianchi by using modified AHP method and <sup>137</sup>Cs dating. (2008) *Frontiers of Environmental Science and Engineering in China*, 2 (3), pp. 370-379.

Zhang, Y., Zhang, H., **Zhong, Z.**, Gao, X., Ni, Y.  
Objectively evaluating environmental comprehensive quality by improved AHP method. (2008) 2nd International Conference on Bioinformatics and Biomedical Engineering, iCBBE 2008, art. no. 4535200, pp. 4645-4649.